**ADDIS ABABA UNIVERSITY**

**ADDIS ABABA INSTITUTE OF TECHNOLOGY**

**AFRICAN RAILWAY CENTER OF EXCELLENCE**


# THE EFFECT OF TRAFFIC ON BALLAST SETTLEMENT

**A Thesis in Railway Civil Engineering**

By Sisay Atumo G/mariam

September 2019

Addis Ababa

A Thesis

Submitted in Partial Fulfillment of the Requirements for the Degree of Master of Science

The undersigned have examined the thesis entitled '**The effect of traffic load on ballast settlement**' presented by **SISAY ATUMO G/MARIAM**, a candidate for the degree of **Master of Science** and hereby certify that it is worthy of acceptance.

| | | |
|---|---|---|
| Mequannent Mulugeta (MSc.) | | |
| Advisor | Signature | Date |
| Zewdie Moges (MSc.) | | |
| Internal Examiner | Signature | Date |
| Matias Kabtamu (MSc.) | | |
| External Examiner | Signature | Date |
| Abrham Gebrie (PhD.) | | |
| Chair person | Signature | Date |

## UNDERTAKING

I certify that research work titled “The effect of traffic load on ballast settlement” is my own work. The work has not been presented elsewhere for assessment. Where material has been used from other sources it has been properly acknowledged / referred.

Sisay Atumo G/mariam

## ABSTRACT

Many of the world's railways run on ballasted track, which has for nearly 200 years provided a stable support for train operation. However, with trafficking the geometry of the track deteriorates, mainly as a result of the development of differential settlement of the track-bed.

The main factor that contribute for the deterioration of track components is traffic load. Explanations on how the speed, load and repetition of traffic influence the long-term settlement of ballast in ballasted track is very scarce. Having in mind that tracks subjected to the same load show different settlement behavior, explanations of track settlements in accordance with the speed, load and repetition is needed. This study is motivated to show how traffic affects the long-term settlement of ballast and how the traffic parameters (speed, load and repetition) contributes in the process.

Using finite element modeling software, three-dimensional track is modeled and analyzed for different values of speed, load and no of repetitions. Drucker Prager plastic model is applied for the ballast and sub-ballast materials of the track. To get the parameters for the Drucker Prager plastic model of granular materials, triaxial test simulation is performed using discrete element software. Hertz contact theory is used to model the contact between the wheel and rail. The long-term settlement behavior of ballast material is analyzed by applying 10,000 cycle of moving axel load.

According to the analyses a change in the speed and the number of repetitions of train movement changes the permanent settlement of ballast more than the variation in load. Increase in the speed of train movement by 20km/hr will increase the stress transferred to the subgrade by up to about 1000kpa. Speed of train movement is most contributing parameter in the degradation of ballast material more than the load and no of repetition. In a conventional ballasted track after about 6,000 repetition of train movement ballast material will start to decrease its performance. So, careful monitoring and periodic maintenance will be necessary.



**KEY WORDS:** Ballast, Speed, Axel load, Number of repetitions, Settlement, Modeling…

## ACKNOWLEDGMENTS

I am grateful to my Advisor, Mr. Mequanent Mulugeta (Msc), for his encouragement, thoughtful guidance, invaluable help and patience throughout this research project. His valuable suggestions, numerous comments and advices during various stages of this research, including the preparation of this thesis, are gratefully acknowledged.

I would like to thank the Ethiopian Railway Corporation (ERC) and Addis Ababa Institute of Technology (AAiT) for the M.Sc. program and financial support given.

I also owe my gratitude to the contractor of the Ethio-Djibouti railway line, China Railway Group Limited (CREC) especially Mr. Chen for their cooperation in giving valuable test data.

## TABLE OF CONTENTS

## LIST OF TABLES

## LIST OF FIGURES

# CHAPTER 1 INTRODUCTION

Many of the world's railways run on ballasted track, which has for nearly 200 years provided a stable support for train operation. However, with trafficking the geometry of the track deteriorates, mainly as a result of the development of differential settlement of the track-bed. When the geometry defects become too severe, maintenance is needed to realign the track to enable the continued safe running of trains. [72] Ballast failure is the reduction of the original quality due to various influences. The most significant factor contributing to the deterioration is the dynamic load. The dynamic load is directly related to the axle load and track geometry. [49] The factor that contribute to the degradation of railway infrastructure are usage (wear by physical contact and dynamic load), environmental conditions (climatic influence and water) and failures (faulty components, bad construction) [49]. And the process of track deterioration is mainly wearing and fatigue then finally settlement [48].

The study of the track structures and their response to applied traffic conditions are easier to study using software models. As the railway industry improves, the modeling of railway track is becoming more realistic and representative of the real conditions. Track modeling is used to predict the performance of railway track components with the application of train movement and environmental conditions. Based on the complexity, railway track modeling techniques can be classified as two dimensional (2D), three dimensional (3D) and two point five dimensional (2.5D). [14] From the very beginning track has been modeled with the concept of Beam on Elastic Foundation (BOEF) which was developed by Winkler's theory or Zimmermann method. These are categorized as two-dimensional analysis of a railway structure and are simplification of a beam (rail) laid on a continuous support (soil's subgrade or foundation). [14] Through time the modeling technique become more realistic to three-dimensional finite element modeling (FEM). [47] For granular materials like ballast and sub-ballast, discrete element modeling (DEM) is better representative. [2]

In this thesis the effect of traffic load parameters on the settlement of ballast material is studied based on the analysis of three-dimensional finite element ballasted track model.

## 1.1. Scope and limitation

In this thesis the effect of vertical load from traffic will be assessed based on three-dimensional finite element modeling of 8.08m track loaded with a moving axel. Drucker Prager plastic model is used to represent the granular behavior of ballast and sub-ballast. Lateral and longitudinal load components of traffic are not taken in to consideration. The effect of vibration and impact load caused by different factors are not included in the analysis. Irregularities in track and wheel are not considered.

## 1.2. Statement of problem

A considerable maintenance work is needed for ballasted tracks due to the track deterioration. Therefore, it is very important to understand the mechanism of track deterioration and to predict the track settlement or track irregularity growth rate in order to reduce track maintenance costs and enable new track structures to be designed. Explanations on how the speed, load and repetition of traffic influence the long-term settlement of ballast in ballasted track is very scarce. Having in mind that tracks subjected to the same load show different settlement behavior, explanations of track settlements in accordance with the speed, load and repetition is needed. This study is motivated to show how traffic affects the long-term settlement of ballast and how the traffic parameters (speed, load and repetition) contributes in the process.

## 1.3. Aims/Objectives

### 1.3.1. General

To assess the effect of traffic load on the settlement of ballast.

### 1.3.2. Specific

- To quantify the contribution of traffic parameters (speed, load and repetition) on the settlement of ballast.
- To assess the long-term effect of traffic on the settlement of ballast

## 1.4. Methodology

### 1.4.1. Plan and procedure

Input parameters for the discrete element modeling software are extracted from typical ballast test result to simulate triaxial compression test using PFC$^{3D}$ software. The simulation includes the following main features:

- Irregular and angular ballast shape
- Ballast breakage
- Confining pressure

Get the plastic behavior of the ballast material from the triaxial test simulation. Using ABAQUS software, three-dimensional conventional ballasted track is modeled and result from the discrete element modeling software is used to represent the Drucker Prager plastic behavior of ballast system. Three-dimensional rail, sleeper and ballast structures are modeled. And cyclic axel load is applied. Four models for each traffic parameters (speed, load and repetition) are analyzed.

Stress strain diagram from FEM simulation is interpreted and used to compare the effects of each parameter on the settlement of ballast material and to predict the behavior of ballast in the long-term.

# CHAPTER 2 LITERATURE REVIEW

## 2.1 Introduction

Ballast is a crushed granular material placed as the top layer of the substructure and between sleepers in a track. Ballast material is the individual particles of crushed stone but ballast system is the whole ballast layer as one material. Ballast is most important material in conventional ballasted track that has significant functions. The most important functions of ballast are to resist vertical, lateral, and longitudinal forces applied to the sleepers and to provide resiliency and energy absorption for the track. Moreover, voids provide drainage of water in the track. However, the voids in the ballast will eventually be filled with fouling material and thus the ballast will need to be cleaned or replaced. [2]

The ballast layer is subjected to both the traffic load and environmental changes. In consequence, the ballast bed deforms and degrades highly affecting the performance of the railway track. Therefore, it is imperative to investigate in detail the deformation behavior and degradation characteristics of 'fresh' ballast for typical loading and drainage conditions specific to railway tracks. Also, it is necessary to identify the factors that highly affect their variation. Better design of ballasted foundation provides higher track performance and ensures reduced maintenance costs. Also, the degradation caused by traffic loading requires proper measure based on detailed specifications in order to effectively plan the ballast-cleaning cycles so the maintenance costs are kept under control. [2]

Studies show that ballast selection criteria depend on the local conditions and the traffic and drainage requirements. Good ballast materials are angular crushed hard stones and rocks, uniformly graded, free of dust and dirt, not prone to cementing action, and that have high specific gravity [6]

## 2.2 Requirements

### 2.2.1 Functions

- To provide level and hard bed for sleepers. and to hold the them in position. [22]
- To transfer and distribute the loads to a wider area. so that, to reduce the excessive settlement in the formation level. [22]

- To provide elasticity and resilience to the track. In doing this it reduces noise and vibration in the track structure due to impact load.
- To provide longitudinal and lateral stability.
- To provide an efficient and effective drainage [22]

### 2.2.2 Requirements

The ballast material and system should fulfill some requirements in order to perform its function appropriately.

- Toughness and able to resist wear which defines the resistance to impact.
- Hardness is another property which defines the abrasive nature of the material. [22]
- Ballast aggregate should be cubical or it should have sharp edges by which all the materials get inter locked so that there will be a cohesive mass and the load transfer capabilities will be there.
- Ballast should be non-porosity and non-water absorbent. [22]
- Resistant to attrition.
- Ballast materials should be durable enough; the durability is in terms of its resistance to the weathering action. [22]
- Ballast cost should be economical and it should not happen that the material is transported from far distance.

## 2.3 Ballast Gradation

The gradation of aggregate mix can be classified as, well graded (dense or broad graded), uniformly graded (open) and gap graded based on the particle size included on the composition.

Even though there is major problem in degradation and permanent deformation, uniformly graded aggregates are used in ballast structure construction for the sake of drainage and resiliency (damping) requirement. When broadly or well graded aggregates used, settlement will be minimized but, there will be drainage problem due to the fine materials.

Naturally obtained and crushed, angular, rock material is good for ballast construction. To achieve on better particle interlocking and to get the required resistance to dynamic loading in the transverse and longitudinal direction, angular stones are the best than rounded shape.

When particles used bigger than the maximum size of the particle, there will be only some particles beneath the tie or sleeper which will distribute the load insufficiently to the subgrade. In the other hand, when too much smaller size particles used than the minimum, the void between the bigger sizes will be filled with these particles exposing the structure for further drainage problem. [2]

Different researches are undergoing on gradation and shape of the particle to reason out their effects on the performance of the ballast structure. But still different countries use different gradation and shape of aggregates without definitely knowing the effects on the performance of the ballast structure.

Research shows that using broadly graded aggregates will resist permanent deformation better than uniformly graded in cyclic loading. It is because; smaller particles will fill the gap between the larger which will improve the package. The total load coming from the super structure is finally resisted by the underlying subgrade structure. So, the gradation of the ballast structure is depending on the subgrade stiffness when recoverable deformation is considered [6]

Specified ballast gradation must have the following two key objectives [74]:

- Ballast must have higher strength to provide increased stability and minimal track deformation. This can be achieved by specifying broadly-graded (well graded) ballast.

- Ballast must have high permeability to provide adequate drainage, hence readily dissipating excess pore water pressures and increasing the effective stress. This can be insured by specifying uniformly graded ballast.

These two objectives are contradictory in terms of required particle size distribution and the optimum ballast gradation needs a balance between the uniform and broad gradation.

## 2.4 Ballast Degradation

Ballast failure is the reduction of the original quality due to various influences. The most significant factor contributing to the deterioration is the dynamic load. The dynamic load is directly related to the axle load and track geometry [49]

Ballast material fails by [22]:

- Crushing: due to overloading and mechanical maintenance (Machine and manual tamping)
- Abrasion: due to tamping and dynamic track movement under traffic
- Attrition: due to exacerbation by the presence of water

The ballast system degrades due to the following factors [5]:

- Creation of fines
- Ingress of fines from above (spillage from trains, wind borne material)
- Ingress of vegetable matter
- Ingress of material from the formation

The following factors may be distinguished that contribute to the degradation of railway infrastructure [49]:

- **Use:** wear by physical contact and dynamic load
- **Environment:** climatic influence, water
- **Failures:** faulty components, bad construction

And the process of track deterioration is [48]:

- **Wear**: due to physical contact between individual particles
- **Fatigue:** due to dynamic load on compacted or rearranged materials
- **Settlement:** due to traffic load on wearied materials. Settlement of track may not always be even. (I.e. differential settlement of track is common failure mechanism of track). This type of track failure usually leads to geometric failure or alteration.

Generally, the track components deterioration is driven by the three forces (these are the static, quasi-static and dynamic forces). These forces can be created due to the factors related to both the vehicle and the track components [48].

Technically ballast failures can be termed as ballast fouling or formation of ballast pocket [2].

- ***Ballast fouling:*** it can be defined as the presence of more fines in the ballast material. As mentioned in [2], even though there are conditions where one of the above conditions dominates for the formation of fines, the most and frequent cause of ballast fouling is from ballast particles breakdown.

- ***Ballast pocket:*** The depression developed beneath the sleeper and forms ballast pocket where it is filled with water. Further accumulation of the water in the ballast pocket causes bearing capacity failure progressive failure observed in the sub-grade due to continuous loading on the track and compression on sub-grade, squeeze out of shoulders. [2]

## 2.5 Ballast maintenance

Maintenance of the ballast layer is an important part of track maintenance. The most common methods of ballast maintenance are discussed below.

### 2.5.1 Tamping

Tamping is the most commonly used method of adjusting track geometry faults, rearranges ballast particles to fill the gaps beneath the ties resulting from differential settlement of ties. In this process the ballast is loosened and damaged; therefore, tamping should be used only where and when necessary. The tamping process also reduces the lateral stability of the track which will be restored gradually by repeated loading from traffic. The wheel load magnitude affects the rate of settlement, the heaviest loads controlling the magnitude of the total settlement. The tamping of ballast can also cause accelerated breakdown of ballast [11].

### 2.5.2 Stone blowing

Stone blowing is a process of track geometry adjustment that involves adding crushed rock to the surface of ballast under the lifted tie to shim the track. This is an alternative method to tamping in which the ballast particles are rearranged to fill the void under the lifted tie. [35]

### 2.5.3 Ballast cleaning

Ballast cleaning and renewal is an expensive and time-consuming process, which is also highly disruptive to train traffic. Thus, the need for this process must be considered carefully. Basically, ballast cleaning and renewal is required when the ballast becomes so fouled that it cannot fulfill its functions [35].

## 2.6 Modeling

### 2.6.1 Railway track modeling

Railway track modeling includes the model of track components and simulation of the real conditions of train-track interaction. As the railway industry improves, the modeling of railway track is becoming more realistic and representative of the real conditions. Track modeling is used to predict the performance of railway track components with the application of train movement and environmental conditions.

Based on the complexity, railway track modeling techniques can be classified as two dimensional (2D), three dimensional (3D) and two point five dimensional (2.5D).

#### *2.6.1.1 Two-dimensional track modeling*

From the very beginning track has been modeled with the concept of Beam on Elastic Foundation (BOEF) which was developed by Winkler's theory or Zimmermann method. These are categorized as two-dimensional analysis of a railway structure and are simplification of a beam (rail) laid on a continuous support (soil's subgrade or foundation). These methods are still applicable for simple track analysis, but for more complex and realistic analysis, it is not suitable because it neglects the effect of the other one dimension, the discrete support provided by sleeper, ballast and sub-ballast material, interaction between support materials (i.e. ballast, sub-ballast, and subgrade materials), and different track supporting layers are not clearly distinguished (i.e. track support is considered as a one-layer component).

The basic concept of Winkler's model is beam (rail) supported on elastic support at a regular interval (sleeper spacing).

Winkler's theory assumptions are:

- Sleepers have no deformation because they are supported from below and from the sides by ballast bed.
- Ballast bed cannot be deformed
- At each point of support the compression stress is proportional to the local compression.
- Supporting sleepers fastened tightly to the rail would resist against rail bending through their rotational stiffness.

Based on Winkler's theory, Zimmermann developed a method to determine the forces and deflections which occur in a single supported track loaded by trains. In this theory rail is assumed to be supported continuously by an elastic support system. The supported areas are transformed by connecting the support areas of adjacent sleepers to come with a theoretical continuously supported rail.

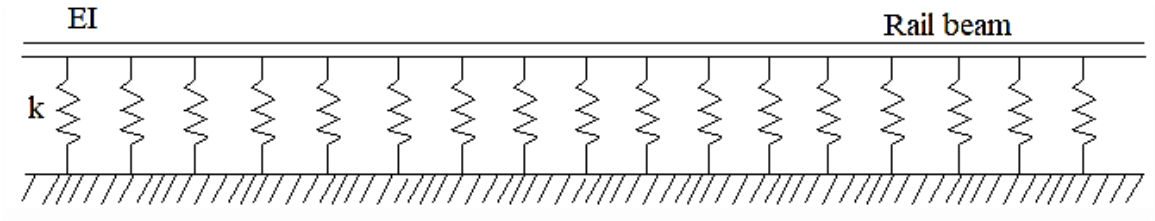


**Figure 2.1: Rail track model supported on elastic foundation**

Using this theory many researchers developed 2D rail track models for analysis of train-track interactions.

As explained in [14], J.J. Kalker (1996) introduced a discretely supported beam model, which is shown in Figure below. In this research, the rail is modeled as a Euler beam and its vertical displacement due to a travelling vertical point load of variable intensity is calculated.

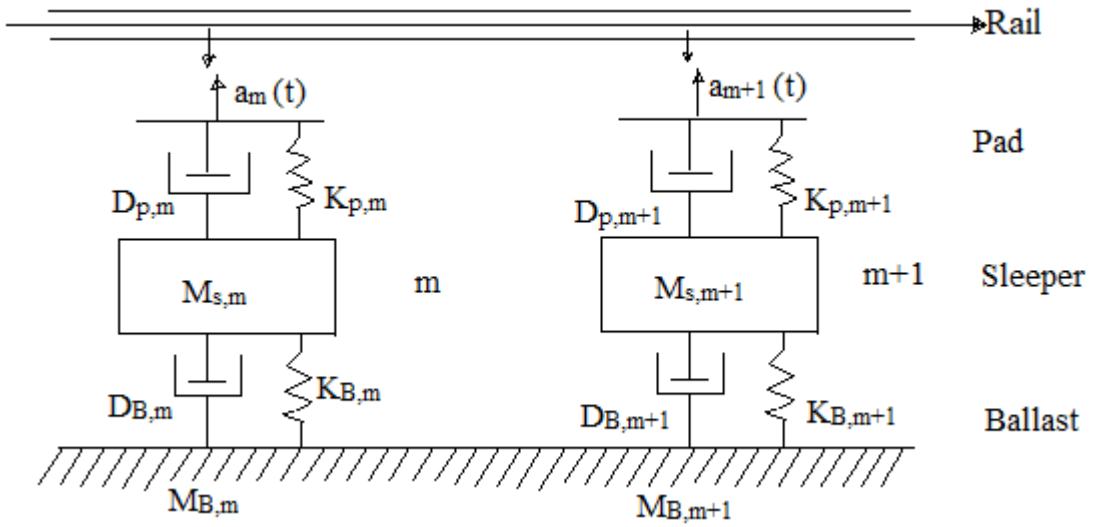


**Figure 2.2: 2D discretely supported rail track model [14]**

And another model is developed by other researcher to include ballast mass as shown in the figure below. In [16] 2D FEM analysis is employed in the long-term analysis of track settlement and influence of different factors. Alves Ribeiro settlement model is used for prediction of long-term behavior of ballast. [47] and [11] also employed the same method to predict settlement of ballast in the long term using Guérin model.

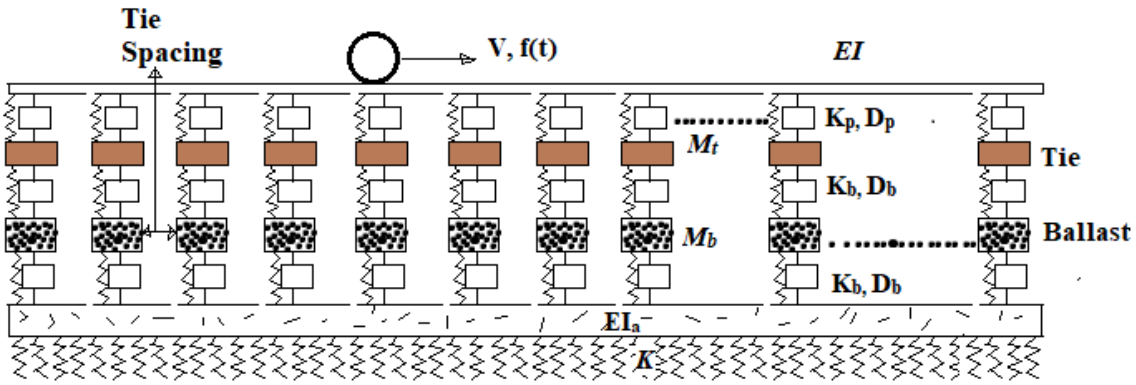


**Figure 2.3: 2D discretely supported railway model including ballast mass [16]**

### *2.6.1.2 Three-dimensional track modeling*

Then a 3D model is introduced with coupling spring/damper elements, representing the mechanism of rail pads, sleepers and ballast bed. The rail can be either modeled as R-T beam or E-B beam to describe the rails which are discretely coupled with sleepers. Another beam element with mass is placed to model the sleepers. The sleeper rests on another spring-damper system. [47]

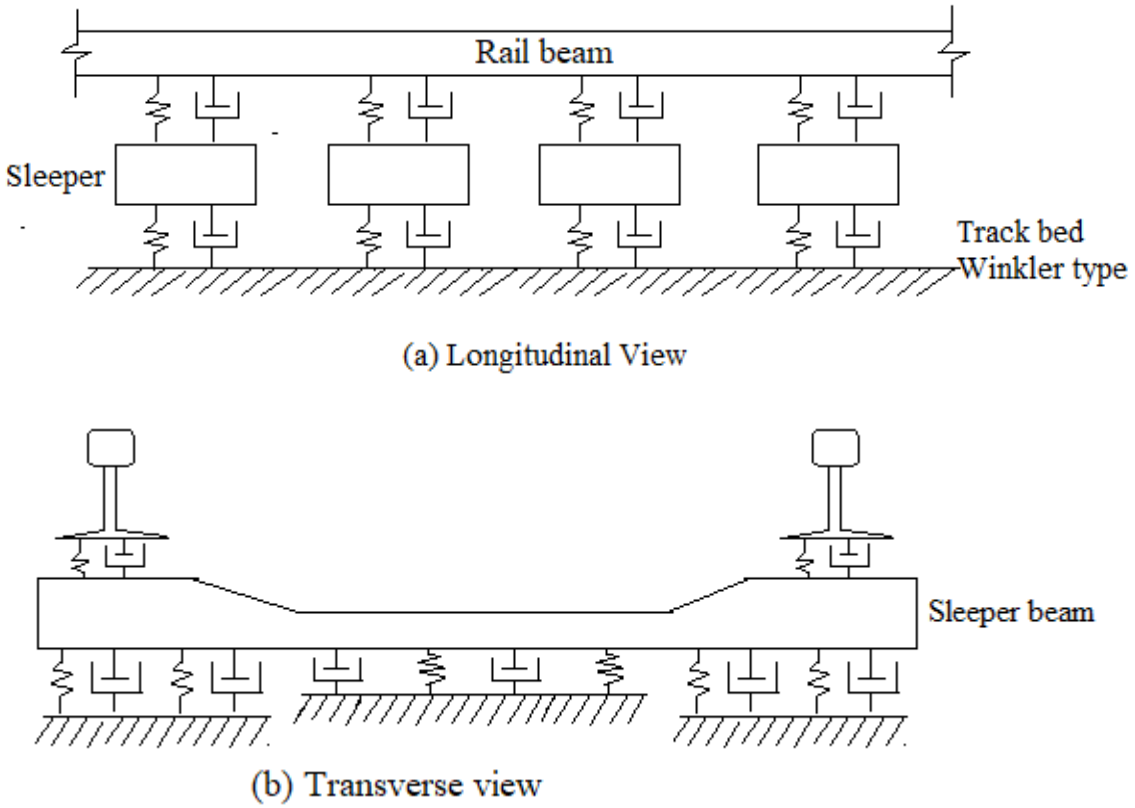


**Figure 2.4: 3D model of rail on discrete support [47]**

This model didn't include the granular behavior of ballast material. Due to this another 3D modeling system is introduced. 3D finite element modeling techniques are most widely

applicable ways of modeling many engineering problems. It is based on the division of the problem domain into a finite number of subdomains (elements). Then, known physical laws are applied to each element, which usually has a very simple geometry. As the result, FEA reduces the problem complexity by solving matrix equations of each element by iteration at specific points, referred to as nodes.

#### *2.6.1.3 2.5D track modeling*

The 3D FEM analysis is time consuming, and realizing this, researchers developed an innovative model called 2.5D FEM assuming the track property remains uniform along the direction of train movement; only a profile of half-space vertical to the direction of load movement is considered. In other words, it is two dimensional elements acting in three directions. [16]

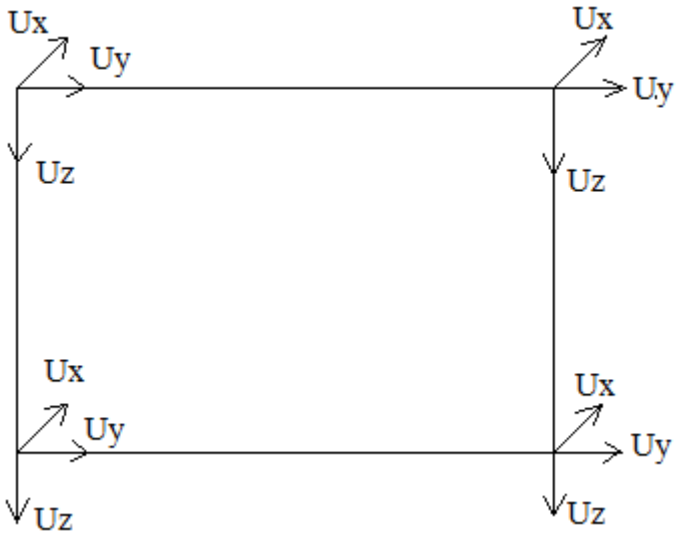


**Figure 2.5: 2.5D element (2D element, 3D motion) [16]**

### 2.6.2 Discrete element modeling (DEM) of Ballast

Simulation of railway ballast structure using the above methods of modeling techniques doesn't include the simulation of the discrete nature of granular material such as individual movement of the particles and physical interaction at contact points. This behavior of ballast material can be represented in discrete element modeling (DEM). In most cases, simple spherical particles are used. But particle shape has a strong influence on resulting behavior of the particle assembly. So, researches developed different representations as mentioned in [14].

DEM as a simulation tool for granular media was introduced by Cundall and Strack (1979) and found wide application and further development in the following decades. Various lab tests have been analyzed using DEM. Direct shear tests for different materials have been modeled [63], [18], [71]. Odometeric compression tests have also been simulated using DEM [18], [70]. Notably, DEM is very suitable and effective to simulate triaxial compression test of granular material [10], [29] [32], [46], [58], [70], [73], [77], [53], [57], [50]. Besides, many special tests for granular materials which could not be modeled using continuum methods have been simulated by DEM, such as the repose test, dumping and compaction tests and rotating drum test.

As mentioned in [2] there are three major operations in DEM techniques:

A. Computation of element contact forces
B. Computation of particle motion and
C. Detection of contacts

There are different parameters to be considered in representing ballast using discrete element method. Some of them are explained based on previous researches below.

#### *2.6.2.1 Shape*

Shape of ballast particles is the main factor which highly influences the behavior of the ballast structure. The easier and non-time-consuming representation of ballast particle is representing them with spherical elements. Concentrating on the other factors like particle size distribution and contact friction, [30] modeled track structure including ballast as circular element using $PSD^{3D}$. [29] simulated triaxial test using clumped and spherical ballast particle shape. The results from the analysis of ballast material modeled as spherical element have much deviation from the laboratory test results. [29]

In many discrete element software, ballast particles shape can be simulated by sphere clumps [26]. It introduced two innovative approaches to capture stone angularity by fitting circular shapes into each stone shapes. These methods are using MATLAB and AutoCAD, and it is found that the MATLAB method yields more realistic results (i.e. the angular and semi rounded shapes present very small permanent deformation). [46] also performed a numerical analysis of railway ballast material using spherical clumps to analyze the field behavior of ballast material mainly lateral resistance test and checked the influence of varies factors (such as friction between ballast stones, friction between ballast and bottom of sleeper, sleeper load influence) on the lateral resistance of track structure.

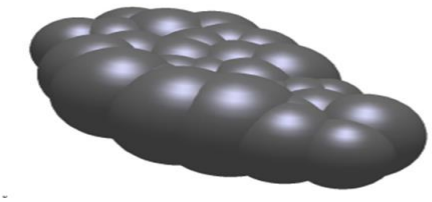

**Figure 2.6: sphere clump representation of ballast particle in DEM [26]**

Researches showed that, ballast particles can be modeled in a better way to get a more precise result to the reality. [33] modeled a promising ballast particle shape using Image aided discrete element modeling approach. In which it created a three-dimensional real shape of ballast particles using three views (top, front and side) processed in university of Illinois aggregate image analyzer. In this thesis, the behavior of fouled ballast material is evaluated by track settlement. Calibration and validation of the model is performed by comparing direct shear test results in the model and laboratory. And it is found that the settlement of track is most of contributed by shoulder settlement due to fouling. [23] used the same method for evaluation of ballast settlement applying different shapes, angularity, and surface roughness. The same method of shaping ballast particle is used in [24] the simulation of field validated ballast settlement behavior, employing various shape, gradation and compaction conditions.

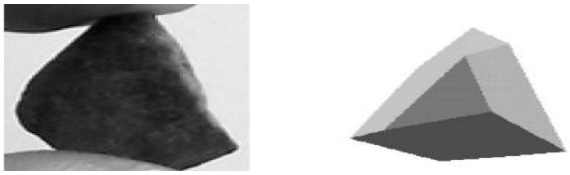

**Figure 2.7: Comparisons of an actual aggregate particle with the discrete element representation generated [33]**

[43] Presented convex polyhedrons generated pseudo-randomly via Voronoi tessellation. And applied this in the simulation of a large odometric test to evaluate ballast settlement due to cyclic load and compared with an experimental data from literature.

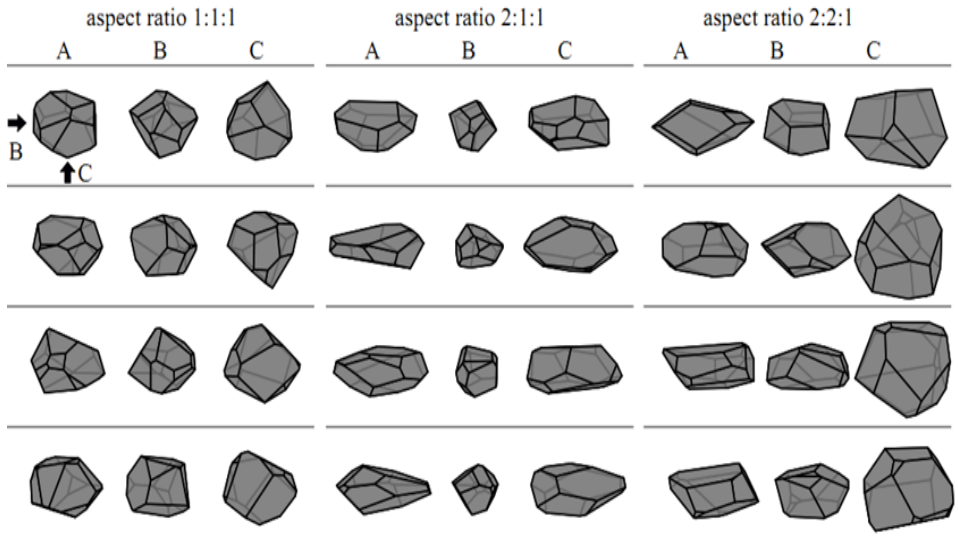


**Figure 2.8: Randomly shaped grains generated via Voronoi tessellation. Three variants differ by pre-scribing different scaling factors along x, y and z axes. Each polyhedral grain is showed in front (A), side (B) and bottom (C) view [43]**

#### *2.6.2.2 Contact*

In DEM two elements are in contact if the distance between the centers of two adjacent elements is equal to or less than the summation of their radii. The contact behavior is described using up to three models: slip (The slip model allows slipping to occur between discrete elements by limiting the shear force. The input parameter for this model is the friction coefficient (μ)), stiffness (The stiffness model relates the contact forces and relative displacement in the normal and shear directions (normal and shear stiffness)), and bonding (While the bonding model is a strength parameter above which a bond breaks). Loop detection of contact between ballast particles applying separating plane detection is employed in different researches. [27]

#### *2.6.2.3 Crushing or breakage*

Simulating crushing or breakage of ballast particles due to cyclic load is significant in modeling the ballast characteristics. This can be done by modeling ballast particles with sphere clumps and allow breaking of bonds between the spheres in the clumps during loads greater than the bond strength. Replacing initially modeled particles with smaller particles of equivalent property is another method to simulate ballast crushing as employed in [64].

### 2.6.3 Reliability of simulation of triaxial test using discrete element modeling

As it has been discussed on previous sections triaxial test is simulated using different DEM software in many former studies. [10], [29], [32], [46], [58], [70], [73], [77], [53], [57], [50]. Some of them also compared the result of this simulation with actual laboratory test results. The deviation of test simulation results from the laboratory test results in the stress-strain curve and volumetric strain-axial strain of some researches are calculated and the average percentage of error is calculated.

#### *2.6.3.1 Percentage error of result on stress-strain diagram*

- [10] simulated triaxial test for crushable sand particles, and compared it with experiment. As it is mentioned on the thesis deviator stress and the corresponding volumetric strain are over estimated in the DEM simulations by factors of about 1·2–1·4. This is about 5-6% error.

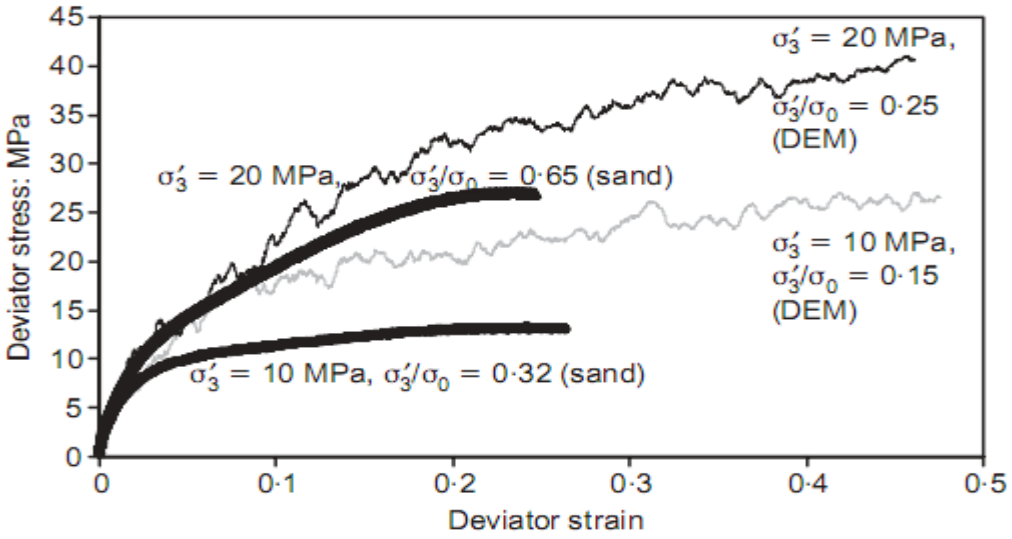


**Figure 2.9: stress-strain diagram of DEM simulation and Experiment**

- In [77] the DEM simulation of triaxial test of coarse graded soil material is compared with the laboratory test. Here the results from the simulation embody to the laboratory test especially at lower and medium confining pressures, making the error about 1-2%.

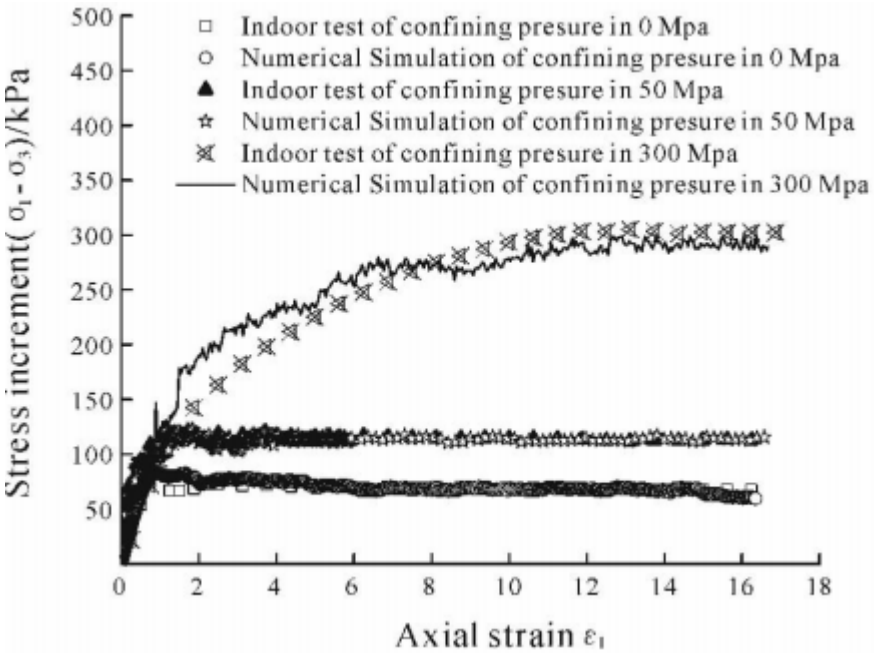


**Figure 2.10: Deviatoric stress vs. axial strain diagram of DEM simulation and laboratory triaxial test**

- [73] used PFC$^{3D}$ to simulate the triaxial test of sand material applying clumped particles. The results from this simulation is has an error of about 0.46 to 5%.

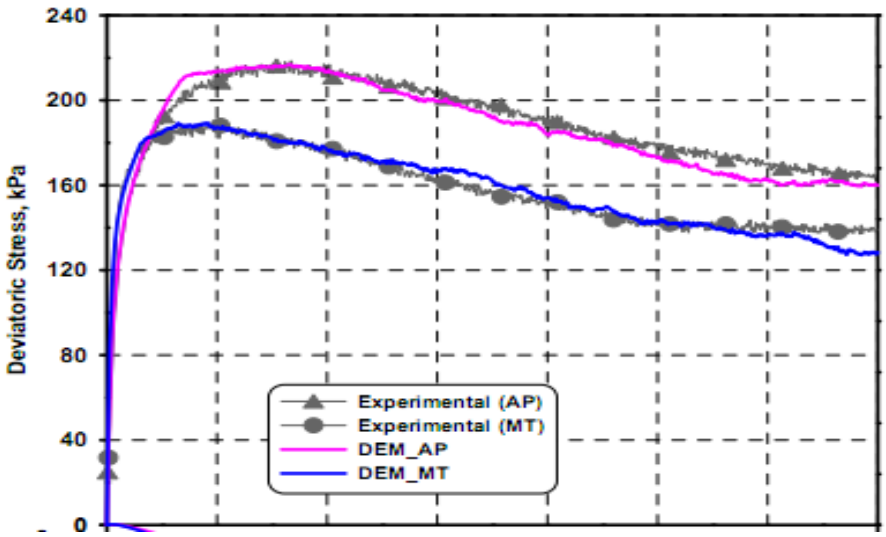


**Figure 2.11: deviatoric stress vs. axial strain diagram of DEM simulation and laboratory triaxial test**

Based on the above analysis the use of PFC$^{3D}$ software simulation of triaxial test of course grained material will give very precise stress-strain diagram to the experiment.

### *2.6.3.2 Percentage error on volumetric strain-axial strain curve*

- Clumps of PFC are used by [57] to investigate the behavior of fouled ballast material. The triaxial simulation at 3 different confining pressure resulted precise results of volumetric strain vs. axial strain curve, with an error of about 1-5%.

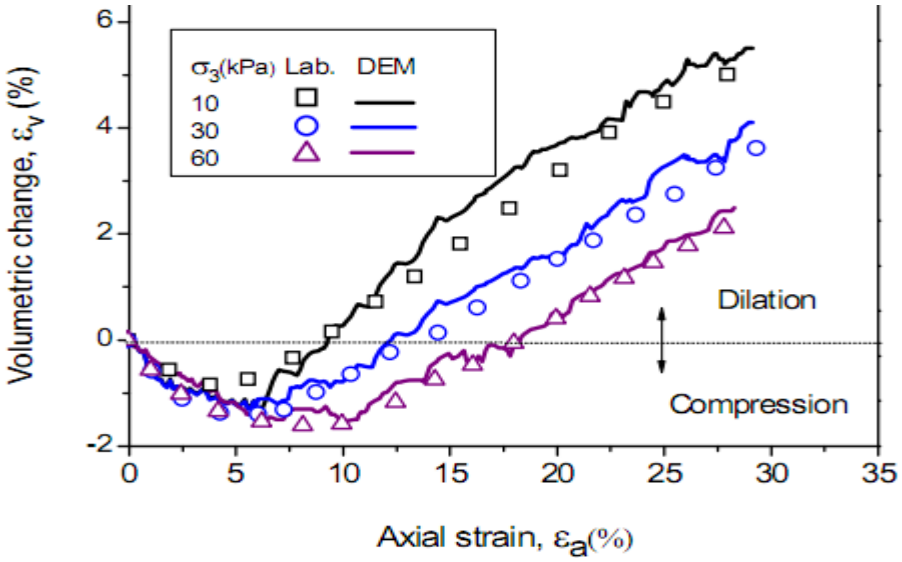


**Figure 2.12: volumetric strain vs. axial strain curve of DEM simulation and experiment of triaxial test.**

- The volumetric strain vs. axial strain curve from DEM simulation of [10] also embodied with the experimental data with an average error about 1 to 10%.

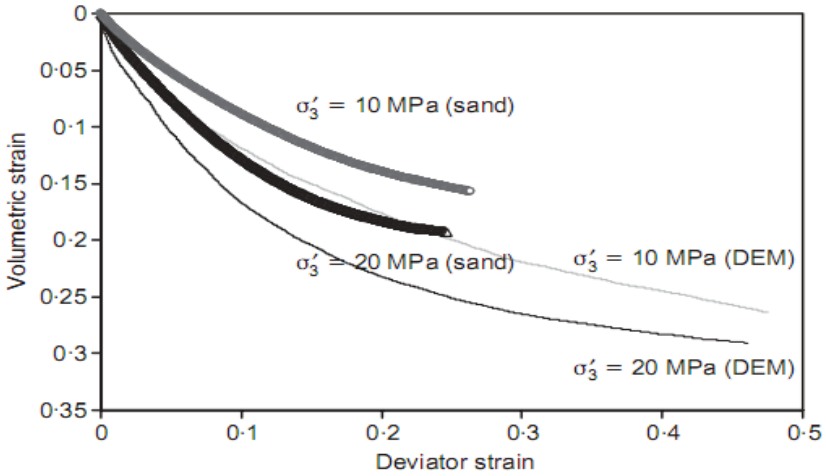


**Figure 2.13: Volumetric strain vs. deviator strain of DEM simulation and experiment**

So, in this paper it is chosen to simulate triaxial compression test to get the plastic behavior of ballast material for finite element modeling of ballasted track. Particle flow code

($PFC^{3D}$) software is used. An over view of the software and the parameters and considerations in the software are discussed in the following sections.

### 2.6.4 Overview of PFC discrete element software

PFC (Particle Flow Code) discrete element modeling software is developed by the ITASCA Consulting Group For commercial use and widely used for many research projects since its first distribution in 1995. The latest version of the software during the time of study is PFC version 5.0. Particles mechanical behavior can be modeled in PFC both in two dimensional ($PFC^{2D}$) and in three dimensional ($PFC^{3D}$) particles. Installation of the software needs paid license but, ITASCA also provides a free demonstration version for limited usage. In this paper demonstration version of the software is used since, the limitations don't highly affect the simulation.

Programming language called Fish is mainly used for generation of particles and application of functions in PFC. It also works with python programming language.

The assumptions made in $PFC^{3D}$ are:

1) The particles are treated as rigid bodies.
2) The contacts occur over a vanishingly small area (i.e. at a point)
3) A soft-contact approach is used in the contacts so that the rigid particles are allowed to overlap one another at the contact points.
4) The magnitude of the overlap is related to the contact force via the force-displacement law.
5) Bonds can exist at contacts between particles.
6) All particles are spherical; however, the clump logic supports the creation of super-particles of arbitrary shape. Each clump consists of a set of overlapping spheres, and acts as a rigid body with a deformable boundary.

In $PFC^{3D}$, the ball and the wall are the two basic entities. Walls allow one to apply velocity boundary conditions to assemblies of balls for purposes of compaction and confinement. The balls and walls interact with one another via the forces that arise at contacts. $PFC^{3D}$ is suitable for modeling the stress-strain response of a granular material, which deformation results primarily from the sliding and rotation of the rigid particles and the interlocking at particle interfaces. More complex behavior of granular materials can be

modeled by allowing the particles to be bonded together at their contact points, so that internal forces (i.e. tensile, shear or moment) are allowed to develop at the contacts. Some basic conceptual models and the mathematical background of PFC$^{3D}$ are presented in the following subsections.

### *2.6.4.1 Computation cycle*

The computation cycle in PFC$^{3D}$ is a time stepping algorithm that requires the repeated application of the law of motion to each particle, a force-displacement law to each contact, and constant updating of wall positions. At the start of each time step, the contacts are updated from the particle and wall positions. The force-displacement law is then applied to each contact to update the contact forces based on the relative motion between the two contacted entities and the contact constitutive model. Then, the law of motion is applied to each particle to update its velocity and position based on the resultant force and moment arising from the contact forces and anybody forces acting on the ball. Also, the wall positions are updated based on the specified wall velocities. [40]

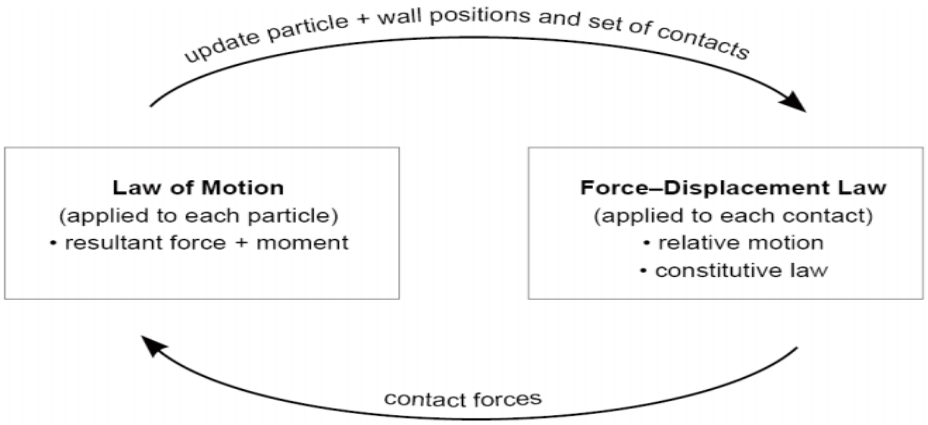


**Figure 2.14: Computation cycle used in PFC$^{3D}$ [40]**

### *2.6.4.2 PFC Model*

The PFC programs (PFC$^{2D}$ and PFC$^{3D}$) provide a general purpose, distinct-element modeling framework that includes a computational engine and a graphical user interface. The PFC model simulates the movement and interaction of many finite-sized particles. The particles are rigid bodies with finite mass that move independently of one another and can both translate and rotate.

The PFC model simulates the movement of particles and their mechanical interaction at pair-wise contacts. We denote each particle as a body to clarify that it is not a point mass,

but instead, is a rigid body with finite mass and a well-defined surface. The PFC model consists of bodies and contacts. There are three types of bodies: balls, clumps and walls. Bodies have surface properties that are assigned to the pieces on the body surface. A ball consists of one piece, which is the ball itself, while the pieces of a clump and wall are called pebbles and facets, respectively. A ball is a rigid unit-thickness disk in 2D or sphere in 3D. A clump is a collection of pebbles that are rigid unit-thickness disks in 2D or spheres in 3D. The 2D model consists of unit-thickness disks *(see*

Figure 2.15*).* Clumps model arbitrarily shaped rigid bodies. The pebbles comprising a clump can overlap but contacts do not exist between them; instead, contacts form between the pebbles on the boundary of a clump and other bodies. A wall is a collection of facets that are linear segments in 2D or triangles in 3D and that form a manifold and orientable surface.

Contacts are created and deleted based on body proximity by the contact-detection logic. A contact provides an interface between two pieces. The interface consists of a contact plane with location ($x_c$), normal direction ($\hat{n}_c$) and coordinate system (nst). The internal force and moment are updated by the particle- interaction law, which takes the relative motion and surface properties of the two pieces as input. Particle-interaction law is referred as a contact model. [38]

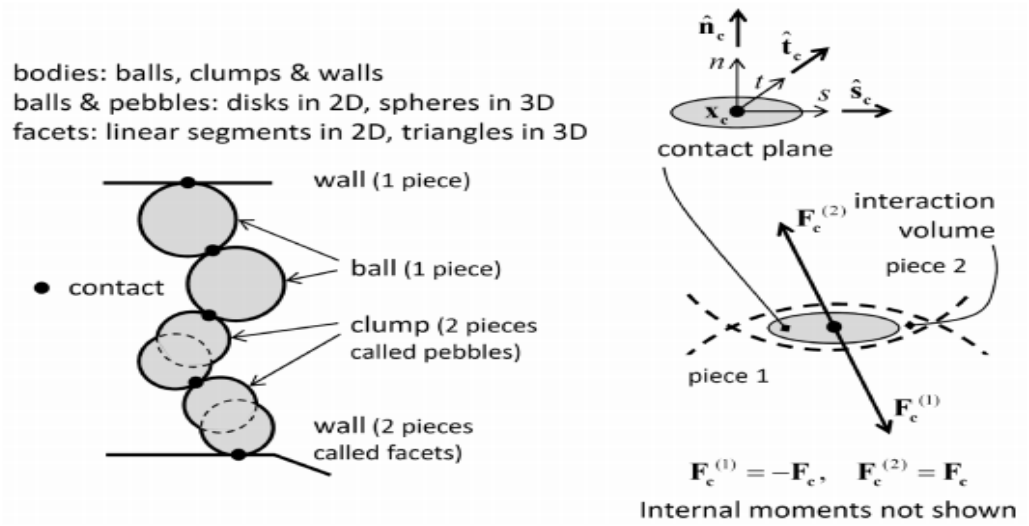


**Figure 2.15: PFC model showing bodies and contacts (left) and contact plane with internal force (right) [38]**

#### *2.6.4.3 PFC Materials and Interface*

A PFC material consists of rigid grains that interact at contacts. The grains of the PFC material can be either balls or clumps drawn from a general grain-size distribution. It is the type of contact model at the grain-grain contacts that defines the material as being linear, contact-bonded, parallel-bonded or flat-jointed. The linear material is a granular material, and the other materials are bonded materials. A user- defined material can also be created. These materials have common properties (which are described by common parameters) and their own particular properties (which depend on the contact models).

##### 2.6.4.3.1 Linear materials

A linear material is a granular assembly in which the linear contact model exists at all grain-grain contacts at the end of the material-finalization phase.

The linear model provides the behavior of an infinitesimal interface that does not resist relative rotation so that the contact moment equals zero ($M_c$=0). The contact force is resolved into linear and dashpot components ($F_c$= $F^l$ + $F^d$). The linear component provides linear elastic (no-tension), frictional behavior, while the dashpot component provides viscous behavior. The linear force is produced by linear springs with constant normal and shear stiffnesses, $K_n$ and $K_s$. The linear springs cannot sustain tension and slip is accommodated by imposing a Coulomb limit on the shear force using the friction coefficient, μ. The dashpot force is produced by dashpots with viscosity given in terms of the normal and shear critical-damping ratios, $\beta_n$ and $\beta_s$. The linear springs act in parallel with the dashpots. [38]

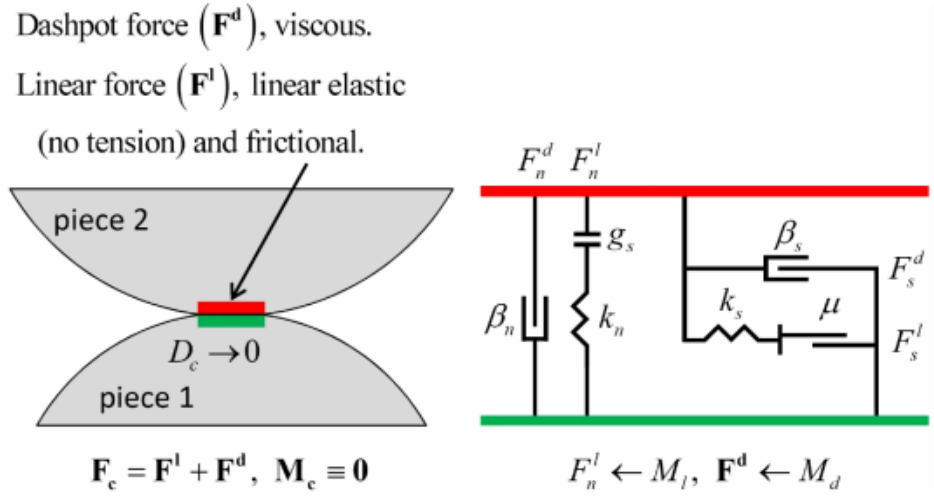


**Figure 2.16: Behavior and rheological components of the linear model [38]**

#### 2.6.4.3.2 Bonded Materials

Bonded materials are analogous to intact rock, which can be viewed as an aggregate of crystals and amorphous particles joined by varying amounts of cementing materials. Three categories of bonded materials are discussed below.

##### *2.6.4.3.2.1 Contact-Bonded Material*

A contact bond can be envisaged as a pair of elastic springs with constant normal and shear stiffnesses acting at the contact point. These two springs have specified shear and tensile normal strengths. The contact bond breaks when the contact force exceeds either the normal contact bond strength or the shear contact bond strength. [38]

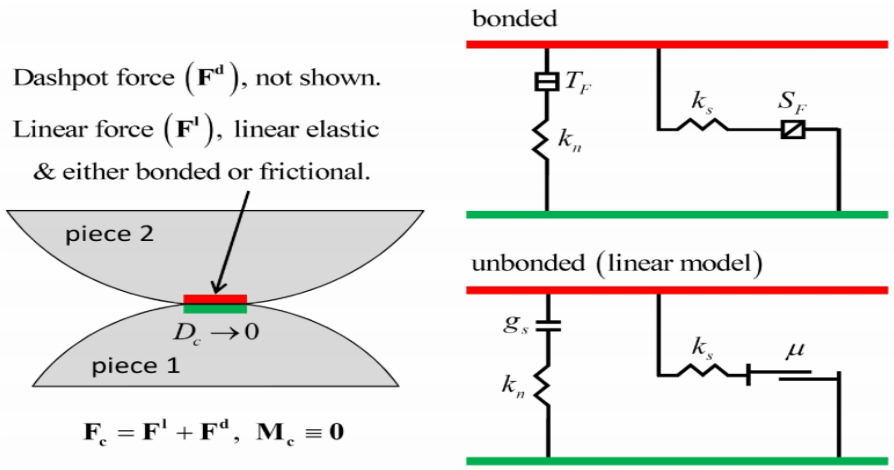

**Figure 2.17: Behavior and rheological components of the linear contact bond model with inactive dashpots [38]**

### *2.6.4.3.2.2 Parallel-Bonded Material*

A parallel bond can be envisaged as column of elastic glue lying on the contact plane. The parallel bond can transmit both forces and moments between particles. The constitutive behavior of the parallel bond is similar to that of the contact bond. Relative motion at the contact causes a force and a moment to develop within the parallel bond as a result of the stiffness of the parallel bond. The parallel bond breaks when the stress in any part of the bond exceeds the parallel bond strength. [38]

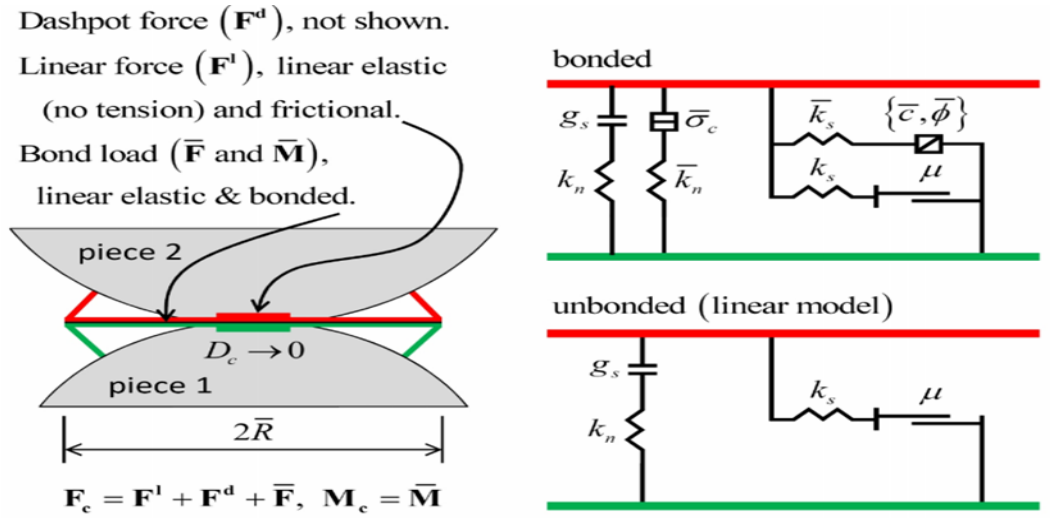


**Figure 2.18: Behavior and rheological components of the linear parallel bond model with inactive dashpots [38]**

### *2.6.4.3.2.3 Flat-Jointed Material*

A flat-jointed material is a granular assembly in which the flat-joint contact model exists at all grain-grain contacts with a gap less than or equal to the installation gap at the end of the material finalization phase; all other grain-grain contacts as well as new grain-grain contacts that may form during subsequent motion are assigned the linear contact model. [38]

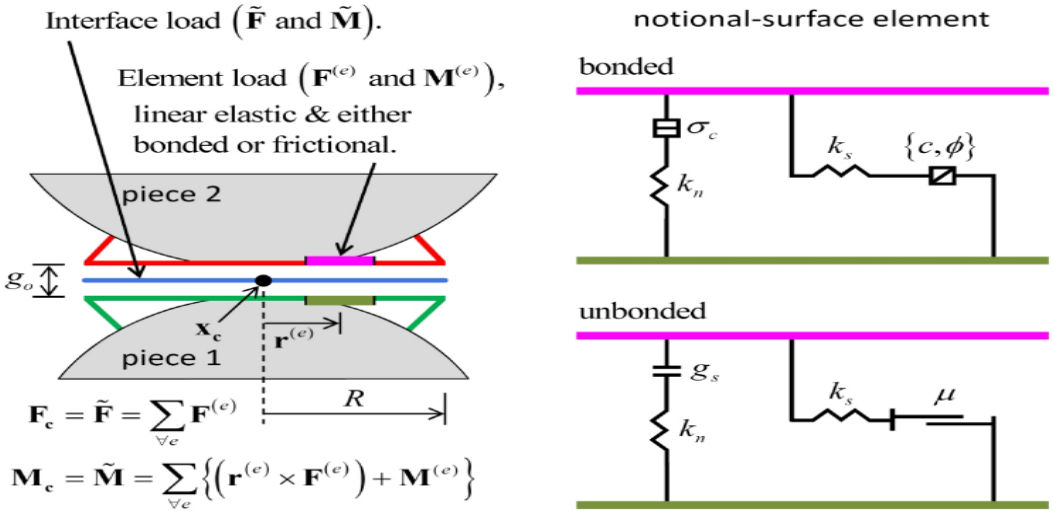


**Figure 2.19: Behavior and rheological components of the flat-joint model [38]**

### *2.6.4.4 PFC Particle Shapes*

Particles in PFC are modeled as rigid circular ($PFC^{2D}$) or spherical ($PFC^{3D}$) elements. But representing angular granular materials like ballast using spherical (3D) or circular (2D) will yield results which more deviate from the experimental results since, the particle shape and angularity have significant influence on the micro and macro mechanical behavior of ballast system. Although there are no yet developed ways of representing the exact shape and angularity of ballast particles in PFC, there are two innovative techniques to model particles of ballast material shape and angularity to some extent. These methods yielded very encouraging results when compared to experimental results as investigated by different researchers. These two techniques are well discussed in the following sections.

#### 2.6.4.4.1 Clumps

The clump logic offers a method of arranging two or more particles to form one rigid super particle, called clump. The particles comprising a clump remain at a fixed distance to each other. Particles within a clump can overlap to any extent and contact forces are not generated between these particles. Clumped particles cannot break apart regardless of the forces acting upon them. [71]

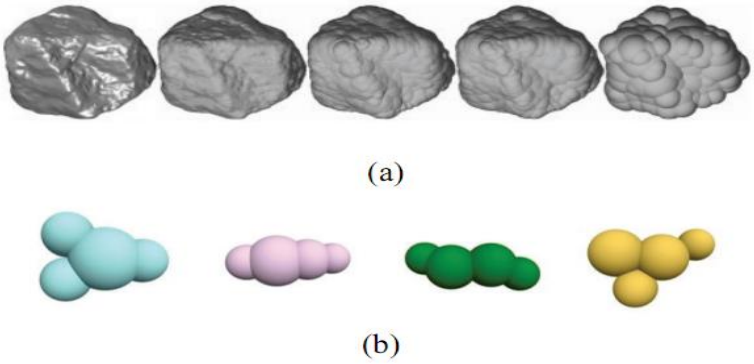


**Figure 2.20: Examples for clumps created by overlapping spheres: (a) Real ballast particle (left) and models with decreasing number of spheres (b) simple clumps with small number of spheres [71]**

#### 2.6.4.4.2 Clusters

A cluster consists of several particles bonded together, so that a deformable super particle with deformable contacts is formed. Clusters can experience disintegration, if bonds break. If contact forces at a specific contact exceed the corresponding bond strength the bond breaks. [56] Clusters and clumps differ significantly:

- ✓ Clusters can crush, clumps not
- ✓ Clusters are deformable, clumps not
- ✓ Particles inside a cluster can rotate while particles in a clump cannot
- ✓ Clusters are more computationally intensive than clumps

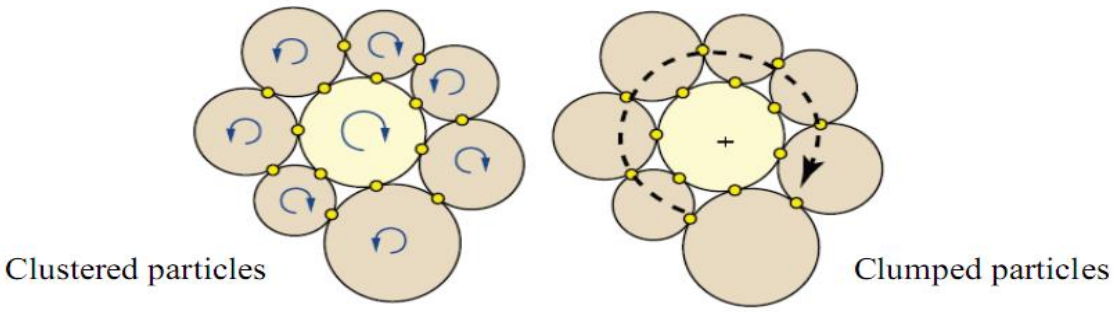


**Figure 2.21: Particle rotation mechanisms in clustered and clumped particles [56]**

# CHAPTER 3 MODELING AND ANALYSIS

## 3.1 Discrete Element Modeling (DEM) of monotonic triaxial test

Experiments are the direct approach to investigate the mechanical behavior of material. Numerical methods can support or partially replace these studies to save costs of experiments and to get deeper insight into the micro-mechanics. In some cases, numerical simulations are the only approach, because it is impossible to perform corresponding experiments.

### 3.1.1 Simulation of triaxial compression test

Due to the need for plastic behavior of ballast material, for the study of the effect of traffic parameters on the settlement of ballast, triaxial compression test is chosen. This test is a promising way of evaluating the compression strength of a sample due to axial stress. Axial and radial strains may be monitored during this test, to determine basic elastic constants (Young's Modulus, E, and Poisson's ratio, ν). Since it is more representative way to simulate the actual field stress conditions, many researchers used the simulation of triaxial test to assess the behavior of ballast system. In this study, triaxial test is simulated to calculate the Drucker Prager parameters to be fed for the FEM analysis of the effect of traffic on the settlement of ballasted track.

#### 3.1.1.1 Ballast particle representation

As mentioned on the sections above, the best way to simulate ballast material is to model particles as clusters of bonded spherical elements called balls to achieve both particle shape and breakability. In this paper, the parallel bonded clusters of spheres are created to simulate three types of ballast particle shapes as shown on the figure below. This is achieved by generating clump templates of the three particle shapes and changing the pebble-pebble contact logic of clumps to parallel bonded pebbles to include breakage in addition to the shape and angularity of ballast particles.

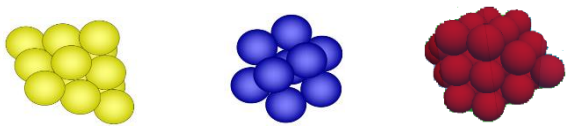

**Figure 3.1: Particle shape used to represent ballast particles in the triaxial test simulation**

***Gradation:*** The clumps representing the particles of ballast material are generated based of the gradation test result collected from the contractor. Every size of the particles is included in the test specimen with percent passing data. Gradation curve of the particle is shown below.

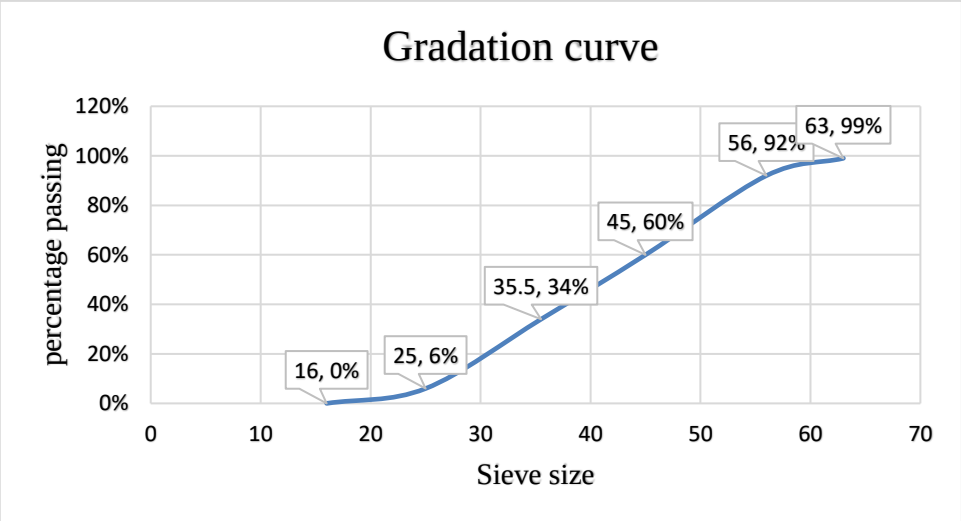


**Figure 3.2: Particle size distribution of ballast material used for the test**

***Particle breakage:*** The particle breakage in PFC can be simulated by modeling particles as cluster of bonded spherical elements and breakage will be assumed to occur when the bond strength between the elements exceeded by the internal forces due to applied load. [65], [66], [67]. In this thesis, the contact model between clumped elements (called pebbles) is changed to parallel bond. With strength parameters mentioned below:

- ✓ Parallel bond normal and shear stiffness ($k_n$ and $k_s$) = 6 x $10^{10}$ N/m
- ✓ Parallel bond normal and shear strength = 5x$10^6$ N/$m^2$

### 3.1.1.2 Test of sample generated

The sample of the particles are inserted in a cylindrical shaped vessel and compressed to achieve a density of 1800kg/$m^3$. The test apparatus includes cylindrical vessel and two top and bottom horizontal plates. Particle compaction and axial and confining pressure are applied by the movement of the plates and the cylindrical vessel. The geometry of cylindrical vessel composed of 20 triangular segments called facets. The top and bottom plates of the apparatus composed of 8 segments. The test is performed under seven different confining pressures (30, 40, 80, 150, 200, 500, 1000kPa). For more detail, the PFC code with explanation for this simulation is shown on APPENDIX A.1.

The size of the apparatus is set to 300x150 mm based on the H to D ratio of 2 (standard of triaxial compression test) and different researches. The test apparatus and the particles assembly are shown in the figure below.

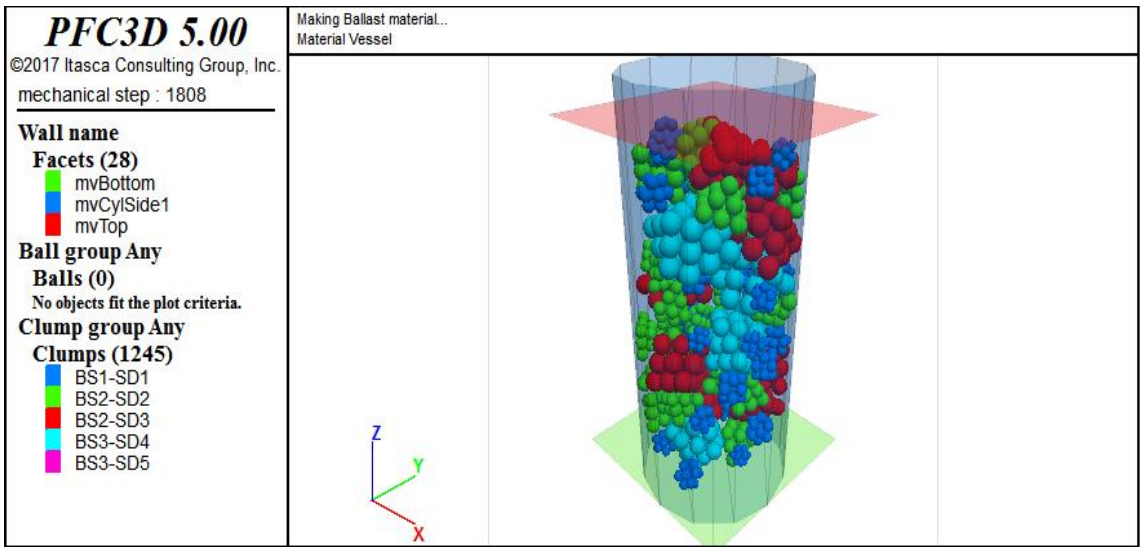


**Figure 3.3: The triaxial compression test simulation using PFC 3D**

#### *3.1.1.3 Test result*

Results of the triaxial compression test simulation under 40Kpa confining pressure are shown below. The triaxial compression test results under the remaining six confining pressures are shown on APPENDIX A.2.

*Deviatoric stress vs. Axial strain:* the graph on *Figure 3.4* shows the relation of deviatoric stress and axial strain due to the loading and unloading of a triaxial test under a confining pressure equal to 40Kpa. As the confining pressure increases, the loading and unloading path of the stress – strain curve becomes closer, that means the material's permanent or plastic strain decreases. These relations for different confining pressure are used to plot p-t graph in Drucker Prager plastic model and then to calculate the friction angle (β) of the ballast material.

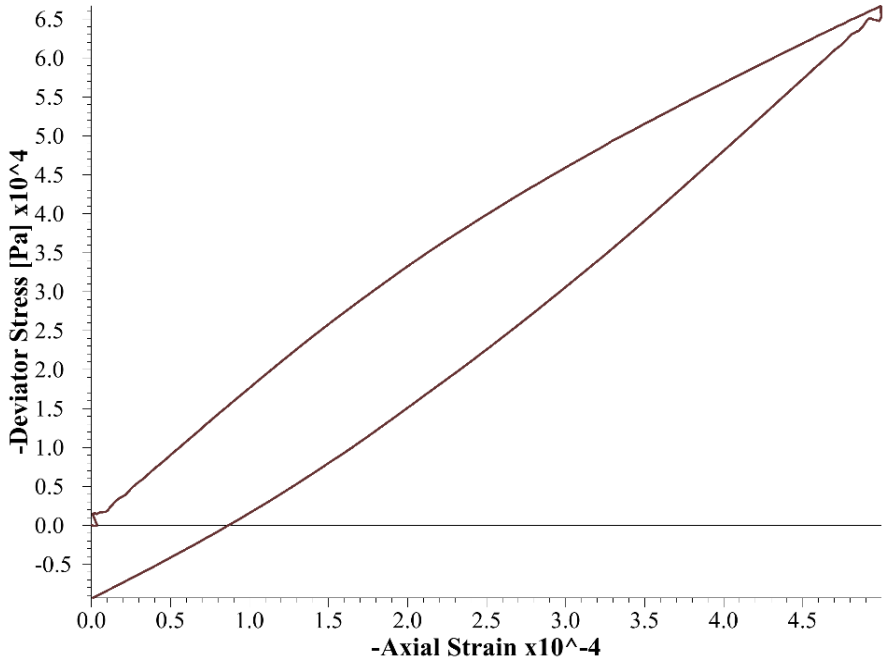


**Figure 3.4: Deviatoric stress vs. axial strain plot from PFC [3D] simulation (40kpa confinement)**

*Axial strain vs. Porosity:* generally the relation between porosity and axial strain is inverse. That is as the compation strain in a material increases the voids in the material decrease that means the material becomes less poros. But, as *Figure 3.5* shows the relation is not smooth, this is because of particle rearrangment in course granular materials.

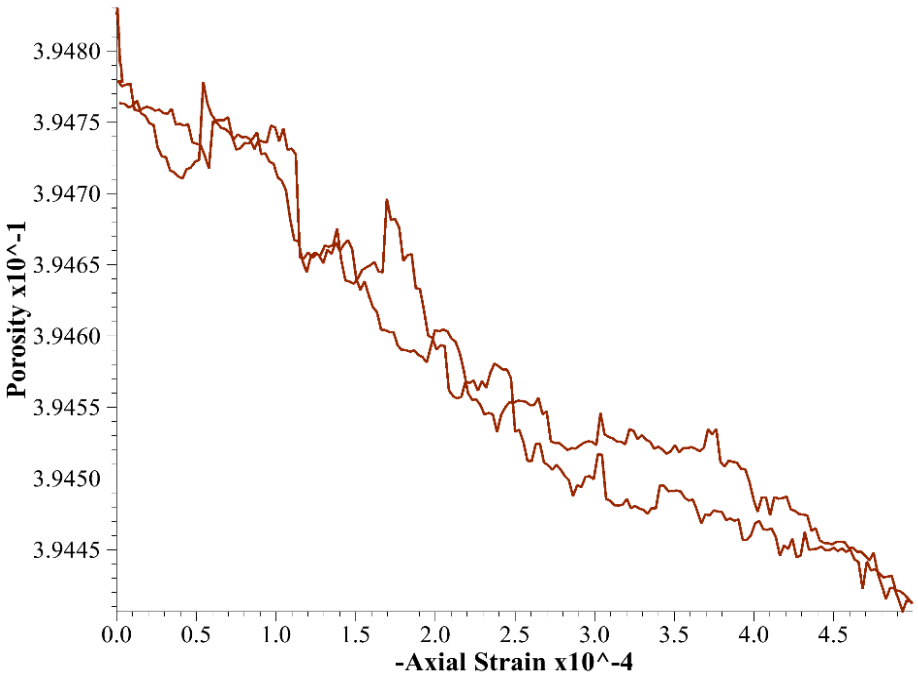


**Figure 3.5: Porosity Vs. Axial Strain plot from PFC [3D] simulation (40kpa confinement)**

*Radial strain vs axial strain:* the radial strain is transversal strain which is perpendicular to the load application. The relation of the radial strain and axial strain is more of direct under high confining pressure.

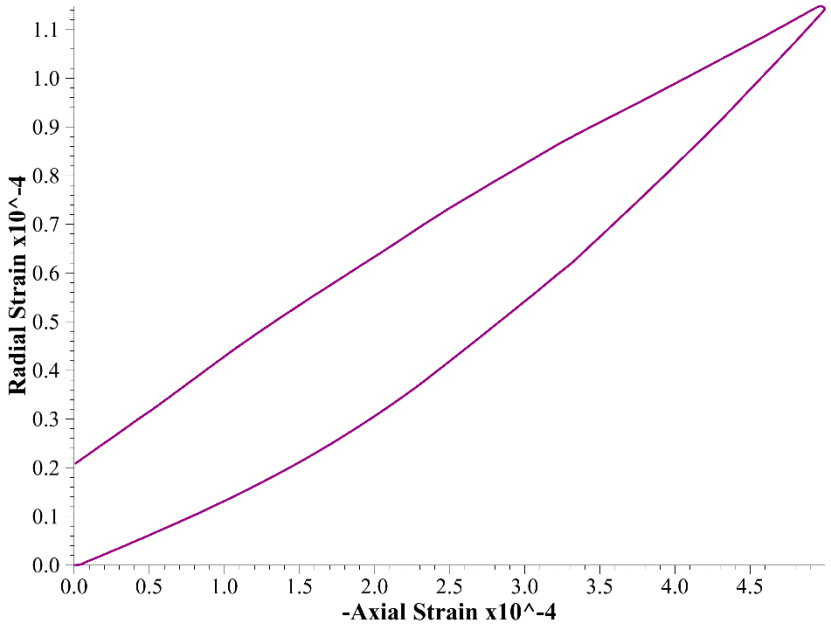


**Figure 3.6: Radial Strain vs. Axial Strain plot from PFC$^{3D}$ simulation (40kpa confinement)**

*Volumetric strain vs Axial strain:* as a compaction stress is applied to a material the volume of the material decreases. That is why the relationship of volumetric strain vs axial strain is inverse. This relation is used to calculate the dilation (ψ) angle in Drucker prager plastic model of ballast material.

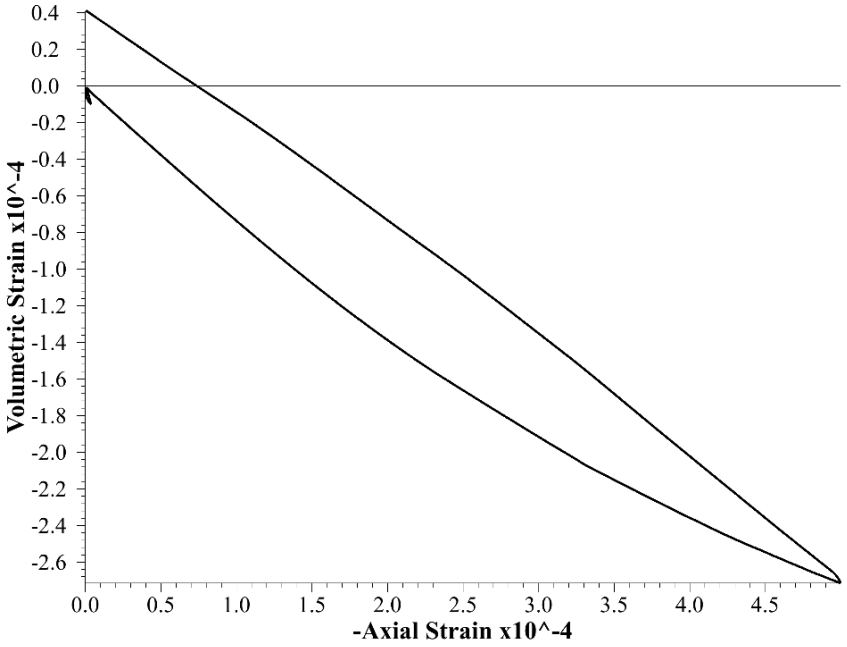


**Figure 3.7: Volumetric Strain vs. Axial Strain plot from PFC$^{3D}$ simulation (40kpa confinement)**

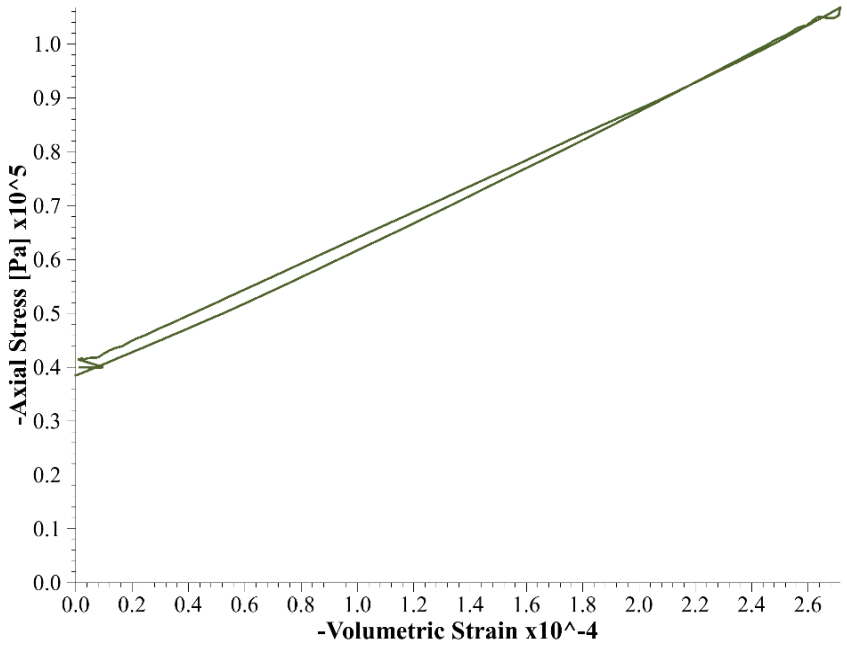


**Figure 3.8: Axial Stress vs. Volumetric Strain plot from PFC$^{3D}$ simulation (40kpa confinement)**

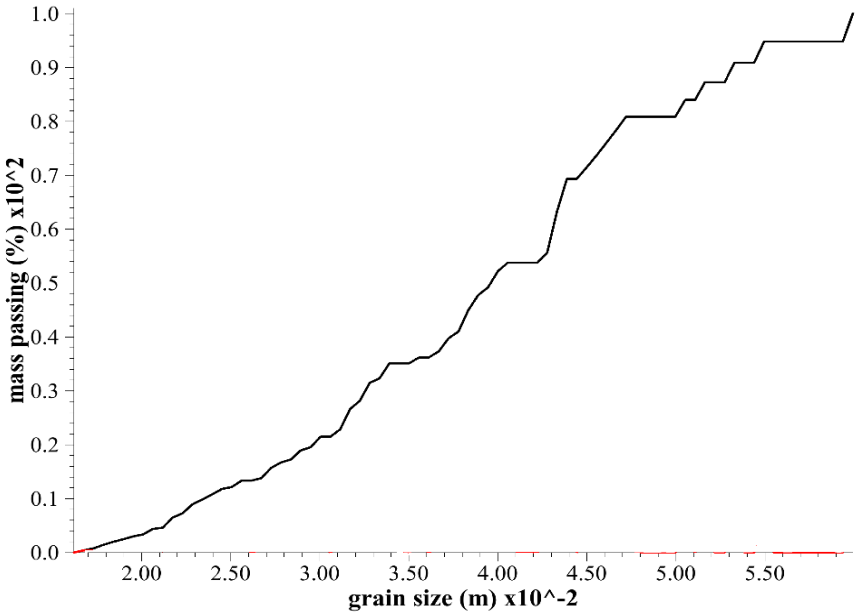


**Figure 3.9: Grain size distribution curve from PFC3D simulation**

The results above will be used as a triaxial test results and will be used to calculate the input parameters of ABAQUS finite element modeling of the ballast material employed in Ethio-Djibouti railway line. An introduction of Drucker-Prager FEM of ballast material and the simulation of the assessment are included in the following section.

### 3.1.2 Reliability of the virtual triaxial test

As it has been discussed on section 2.6.3 triaxial test is simulated using different DEM software (including PFC) in many former studies. The results from these simulations has small errors as compared with the experiment results. In the *Figure 3.10*, the picture on the right is the relation of sieve size and percentage pass of actual laboratory sieve analysis test of typical ballast material. The one on the left is the output of PFC$^{3D}$ simulation. As it is seen from both diagrams the particle size and corresponding passing percentage is well modeled.

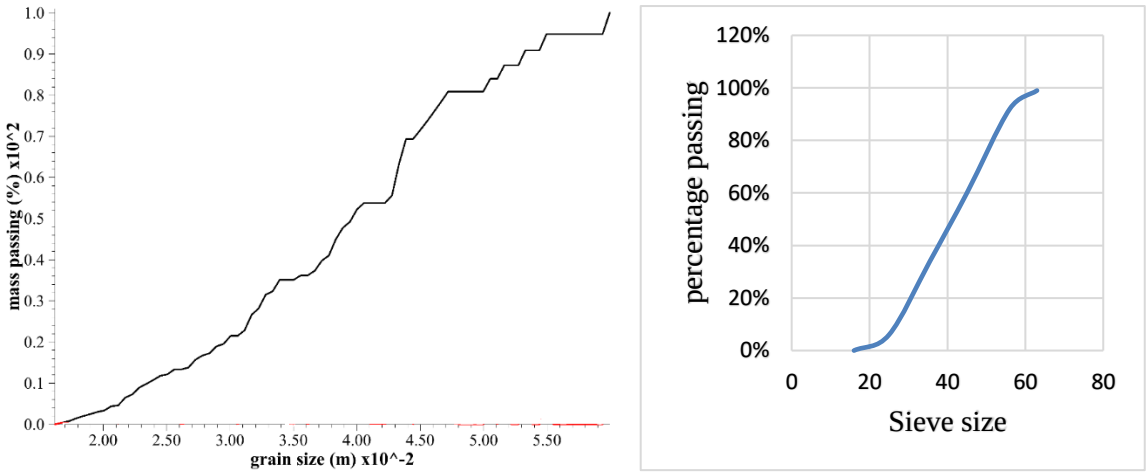


**Figure 3.10 comparison of input gradation curve and PFC output gradation curve**

## 3.2 Finite Element modeling of ballasted railway track

The deformation behavior of ballast materials is very complex. And the precise representation of these behaviors using software simulation is difficult. However, under essentially monotonic loading conditions rather simple constitutive models provide useful information. These constitutive models are essentially pressure-dependent plasticity models that have historically been popular in the geotechnical engineering field.

The model used in this thesis (The Extended Drucker-Prager model) is extension of the original Drucker-Prager model (Drucker and Prager, 1952). In the context of geotechnical materials, the extensions of interest include the use of curved yield surfaces in the meridional plane, the use of noncircular yield surfaces in the deviatoric stress plane, the use of non-associated flow laws and creep. [69]

Drucker Prager model along with its optimized models are successfully been employed to simulate the material response behavior of pressure-dependent soil, rocks and concrete. [4] As described on [68], the Extended Drucker Prager model in Abaqus:

- Used to model frictional materials, which are typically granular-like soils and rock, and exhibit pressure-dependent yield (the material becomes stronger as the pressure increases);
- Used to model materials in which the compressive yield strength is greater than the tensile yield strength, such as those commonly found in composite and polymeric materials;

- Allow a material to harden and/or soften isotropically;
- Generally, allow for volume change within elastic behavior: the flow rule, defining the inelastic straining, allows simultaneous inelastic dilation (volume increase) and inelastic shearing;
- Can include creep in Abaqus/Standard if the material exhibits long-term inelastic deformations;
- Can be defined to be sensitive to the rate of straining, as is often the case in polymeric materials;
- Can be used in conjunction with either the elastic material model or, in Abaqus/Standard if creep is not defined, the porous elastic material model.
- Can be used in conjunction with an equation of state model to describe the hydro dynamic response of the material in Abaqus/Explicit;
- Can be used in conjunction with the models of progressive damage and failure to specify different damage initiation criteria and damage evolution laws that allow for the progressive degradation of the material stiffness and the removal of elements from the mesh; and
- Are intended to simulate material response under essentially monotonic loading.

Three yield criteria are provided in this set of models. They offer differently shaped yield surfaces in the meridional plane (p–q plane): a linear form, a hyperbolic form, and a general exponent form. The choice of model depends largely on the material, the experimental data available for calibration of the model parameters, and on the range of pressure stress values likely to been countered. [69]

The linear model (available in Abaqus/Standard and Abaqus/Explicit) provides a noncircular section in the deviatoric (II) plane, associated inelastic flow in the deviatoric plane, and separate dilation and friction angles. [69] The hyperbolic and general exponent models (available in Abaqus/Standard only) use a Von Mises (circular) section in the deviatoric stress plane with associated plastic flow. A hyperbolic flow potential is used in the meridional plane, which in general means non-associated flow. [69]

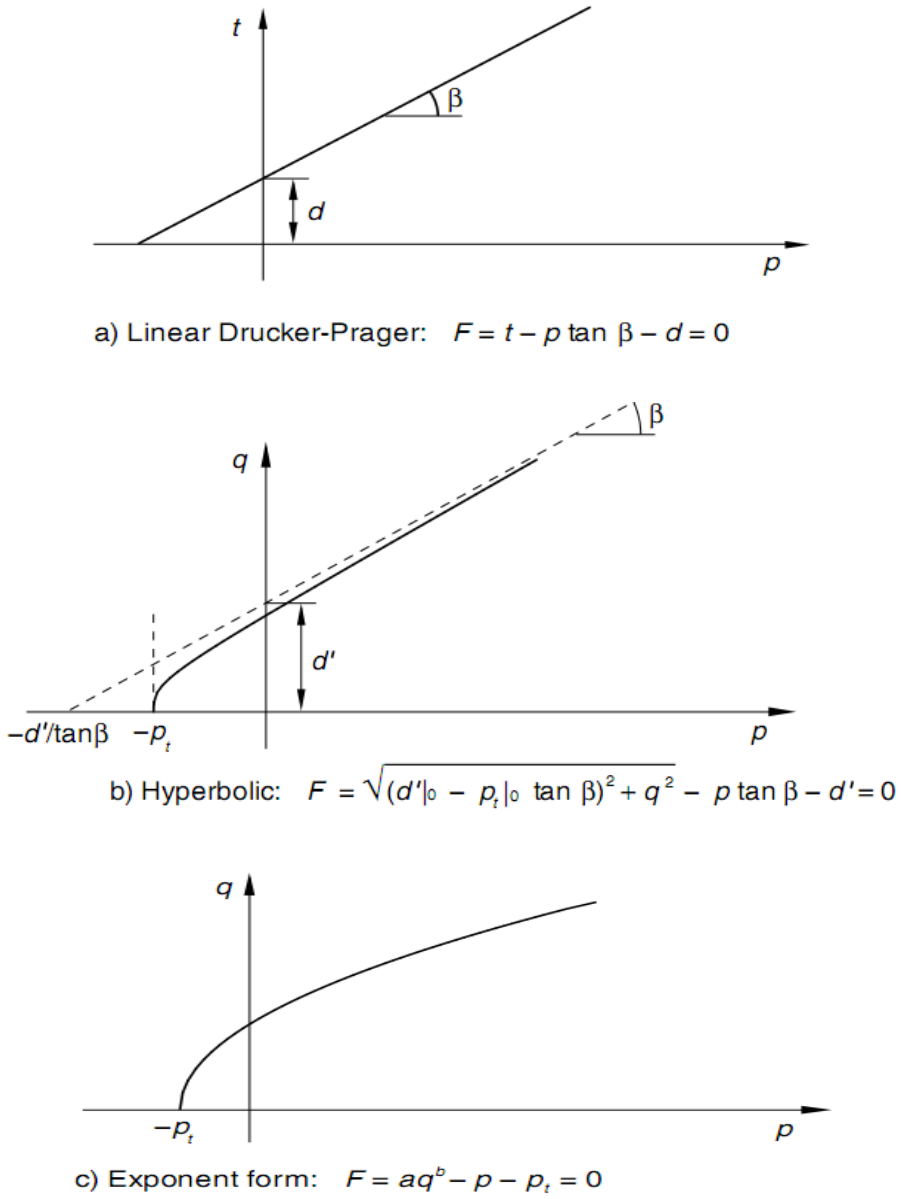


**Figure 3.11: Yield criteria in the meridional plane**

### 3.2.1 Drucker-Prager model used for the thesis

In this thesis, the linear Drucker-Prager model is employed because it is suitable for ballast material. According to [69] and [68], the linear Drucker-Prager model provides for a possibly noncircular yield surface in the deviatoric plane to match different yield values in triaxial tension and compression, associated inelastic flow in the deviatoric plane, and separate dilation and friction angles.

#### *3.2.1.1 Yield Criterion*

The linear Drucker-Prager criterion (*see figure 3.23 a)*) is written as [68]

$$F = t - p\tan\beta - d = 0 \quad (3.1)$$

Where: $t = \frac{1}{2}q\left[1 + \frac{1}{K} - \left(1 - \frac{1}{K}\right)\left(\frac{r}{q}\right)^3\right]$ (3.2)

$\boldsymbol{\beta(\theta,\varphi)}$ – is the slope of the linear yield surface in the p–t stress plane and is commonly referred to as the friction angle of the material;

$\boldsymbol{d}$ – Is the cohesion of the material; and

$\boldsymbol{K(\theta,\varphi)}$ – is the ratio of the yield stress in triaxial tension to the yield stress in triaxial compression and, thus, controls the dependence of the yield surface on the value of the intermediate principal stress *(see*

Figure 3.12*).*

When K = 1, t = q, which implies that the yield surface is the von Mises circle in the deviatoric principal stress plane, in which case the yield stresses in triaxial tension and compression are the same. To ensure that the yield surface remains convex requires 0.778 ≤ K ≤ 1.0. [68]

#### 3.2.1.1.1 Plastic flow

G is the flow potential, chosen in this model as: [68]

$$G = t - p\ \tan\psi \quad (3.3)$$

Where: $\psi(\theta,\varphi)$ is the dilation angle in the p-t plane as shown in *Figure 3.13*.

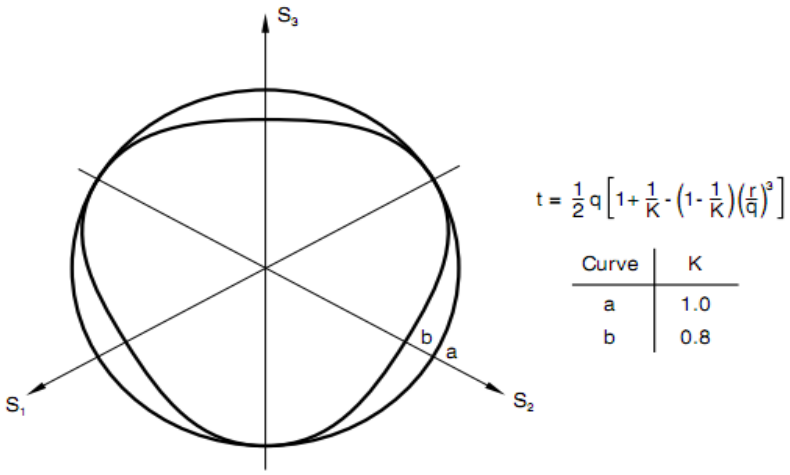


**Figure 3.12: Typical yield / flow surfaces of the linear model in the deviatoric plane.**

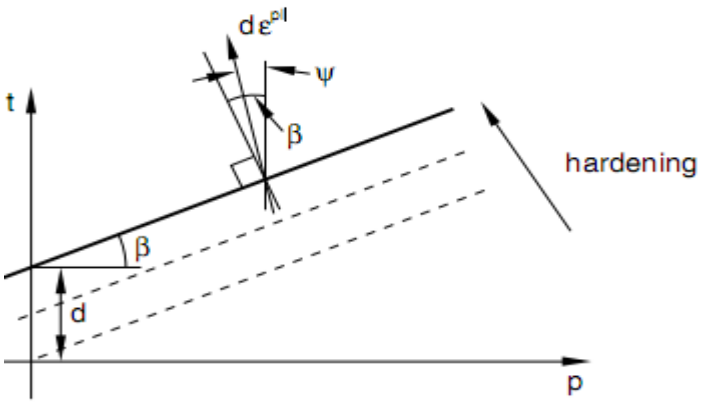


**Figure 3.13: Linear Drucker-Prager model: yield surface and flow direction in the p–t plane**

The input parameters (dilation angle [ψ], friction angle [β], flow ratio [K]) for the linear Drucker-Prager analysis are calculated based on the triaxial test simulation results. These parameters description and their respective calculation for this thesis are discussed in the following sub sections.

The stress invariants of the model can be written in terms triaxial compression principal stresses as:

$$p = -\frac{1}{3}(2\sigma_1 + \sigma_3) \quad (3.4)$$

$$q = \sigma_1 - \sigma_3 \quad (3.5)$$

$$r^3 = -(\sigma_1 - \sigma_3)^3 \quad (3.6)$$

***Where:*** $\sigma_3$ *and* $\sigma_1$ are the principal axial and lateral stresses respectively. Both are negative (compression).

The triaxial compression results can, thus, be plotted in the meridional plane.

Based on the equations above and rules the three input parameters of ABAQUS Linear Drucker-Prager model are calculated as follows.

***Friction angle (β)***

This parameter is calculated by plotting and fitting the best straight line through the t-p drawn from triaxial compression results.

According to [4], for triaxial compression $t = q$. Therefore, using *Eq 3.4* and *Eq 3.5*, t-p plot is generated from triaxial compression stress-strain plots of different confining pressure and best straight line fitted on the points as shown on *Figure 3.14*.

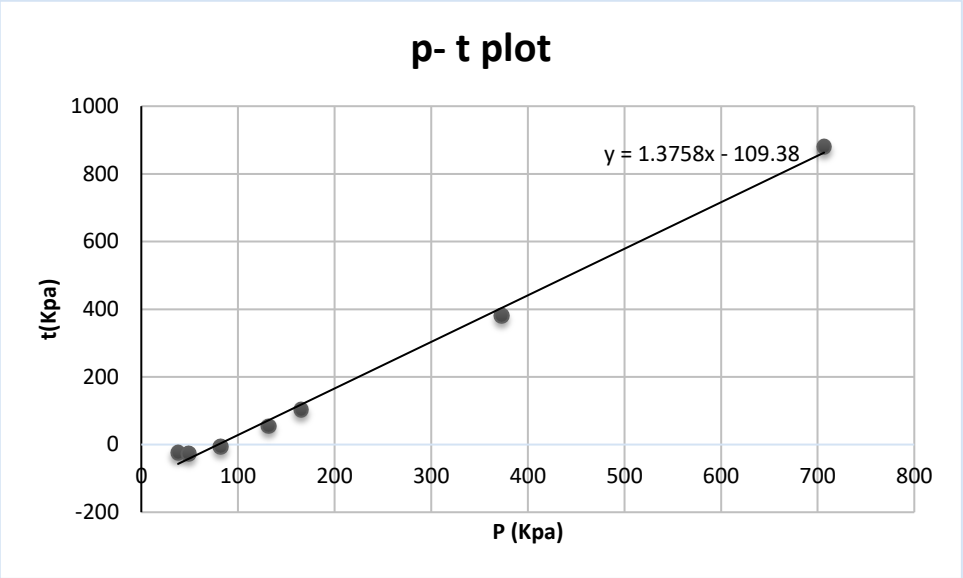


**Figure 3.14: t-p plot generated from the triaxial compression test simulation results**

Then the value of β calculated from the equation of the fitted line and is equal to 54°.

***Dilation angle (ψ):***

It is the volume change observed in granular materials when they are subjected to shear deformations. This effect was first described scientifically by Osborne Reynolds in 1885/1886 and is also known as Reynolds dilatancy. [37]

Unlike most other solid materials, the tendency of a compacted granular material is to dilate (expand in volume) as it is sheared. This occurs because the grains in a compacted state are interlocking and therefore do not have the freedom to move around one another. When stressed, a lever motion occurs between neighboring grains, which produces a bulk expansion of the material. On the other hand, when a granular material starts in a very loose state it may initially compact instead of dilating under shear. A sample of a material is called dilative if its volume increases with increasing shear and contractive if the volume decreases with increasing shear. [37]

This parameter is calculated by using the formula recommended by [42], from the plot of volumetric strain-axial strain.

$$\psi = \sin^{-1}\left(\frac{\frac{d\varepsilon_v}{d\varepsilon_a}}{\frac{d\varepsilon_v}{d\varepsilon_a}-2}\right) \quad (3.1)$$

***Where:*** *$\psi$ is dilation angle in degrees*

*$d\varepsilon_v$ is change in volumetric strain and*

*$d\varepsilon_a$ is change in axial strain*

The value of the dilation angle of the ballast are calculated for each confining pressure (30, 40, 80, 150, 200, 500, 1000Kpa) and are equal to 12.84$^o$, 14.22$^o$, 15.9$^o$, 16.2$^o$, 16.24$^o$, 16.36$^o$, 16.7$^o$ respectively. As written on different researches the confining pressure of real ballast material is 30 to 40Kpa. So, the dilation angle for 40Kpa confining pressure which is equal to 14.22$^o$ is chosen.

***Flow stress ratio (K)***: is the ratio of the yield stress in triaxial tension to the yield stress in triaxial compression. To ensure that the yield surface of a Drucker-Prager model remains convex requires $0.778 \leq K \leq 1.0$.

In this paper, this parameter is estimated in range to be 0.8, because the compression strength of ballast is much greater than its tensile strength.

***Elastic parameters:*** Modulus of Elasticity (E) = 320Mpa and Poisson's ratio ($\nu$) = 0.3 calculated from the test results under 40Kpa confining pressure.

### 3.2.2 Modeling of components using ABAQUS

Twelve 8.08m long three-dimensional track models are created (i.e. four for each three parameters of traffic load: speed, load and number of repetition). For speed parameter four models are created making number of pass and load constant; with four speed variations of 80km/hr, 100km/hr, 120km/hr and 160km/hr. And four models with varying load of 15, 20, 25 and 30tons, making number of pass and speed constant. Four models also made varying number of pass of 2, 4, 6, and 8 repetitions, with constant speed and load. To assess the long-term behavior of ballast material due to cyclic traffic load, the model is subjected to an axel load of 25 tons with 120km/hr speed for 10,000 cycles. The properties of components of the track are summarized in the table below as collected from different sources.

**Table 3.1: Summary of properties of track components**

| ***Materials*** | ***Part type in ABAQUS*** | ***Modulus of elasticity, E (Mpa)*** | ***Poison's Ratio, v*** | ***Density, ρ (kg/m$^3$)*** | ***Drucker Prager parameters*** | | | ***Source*** |
|---|---|---|---|---|---|---|---|---|
| | | | | | *Friction angle, $\phi$* | *Dilation angle, $\psi$* | *Flow stress ratio, K* | |
| Wheel & axel *(see Figure 3.17)* | 3D deformable | 210000 | 0.28 | 78500 | - | - | - | - |
| Rail *(see Figure 3.15)* | 3D deformable | 210000 | 0.28 | 78500 | - | - | - | [12] |
| Sleeper *(see Figure 3.16)* | 3D deformable | 39117 | 0.3 | 24000 | - | - | - | [21] |
| Ballast | 3D deformable | 320 | 0.3 | 1800 | 54 | 14.22 | 0.8 | Test result |
| Sub-ballast | 3D deformable | 80 | 0.3 | 1800 | 40 | 11 | 0.8 | - |
| Subgrade | 3D deformable | 10 | 0.3 | 2000 | - | - | - | - |

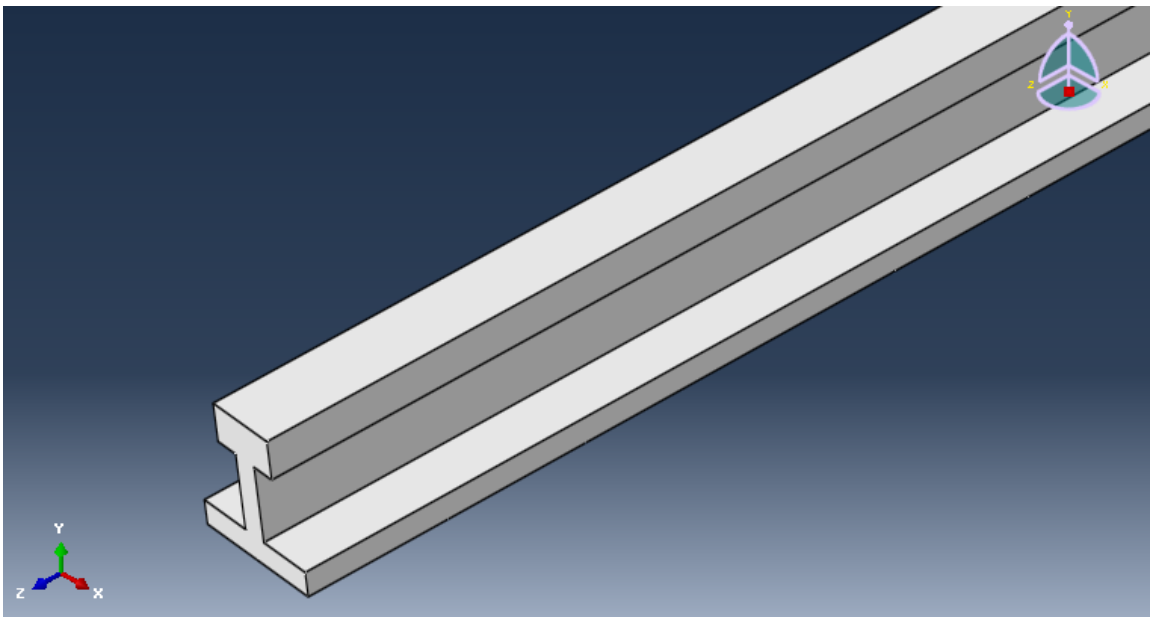


**Figure 3.15: rail model from ABAQUS**

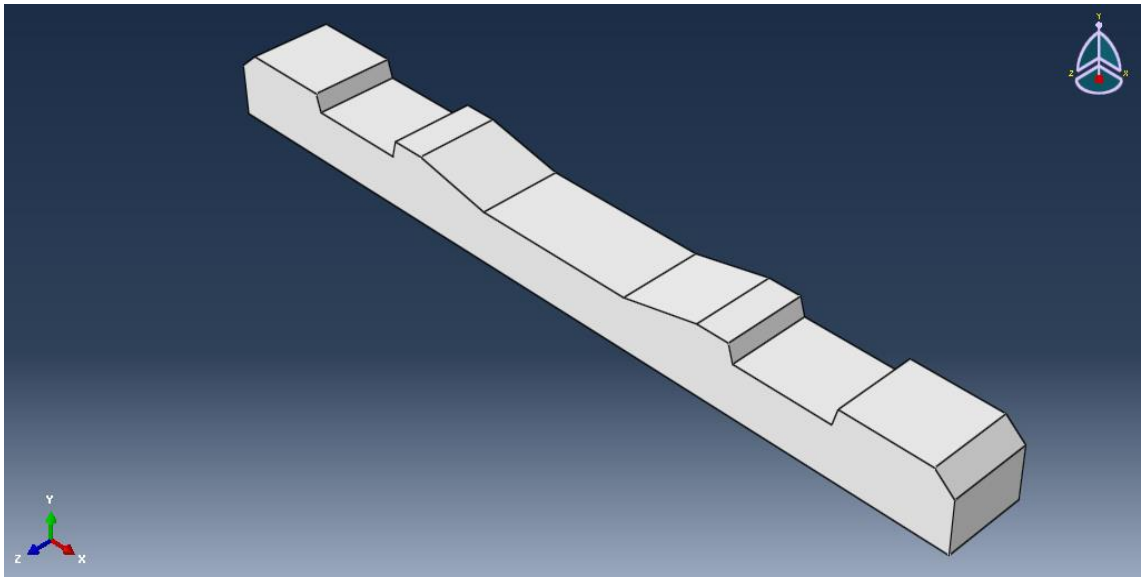

**Figure 3.16: Sleeper model from ABAQUS**

### *3.2.2.1 Step Module*

In this module two steps are created one for the application of the axel load. Its total time is 0.1sec, and the other for the cyclic movement of the axel. Both the steps are Dynamic-Explicit to avoid the convergence problem.

### *3.2.2.2 Interaction Module*

Parts created were assembled to their appropriate place but the connections and interactions between them should be defined and assigned. Before interactions are applied to the parts, ABAQUS will treat them as separate elements even though they are connected in assembly module.

#### 3.2.2.2.1 Constraints

Kinematic coupling the middle rod with wheels is performed defining reference point at the center of axel *(see Figure 3.17).*

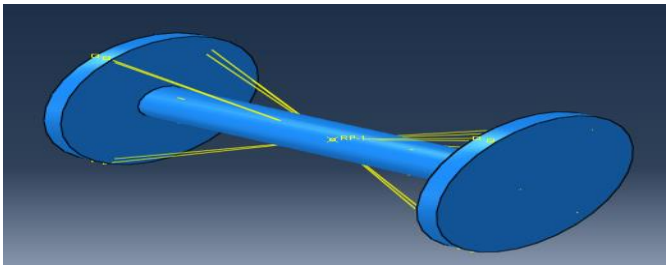

**Figure 3.17: Coupled axel components**

#### 3.2.2.2.2 Interaction properties

Two contact interaction properties are created. One is for the wheel-rail contact and the other for other contacts in the model.

- ✓ ***Wheel-rail contact:*** friction less tangential behavior and Hertz normal contact behavior is created based on [78]. The contact pressure-over closure relationship curve is shown below.

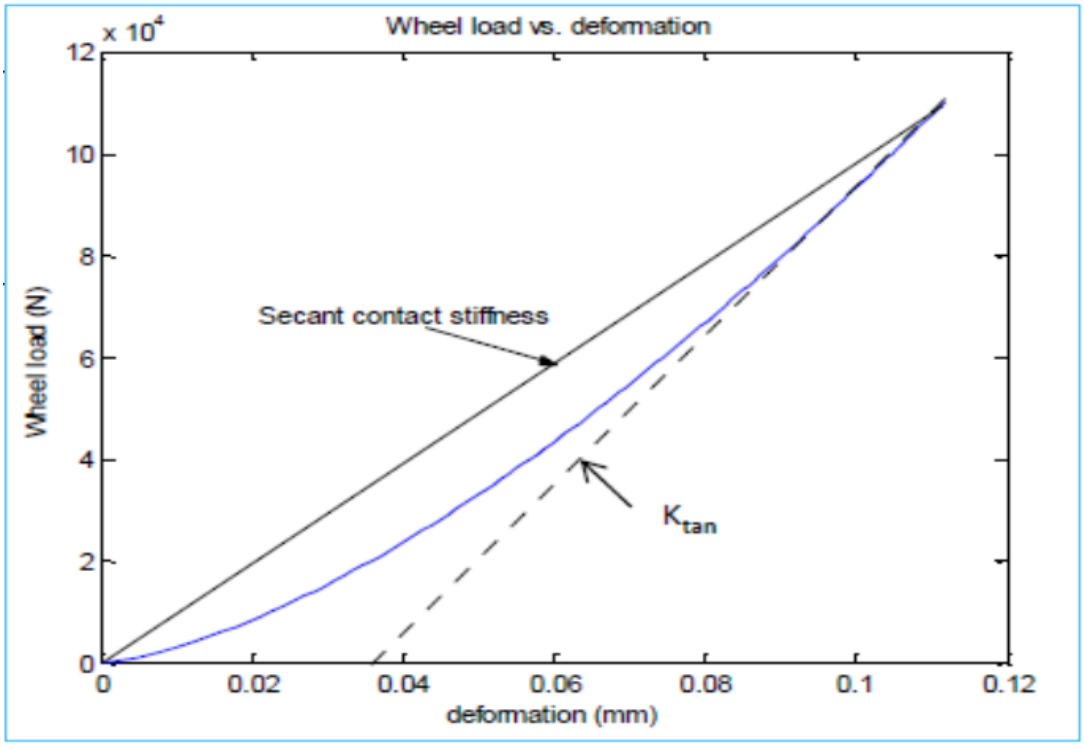


**Figure 3.18: secant pressure- over closure relationship**

- ✓ ***Other contact:*** a contact behavior with penalty frictional tangential behavior of friction coefficient equal to 0.7 and normal contact pressure-over closure relationship of linear type with stiffness of 400,000N/m is created for the other contacts in the model.

#### *3.2.2.2.3 Spring/ Dashpots*

The rail pads are represented by spring/dashpot elements connecting the sleepers and the rails. Three spring elements with spring stiffness of $1.2x10^8 N/m^2$ and dashpot coefficient of $75000 Ns/m^2$ are created per sleeper.

### 3.2.2.3 Load Module

In this module, two types of loads are created. The first is a concentrated axel load which is applied at the reference point created on the previous part. And the other is uniformly distributed (pressure) which is the sum of the dead load of the components of the track is applied on ballast, sub ballast and subgrade. The loads are applied based on the amplitudes defined.

#### *3.2.2.3.1 Boundary conditions (BC)*

Three types of boundary conditions are created. The first one is a velocity/angular velocity type boundary condition which is applied to the axel to constrain the axel from any movement during loading step and to allow it to move cyclically with a specified velocity at amplitude created during movement step *(see Figure 3.19)*. And the second is to constrain the lateral and longitudinal movement of track components. In the third BC the bottom of the subgrade is constrained from all displacements and rotations.

#### *3.2.2.3.2 Amplitude*

Amplitudes are created to define the repetition of load or boundary conditions in cyclic actions. Here two amplitudes are created; one is for the axel load (*Amp1*) and the other is for cyclic movement of the loaded axel on the track (*Amp 2*).

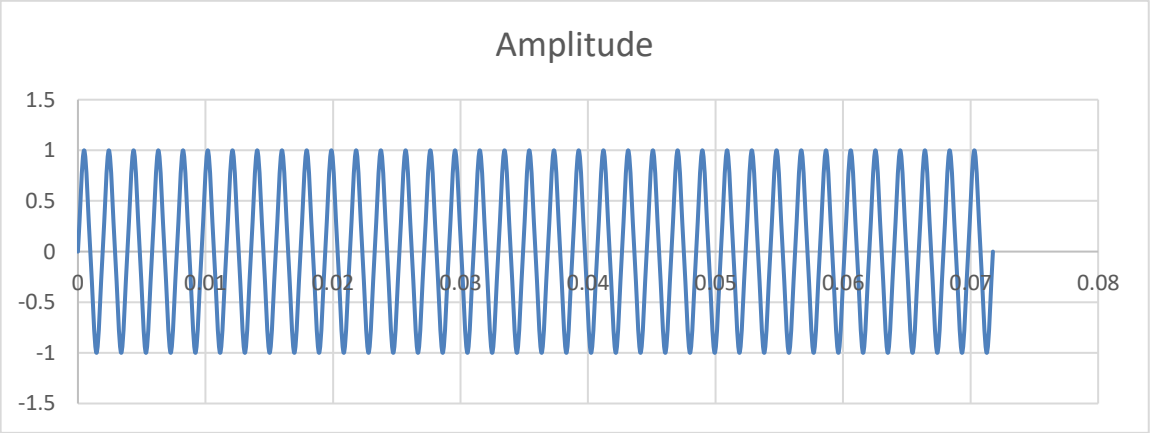


**Figure 3.19: Constant amplitude (Amp 2) used for cyclic movement of axel**

### 3.2.2.4 Mesh

The components assembled above are meshed separately based on their size to a total no of mesh elements equal to 9,111. *(See Figure 3.20)*

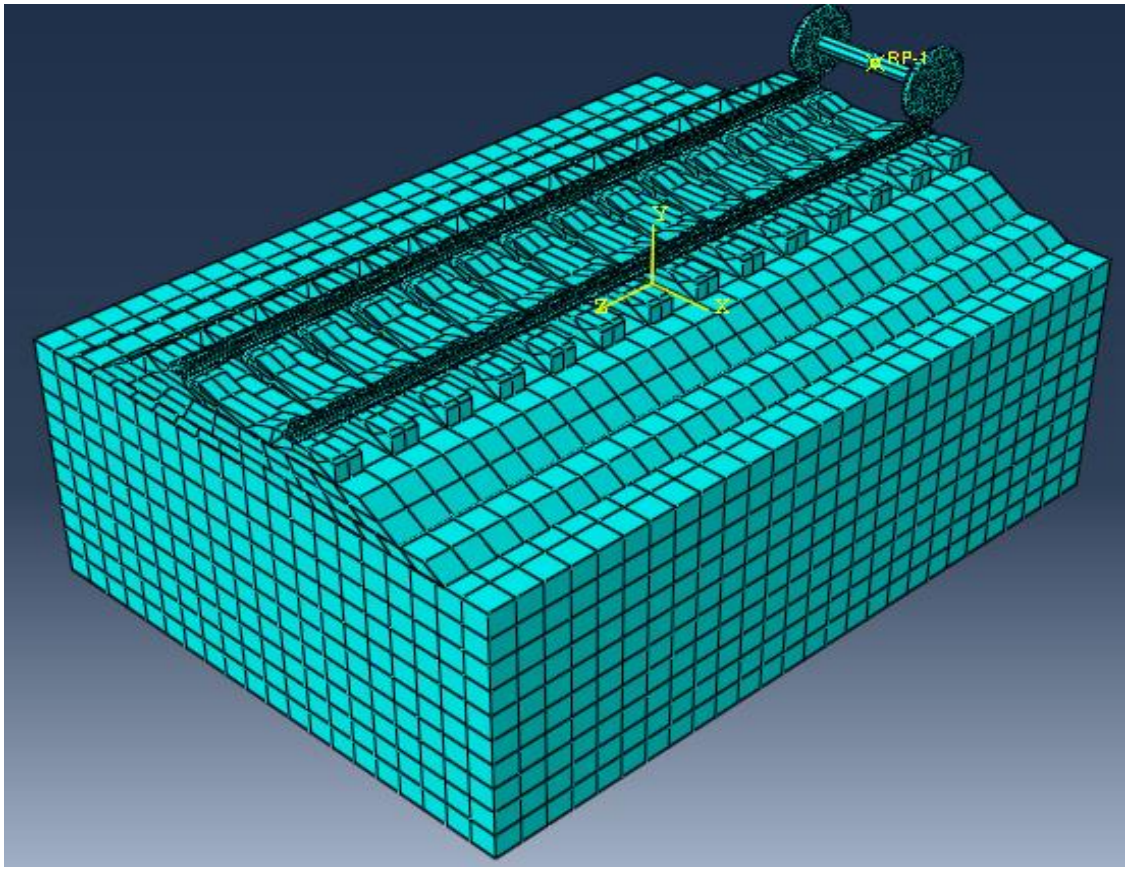


**Figure 3.20: Meshed components of track model**

# CHAPTER 4 RESULT AND DISCUSSION

In this chapter, results from finite element track model analysis are shown and discussed in detail. The results of each model are used to compare the effect of traffic load parameters. The effect of traffic load in the long run is assessed and discussed based on the results from the 10,000-cycle track model analysis. The results used to meet this objective are stress-strain relationship of ballast, strain-time relationship of ballast, and stress-time relationship of subgrade and contours showing the distribution of stress and strain.

## 4.1 The effect of traffic parameters on ballast strain

The cumulative plastic strain-time relations of ballast for each model of varying axel speed, axel load and number of cycles are plotted using excel; extracting the x-y data from Abaqus. Then the maximum cumulative strain that means the total plastic strain of each speed categories are plotted against the corresponding axel speeds (*see Figure 4.1*). The increase in the axel speed by 20 Km/hr increases the cumulative plastic strain of the ballast drastically in the first stage and gradually the slope became gentle; this is because in the first stages, the strain can be increased due to voids but gradually the amount of void between the particles will decrease.

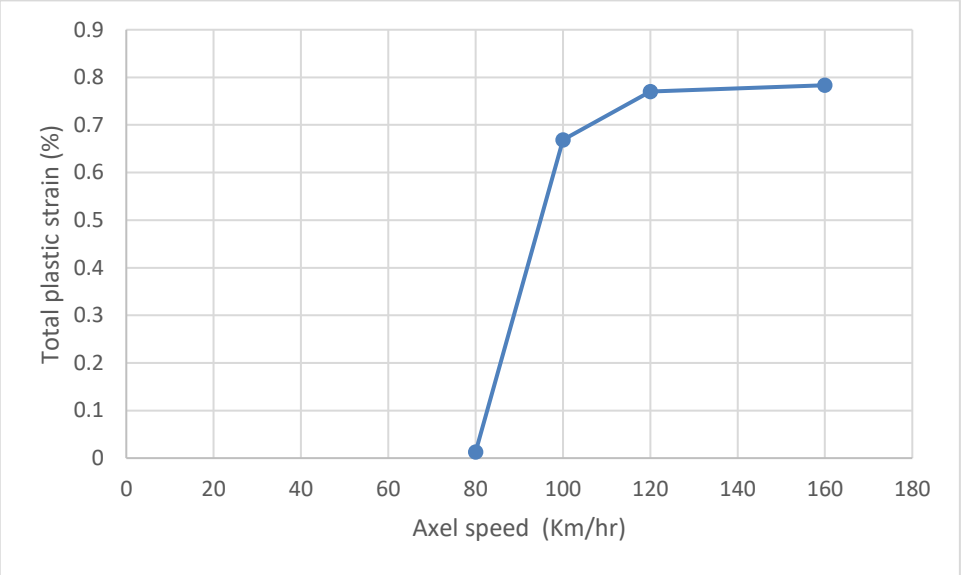


**Figure 4.1 Axel speed Vs Total plastic strain**

Similarly, the relation of total plastic strain due to axel load and number of cycles variation are plotted (*see Figure 4.2 and Figure 4.3)*

As shown in the figure below, the increase in axel load by 5 tone will cause a small increase in the total plastic strain of ballast. This graph has gentler slope than the speed – strain graph.

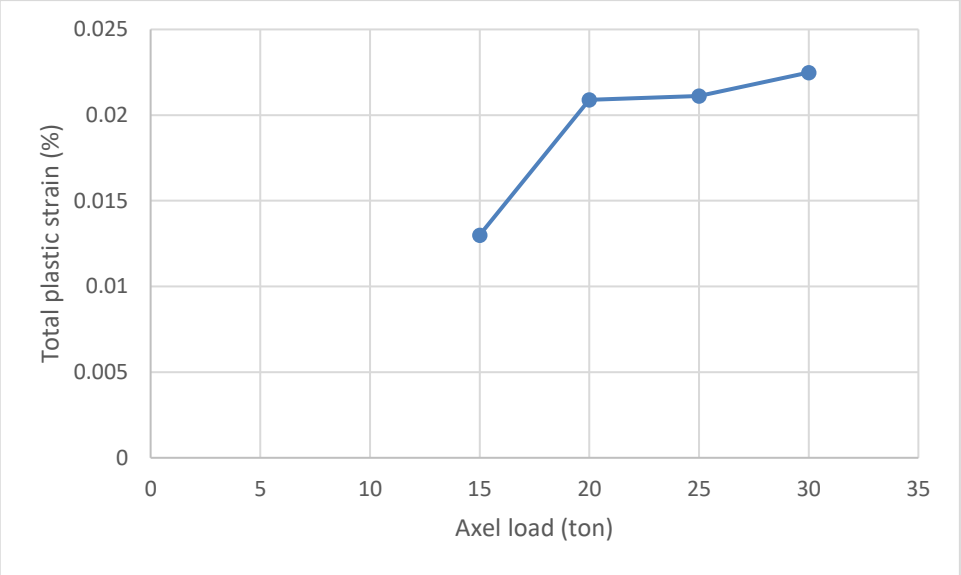


**Figure 4.2 Total plastic strain Vs Axel load**

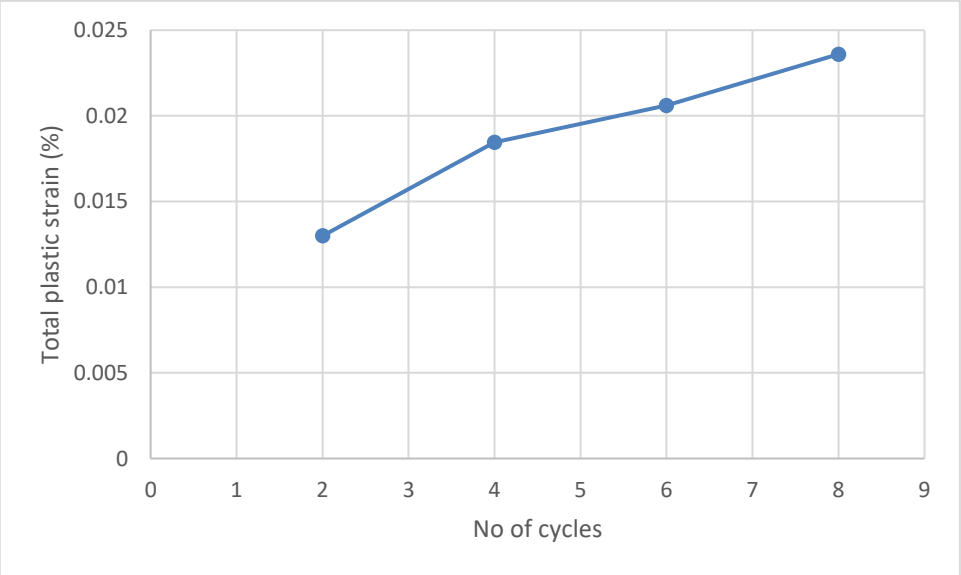


**Figure 4.3 Total vertical plastic strain Vs Number of cycles**

## 4.2 The effect of traffic parameters on the stress transfer to subgrade

One of the most important performance criteria of ballast material is to resist load and to distribute it to wider area to minimize the stress transferred to the subgrade. Here the stress transferred to the subgrade Vs. time graphs of each model were extracted from the software. The maximum stress values are plotted against the corresponding speed, load and number of cycles.

The relation of speed and the stress transferred to subgrade is comparable. The increase in the speed of train drastically increases the stress transferred to the subgrade in the first increases. But gradually the effect decreases this is because of plastic hardening. *(See Figure 4.4)*

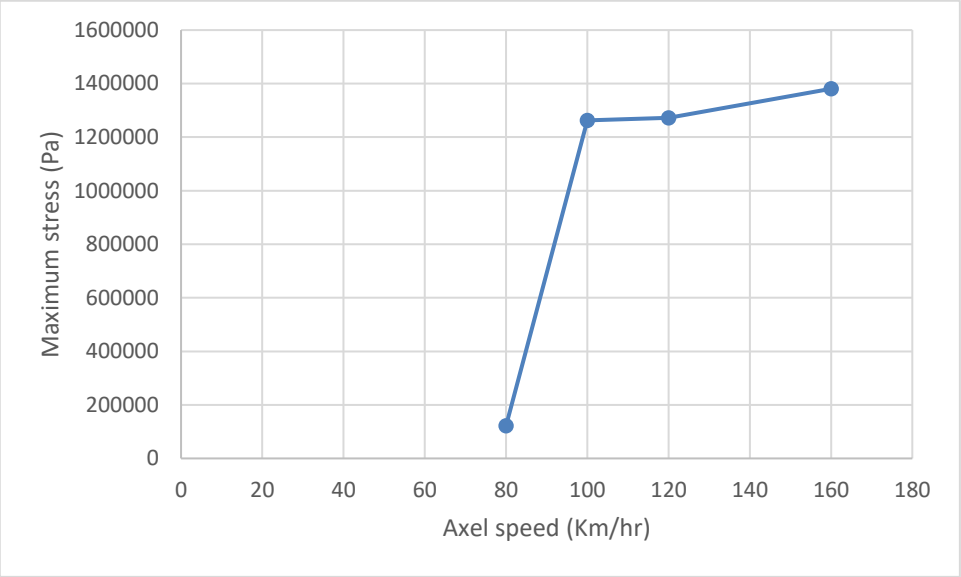


**Figure 4.4 Maximum stress on subgrade Vs Axel speed**

The relation between traffic load and the stress transferred to the subgrade is direct but, as it can be seen on the graph, the slope varies frequently, this shows effect of traffic load on the stress transferred to subgrade depends on other traffic parameters. *(See Figure 4.5)*

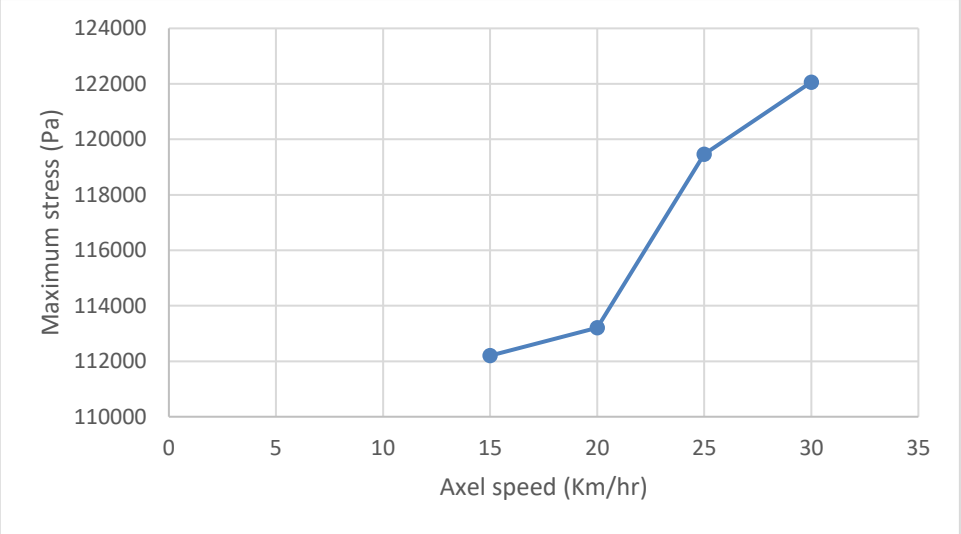


**Figure 4.5 Maximum stress on subgrade Vs Axel load**

Increasing the number of cycles of train movement by 2 may cause a change up to 20kpa on the stress transferred to the subgrade. These means careful monitoring of maintenance period of ballast should adopted because improper additional cycles of train movement beyond maintenance period will cause damages to subgrade.

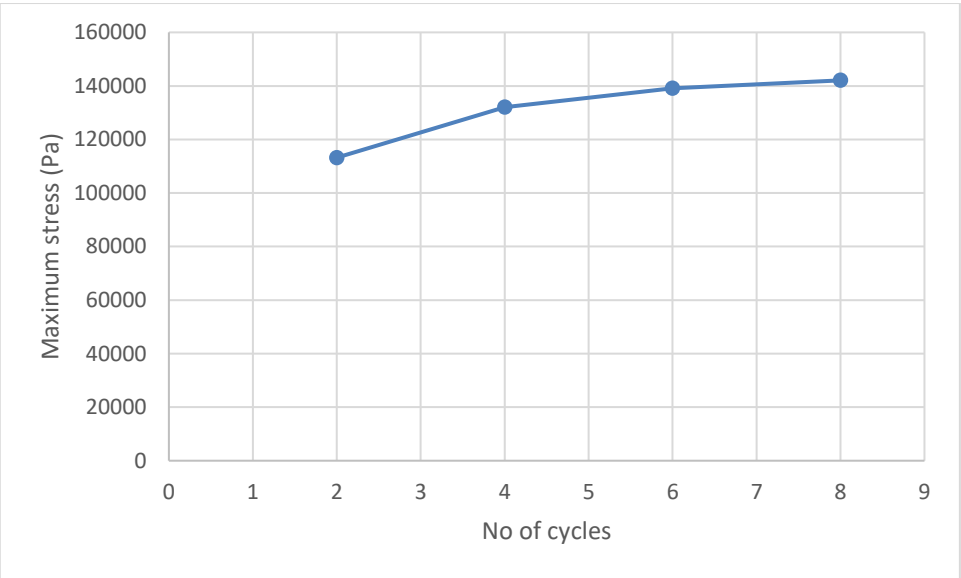


**Figure 4.6 Vertical stress – time curve of subgrade**

In this chapter, results from finite element track model analysis are shown and discussed in detail. The x-y data for each graph is generated from the software (ABAQUS) and plotted on excel sheet.

## 4.3 Contour pictures of deformation and stress distribution

Deformation distribution in ballast, sub-ballast and subgrade layers of the track is shown in the following picture (see *Figure 4.7*). This contour shows the permanent deformation of track after all the loading cycles.

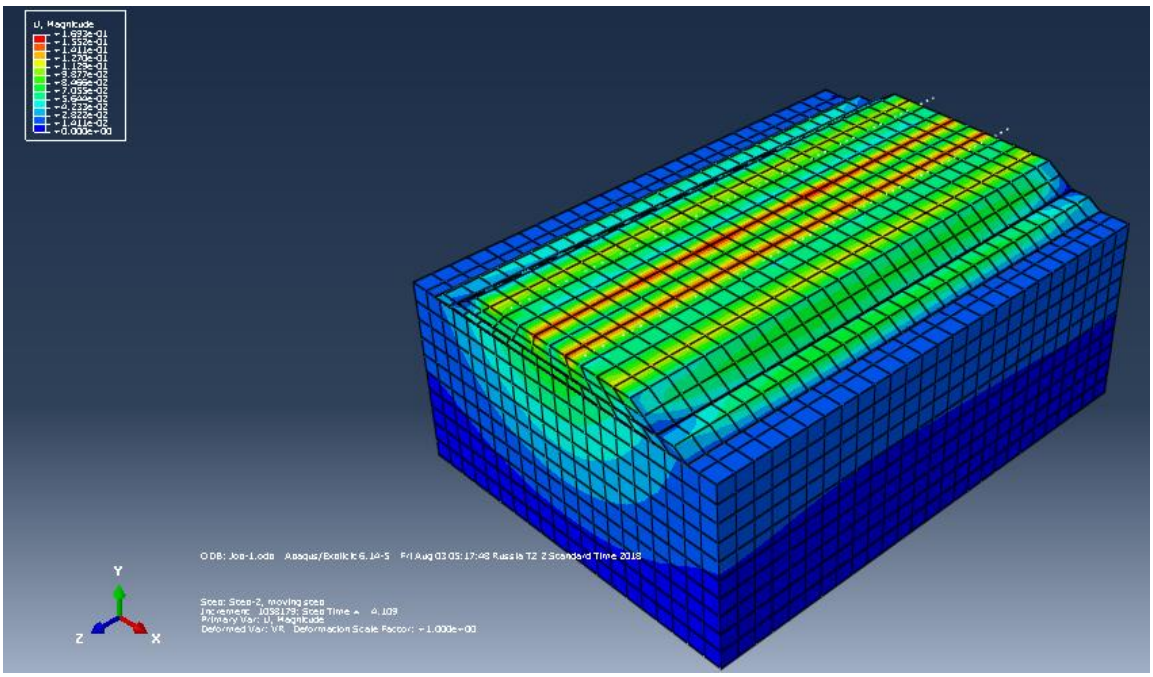


**Figure 4.7 Deformation contour for ballast, sub-ballast and sub-grade**

The vertical stress (at the end of the last loading cycle) distribution in track is shown by the contour representation as shown on the following picture. In the picture the stress begins at a small area at the top and is distributed to a wide area.

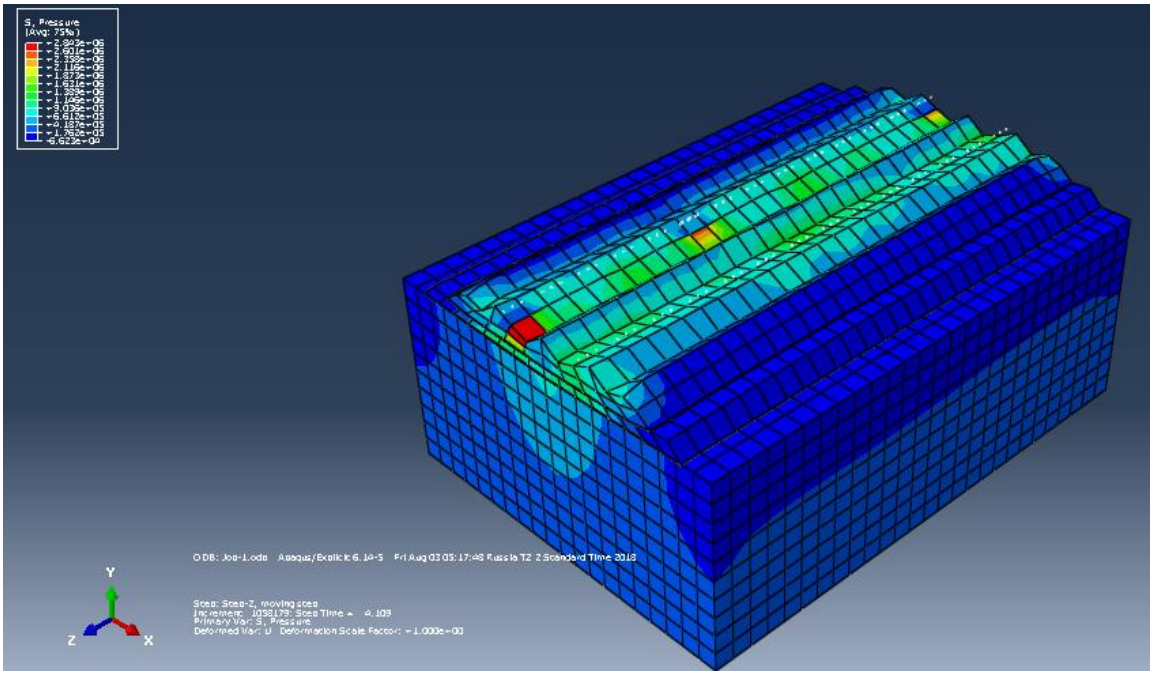

**Figure 4.8 stress contour for ballast, sub-ballast and subgrade**

## 4.4 Stress-strain relationship of ballast

Here stress vs total strain graph is presented. (see

*Figure* 4.9) As shown in the figure, at the beginning the stress value in the track increases rapidly for a little amount of changes in the strain. That means when the axel load is first applied the internal stress in the ballast highly increases. The ballast resists this stress for some cycles with lower and gradually increasing strain; this gradual increasing of ballast strain will continue even after the axel load moved away. In other words, the ballast reaction to the applied load is not fast. When another axel load cycle is applied the ballast will not yet relief from the first strain and internal stress. Through multiple cycles of axel load, the internal stress and strain will be increased to constant numbers. This is because the ballast permanent deformation gradually decreases since the ballast particles broken and the ballast system is compacted enough. As it can be seen from the graph, the stress tends to a constant value of 4Mpa, and the strain to a value of 6.5%. At this stage many of the ballast performances (drainage and damping) will be degraded. The geometric faults will also be expected due to differential settlement.

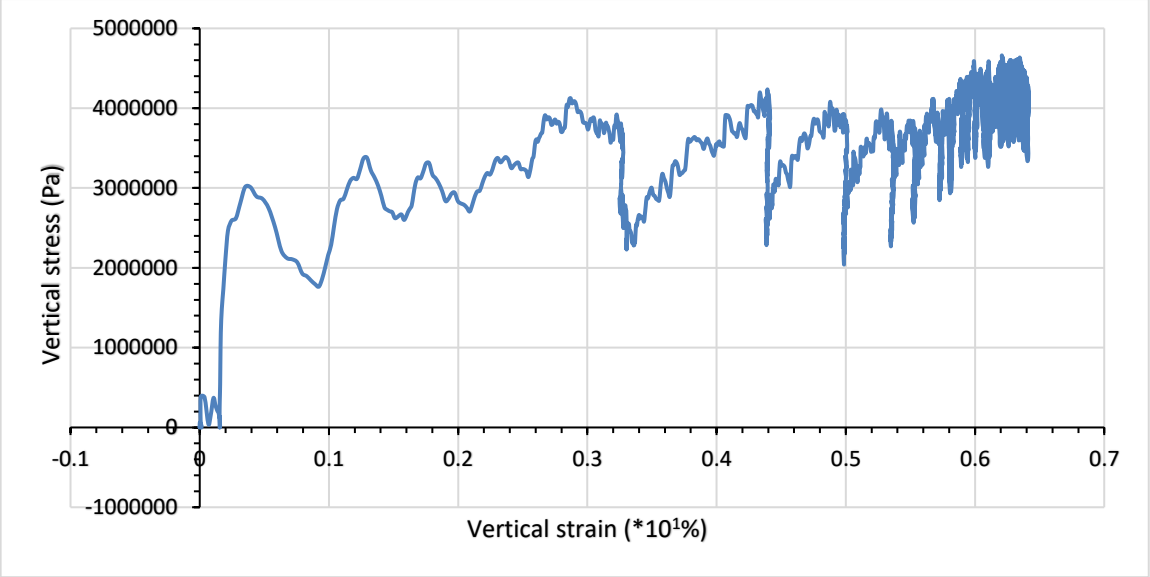


**Figure 4.9 vertical stress – strain graph of ballast**

## 4.5 Stress-time relationship of ballast

*Figure 4.10* shows the vertical stress value in relation to the loading cycles. As it can be seen from the graph, in the beginning the stress increases drastically to a large value, and fluctuates based on the passage of axel loads. Gradually the fluctuation decreases and the stress value tends to a constant value. In this stage the ballast will be subjected to high internal stress weather there is axel load or not. That is because of full compaction of ballast layer.

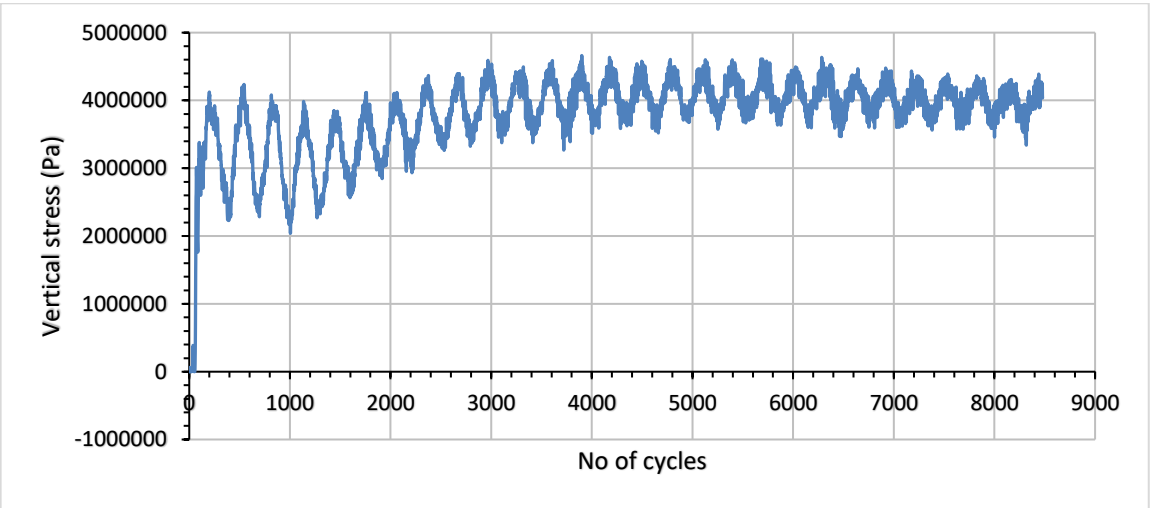


**Figure 4.10 Vertical stress – time graph of ballast**

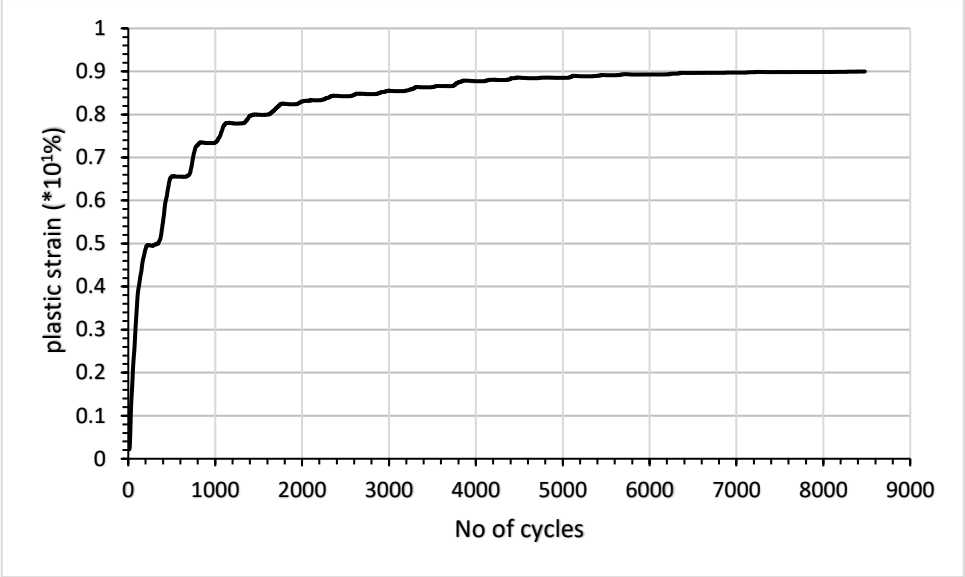


**Figure 4.11 Plastic strain – time graph**

## Strain-time relationship of ballast

Plastic deformation in relation to the number of cycles of moving load is generated from the software and plotted using excel. In the analysis, moving load is applied for 10,000 cycles. (*see Figure 4.11*)

According to the result, in the first about 25 to 30 cycles the ballast shows rapid increasing of plastic strain that is due to reduction of depth as particles begin to interlock. Then up to cycle about 1200 the strain growth rate fluctuates (almost zero strain and then rapid growth). This is because of the particle resistance to stress due to enough interlock, and then particle breakage. In the next cycles up to 5,000 plastic strain grows slowly due to particle final remaining breakage and compaction. Then after the strain rate decreases to have almost constant value. That shows the ballast particles broken and well interlocked again. In this stage the ballast's drainage and damping performance will be lost since its particles are broken and it is compacted enough.

## 4.6 Stress-time relationship of subgrade

In a track structure a layer on the top is stronger than the one below it; so, it is the responsibility of the above layer to protect the layers under it. Here in ballasted track, the increase in stress on the subgrade is due to the degradation of the performance of ballast and sub-ballast to distribute load to wide area. As the thickness of ballast decreases and damping performance decreases the pressure to be transferred to subgrade becomes higher. According to the finite element analysis result, the value of stress on the subgrade fluctuates between the values 0.5MPa and 2MPa and tends to converge to a constant value around 1.5MPa. *(see Figure 4.12)* This is because of the ballast settlement and reduced damping performance.

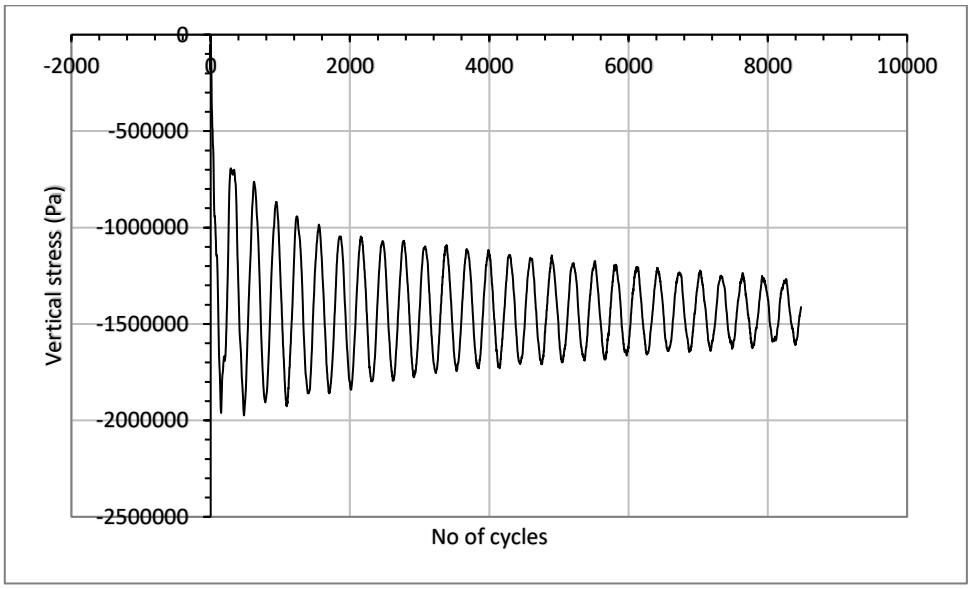


**Figure 4.12 Vertical stress – time curve of subgrade**

# CHAPTER 5 CONCLUSIONS AND RECCOMENDATIONS

## 5.1 Conclusion

The effects of train speed and number of cycles of train movement on ballast settlement are higher than that of the axel load. According to the results the increase in the speed of train movement by 20km/hr. will increase the stress transferred to the subgrade by up to about 1000kpa. Increasing the number of cycles of train movement by four affects the total plastic strain of ballast more than increasing of tonnage by 5 tons.

Ballast maintenance is mainly applied to correct two major deterioration (failure) of ballast material due to cyclic traffic load and environmental conditions. These two failures are differential settlement of ballast layer and the fouling or contamination of ballast material with fine materials. Tamping or stone blowing are the maintenance actions that can be taken to correct differential settlement and other geometrical failure whereas ballast fouling is maintained by ballast cleaning action. Usually ballast differential settlement happens before fouling because the main cause of ballast fouling is particle breakage and wear. According to the results and discussions in the above chapters, the performance reduction due to much settlement is reached at after about 6000 cycles of moving axel load. Therefore, periodic monitoring of the performance of ballast material should be done after 6000 cycle of axel load.

## 5.2 Recommendation for further studies

The study carried out within the scope of this thesis has generated several new aspects of ballast behavior that need to be investigated in more detail. The following issues in particular, are recommended for further research on the behavior of ballast.

1) Traffic load is not the only thing responsible for ballast degradation. Environmental factors such as climate change and weathering conditions contribute a lot for the deterioration of track components especially ballast. So, in future studies the author recommends the study of effect of environmental factors on the life time performance of ballast material or system.
2) The lateral and longitudinal strength failures of track are the major causes of geometric alignment alteration of track. And the track lateral and longitudinal strength are mainly from the shear strength developed between ballast and sleepers. So, the inspection and study of lateral and longitudinal strength performance of ballast system is vital issue.
3) Drainage performance of ballast system is affected by the fouling rate or the growth in percentage of fine materials between coarse particles of ballast and the reduction of spaces between particles due to settlement caused by traffic load or maintenance action like tamping. The drainage performance of ballast system in relation to settlement and the production of fine particles can be one direction for further studies.
4) Maintenance period, the type of measure to be taken, damage or degradation level and type of performance reduction are interrelated issues in the maintenance of ballast system. The author recommends the study of ballast maintenance in relation to degradation level, performance reduction type and period.
5) The simulation of largescale tests in other words virtual tests are easy ways to evaluate properties of materials with limited resources. So, detailed study and comparison of results with actual test results can be the other direction of research.
6) The deferential settlement in track is mainly caused by irrespective of the initial irregularities in the vehicle-track system such as varying ballast densities (varied degree of compaction), different subgrade properties, out-of-round or flat wheel, or in the transitions of ballasted track and slab track. Modeling and analysis of the differential settlement of ballasted tracks incorporating those causes can be another research idea.

## REFERENCES

[1] "Ethiopia – Djibouti high speed railway finally completed" CGTN. 17 January 2017.

[2] Abateneh Y. A. (2011). Survey of Railway Ballast Specification and Aspects of Modeling Techniques. Royal Institute of Technology, Stockholm, Sweden.

[3] Alexey Kolos, Irina Darienko, Anastasia Konon (2017), Mathematical model for forecasting of rail track ballast bearing capacity, Transportation Geotechnics and Geoecology, Saint Petersburg, Russia. Science Direct Publishing.

[4] Amir Mir, Xichun Luo1, Amir Siddiq (2015), Numerical Simulation of Triaxial tests to determine the Drucker-Prager Parameters of Silicon, DMEM, University of Strathclyde, Glasgow, U.K, Dept. of Physical Sciences, University of Aberdeen, Aberdeen, U.K, Proceedings of the 21st International Conference on Automation & Computing, University of Strathclyde, Glasgow, UK, 11-12 September 2015.

[5] Andy Franklin, Professional Head of Civil Engineering Carillion Rail June 2006, Current Practice in Ballast Maintenance & Renewal.

[6] Bhanitiz Aursudkij, (2007). A Laboratory Study of Railway Ballast Behavior under Traffic Loading and Tamping Maintenance. The University of Nottingham, Nottinghamshire, UK.

[7] Biruk G/medhin, (2015). Identifying and optimizing suitable source of ballast material, Addis Ababa institute of technology, Addis Ababa, Ethiopia.

[8] Buddhima Indraratna, Qi Deng Sun, Sanjay Nimbalkar, (2015). Observed and predicted behavior of rail ballast under monotonic loading capturing particle breakage, Faculty of Engineering and Information Sciences, University of Wollongong, Australia.

[9] Cheng Chen, Buddhima Indraratna, Glenn McDowell, Cholachat Rujikiatkamjorn (2015), Discrete element modelling of lateral displacement of a granular assembly under cyclic loading, Centre for Geomechanics and Railway Engineering, Faculty of Engineering and Information Sciences, University of Wollongong, Wollongong City, NSW 2522, Australia. Science Direct Publishing.

[10] Cheng Y.P, Nakata Y & Bolton M.D. (2003). Discrete element simulation of crushable soil, Department of Engineering, Cambridge University, UK. Geotechnique 53, No.7, 633-641, Research gate, England.

[11] Chiara Paderno, (2009). Simulation of ballast behavior under traffic and tamping process, LAVOC - EPFL Conference paper STRC.

[12] Chinese Rail Standard (National Standards of the People's Republic of China GB 2585—2007).

[13] Chinese Railway Standard (TB 10082-2005 PRC Code for design of railway track).

[14] Consta JV and Addis Environmental Services, "Basalt Quarry Investigation for Djibouti -Ethiopia Railway Line Rehabilitation Project (Dire Dawa – Lassarat Section)."

[15] CREC Addis Ababa-Mieso railway project, Testing report for stone ballast No.1 and 2nd testing report for stone ballast.

[16] Catarino, C. Alves-Ribeiro and C. Vale, (2015). Analysis of The Influence of The Permanent Deformation of Ballast Layer in The Railway Track Degradation Based on Numerical Simulations, Civil Engineering Department, University of Porto, Portugal.

[17] Robertson & M.D. Bolton (2001), DEM simulations of crushable grains and soils, Cambridge University Engineering Department, U.K.

[18] D.O. Potyondy and P.A. Cundall (2004), A Bonded-Particle Model for Rock, Department of Civil Engineering, Lassonde Institute, University of Toronto, Toronto, Ont. Canada, International Journal of Rock Mechanics and Mining Sciences 41, 1329-1364.

[19] Daniela Ionescu (2004). Evaluation of the engineering behavior of railway ballast. Faculty of engineering, department of civil mining and environmental engineering, University of Wollongong. Wollongong. Australia.

[20] David Potyondy, PFC 5.0 Technical Memorandum/ Material-modeling-support [fistPkg25] March 16, 2017.

[21] Desalew Fisseha (2014), Analysis and Design of Prestressed Concrete Sleeper, School of Civil and Environmental Engineering, Addis Ababa Institute of Technology, Addis Ababa University, Addis Ababa, Ethiopia.

[22] Dr. Rajat Rastogi, Lecture-12, Ballast. Department of Civil Engineering. Indian Institute of Technology- Roorkee. India.

[23] Tutumluer, H. Huang, Y. Hashash, and J. Ghaboussi, 2007. Discrete Element Modeling of Railroad Ballast Settlement, Civil and Environmental Engineering Department, University of Illinois at Urbana Champaign, Newmark Civil Engineering Laboratory, 205 North Mathews Avenue, Urbana, Illinois 61801, United States.

[24] E. Tutumluer, Y. Qian, Y. Hashash, and J. Ghaboussi, 2011. Field Validated Discrete Element Model for Railroad Ballast, University of Illinois at Urbana-Champaign (UIUC), Transportation Technology Center, Inc. (TTCI), United States.

[25] Ehsan Ghazvinian (2010), Modelling and Testing Strategies for Brittle Fracture Simulation in Crystalline Rock Samples, A thesis submitted to the Department of Geological Sciences & Geological Engineering In conformity with the requirements for the degree of Masters of Applied Science, Queen's University, Kingston, Ontario, Canada.

[26] Enad Mahmoud, A.T. Papagiannakis, David Renteia, (2016), Discrete Element Analysis of Railway Ballast under Cycling Loading, University of Texas Rio Grande Valley, 1201 West University Drive, Edinburg 78539, United States.

[27] Enad Mahmoud, A.T. Papagiannakis, David Renteia, (2016), Discrete Element Analysis of Railway Ballast under Cycling Loading University of Texas Rio Grande Valley, 1201 West University Drive, Edinburg 78539, United States.

[28] Ethiopian Railways Corporation, Addis Ababa/Sebeta – Djibouti Railway Project, Techno-Economic Feasibility Study, Volume I Main Document, April 2012.

[29] Galle Hetti Arachchige Janaka Jagath Kumarad, (2013), Development of Prediction Methods for Deformation Characteristics of Fouled Ballasts Based on Laboratory Experiments and Discrete Element Method, Yokohama National University, Graduate School of Engineering, Japan.

[30] Gino Calderón Vizcarra, Sanjay Nimbalkar, and Michéle Casagrande (2016). Modeling Behaviour of Railway Ballast in Prismoidal Apparatus using Discrete Element Method, Pontifical Catholic University of Rio de Janeiro,Rio de Janeiro, Brazil. University of Wollongong, Wollongong City, Australia.

[31] Hai Huang, Erol Tutumluer (2011), Discrete Element Modeling for fouled rail road ballast, University of Illinois, Urbana, IL61801, United States. Science Direct Publishing.

[32] Hai Huang, Erol Tutumluer (2011), Discrete Element Modeling for Fouled Railroad Ballast, Penn State University, Altoona, PA 16601, United States.

[33] Hai Huang, Erol Tutumluer, (2011), Discrete Element Modeling for fouled railroad ballast University of Illinois, Urbana, IL 61801, United States.

[34] http://www.itascacg.com/material-modeling-support.com, 09/07/2017.

[35] https://en.wikipedia.org/ballast-maintenance-railway-substructure-engineering 7/11/2016.

[36] https://en.wikipedia.org/wiki/Addis_Ababa–Djibouti_Railway. 18 February 2017.

[37] https://en.wikipedia.org/wiki/Dilatancy-(granular material).com 03/10/2017

[38] Itasca Consulting Group, Inc. (2016) PFC — Particle Flow Code in 2 and 3 Dimensions, Version 5.0, Documentation Set of version 5.00. 30 [March 2, 2017]. Minneapolis: Itasca.

[39] Itasca Consulting Group, Inc. PFC 5.0 user manual (PFC 5.0 documentation last updated Jul 28, 2017).

[40] Itasca, (1999). Particle Flow Code in Three Dimensions. Itasca Consulting Group, Inc., Minnesota.

[41] Ivan Deiros, Charles Voivret, Gaël Combe and Fabrice Emeriault, Quantifying Degradation of Railway Ballast using Numerical Simulations of Micro-Deval Test and In-situ Conditions, SNCF, Paris, France Université Grenoble Alpes, 3SR, Grenoble, France. Advances in Transportation Geotechnics 3. The3rd International Conference on Transportation Geotechnics (ICTG 2016)

[42] J. R. Maranha, The experimental determination of the angle of dilatancy in soils, ICIST, IST, Technical University of Lisbon, Portugal.

[43] Jan Elias, (2013), DEM Simulation of Railway Ballast Using Polyhedral Elemental Shapes, Brno University of Technology, Faculty of Civil Engineering, Institute of Structural Mechanics, Czech Republic.

[44] Jian Feng Wang and Haibin Yan (2012) DEM analysis of energy dissipation in crushable soils, Department of Civil and Architectural Engineering, City University of Hong Kong, Hong Kong. Science direct.com

[45] Jianfeng Wang, Haibin Yan, DEM analysis of energy dissipation in crushable soils, Department of Civil and Architectural Engineering, City University of Hong Kong, Hong Kong. Science direct 2012.

[46] Joaquín Irazábal González, June (2015). Numerical Modelling of Railway Ballast Using the Discrete Element Method, Escola Technica Superior d'Enginyeria de camins, canals i ports, UPC Barcelona tech, Spain.

[47] K. Nguyen, J. M. Goicolea and F. Galbadón, (2011). Dynamic Effect of High Speed Railway Traffic Loads on the Ballast Track Settlement.

[48] K. Tzanakakis, Railway Track and Its Long-Term Behavior: A Handbook for Railway Track of High Quality.

[49] Kedir Abdu, (2014). Assessment of Degradation and Performance Improvement of Railway Ballast with Geosynthetics - A Case Study of National Railway Network, School of Civil and Environmental Engineering, Addis Ababa Institute of Technology, Addis Ababa.

[50] M. Stahl, H. Konietzky (2010), Discrete element simulation of ballast and gravel under special consideration of grain-shape, grain-size and relative density, Geotechnical Institute, TU Bergakademie Freiberg, Germany.

[51] Manual for the Calculation of Elastic-Plastic Materials Models Parameters, NPL (National Physical Library) Manuals. 2007.

[52] Mauricio Alberto Tapias Camacho (2016), Particle Model for Crushable Aggregates Which Includes Size, time and Relative Humidity Effects, Division of Geotechnical Engineering and GeoSciences, Department of Civil and Environmental Engineering, UPC, Universitat Politecnica de Catalunya, Barcelonatech, Barcelona, Spain.

[53] Mc Dowell, Glenn R. and Li Huiqi (2016), Discrete Element modelling of scaled railway ballast under triaxial conditions, the university of Nottingham, UK.

[54] Md Wadud Salim (2004), Deformation and degradation aspects of ballast and constitutive modeling under cyclic loading, University of Wollongong, Australia.

[55] Mingfei Lu (2008), Discrete element modeling of railway ballast, Thesis submitted to the University of Nottingham for the degree of Doctor of Philosophy.

[56] N. Cho, C. D, Martin, and D. C. Sego, A clumped particle model for rock, International Journal of Rock Mechanics and Mining Sciences, vol, 44, no. 7, pp, 997-1010, 2007.

[57] N. T. Ngo, B. Indraratna, C. R. Kamjorn (2017), Micromechanics based investigation of fouled ballast using large-scale triaxial tests and discrete element modelling, University of Wollongong, Australia.

[58] P K Thakur, J S Vinod, and B Indraratna, Effect of particle breakage on cyclic densification of ballast: a DEM approach, School of Civil, Mining and Environmental Engineering, University of Wollongong. NSW 2522 Australia. IOP Publishing 2010.

[59] Pei Wang, Chloe Arson, (April 2,2016). Discrete Element Modeling of shielding and size effects during single particle crushing, School of Civil and Environmental Engineering at the Georgia Institute of Technology, Atlantic Drive, Atlanta.

[60] Qideng Sun (June, 2015), An Elasto-plastic Strain-based Approach for Analyzing the Behavior of Ballasted Rail Track, Department of Civil, Mining and Environmental Engineering, University of Wollongong, City of Wollongong, Australia.

[61] Roar Nalsund. (2014). Railway Ballast Characteristics, Selection Criteria and Performance. Norwegian University of Science and Technology, Trondheim, Norway.

[62] Sebastian Lobo-Guerrero and Luis E. Vallejo (2006), Discrete element Method analysis of rail track ballast degradation during cyclic loading, Department of Civil and Environmental Engineering, University of Pittsburgh, Pittsburgh PA 15261, USA.

[63] Sebastian Lobo-Guerrero and Luis E. Vallejo, Discrete Element Method Evaluation of Granular Crushing Under Direct Shear Test Conditions, Journal of geotechnical and geo environmental engineering ASCE/October 2005.

[64] Sebastian Lobo-Guerrero Luis E. Vallejo, 2006. Discrete element method analysis of rail track ballast degradation during cyclic loading.

[65] Sebastian Lobo-Guerrero, S.M. ASCE; Luis E. Vallejo, M. ASCE; and Luis F. Vesga, S.M. ASCE, Visualization of Crushing Evolution in Granular Materials under Compression using DEM, International Journal of Geomechanics © ASCE /May/June 2006.

[66] Shimelis Assefa (2015), Modeling and Analyzing the deformation of Ballast Structures Due to Repetition of Loads, School of Civil and Environmental Engineering, Addis Ababa University, Addis Ababa, Ethiopia.

[67] Shouju Li, De Li, Lijuan Cao and Zichang Shangguan (2014), Parameter Estimation Approach for Particle Flow Model of Rockfill Materials Using Response Surface Method, Dalian University of Technology, Dalian, China.

[68] SIMULIA ABAQUS 6.13 Analysis Guide, Section 23.3.1.

[69] SIMULIA ABAQUS 6.13 Theory Guide, Section 4.4.2.

[70] Toivo Wanne (2009), Bonded-Particle Modeling of Thermally Induced damage in Rock, Graduate department of Civil Engineering, University of Toronto, Toronto, Canada.

[71] Von Quang, Tuan Nguyen (2016) Shafts Back filled with Ballast: Stability and Settlement Predictions Via DEM Simulations, Faculty of Geo-Sciences, Geo engineering and Mining of the Technische University, Germany.

[72] Xiaoyi Shi (April 2009), Prediction of Permanent Deformation in Railway Track, The University of Nottingham, Nottingham, UK.

[73] Ye Lu, (2010), Reconstruction, characterization, modeling and visualization of Inherent and Induced digital sand Microstructures, School of Civil and Environmental Engineering, Georgia Institute of Technology, USA.

[74] Yeserah Gebeyehu, (2012). Standardization of Guidelines for Railway Track Infrastructure Subsystem for Railway System of Ethiopia, School of Civil and Environmental Engineering, Addis Ababa Institute of Technology, Addis Ababa.

[75] Yin Gao, (2013). A 3d Dynamic Train-Track Interaction Model to Study Track Performance under Trains Running at Critical Speed, Department of Civil and Environmental Engineering, the Pennsylvania State University, USA.

[76] Z. Hossain, B.Indraratna, F.darve and P.K.Thakur (2007), DEM analysis of angular ballast breakage under cyclic loading, School of Civil Mining and Environmental Engineering, Faculty of Engineering, University of Wollongong, Wollongong City, NSW2522, Australia. Taylor & Francis Group publishing.

[77] Zhao Shuyun and Li Shibo, (2013), Stress strain analysis of loess triaxial shear test by $PFC^{3D}$, College of Construction engineering, Jilin University, Changchun 130021, China.

[78] Wheel-rail contact mechanics, lecture note, prepared by Mequanent Mulugeta (M.Sc.), school of civil and environmental engineering, Addis Ababa Institute of technology May, 2015, Addis Ababa.

# APPENDIX A

## RELATED TO PFC 3D

## A.1 PFC3D codes used

### A.1.1 material generation

```
; fname: Ethio-Djibouti railway ballast. p3dat

; Specify the material properties:

; common, packing and material groups.

;#####################################################

; change the clump contact logic to linear parallel bond

cmat default type pebble-pebble model linearpbond property kn 5e6
proximity 0.1

contact method bond gap 2.0e-4

; set linear stiffness using methods

contact method deform emod 1.0e9 krat 1.0

; set stiffness of bonds using methods

contact method pb_deform emod 1.0e9 krat 1.0

; set bond strengths

contact property pb_ten 10.0e6 pb_coh 50.0e6 pb_fa 0.0

; set some damping at the contacts

contact property dp_nratio 0.5

; set pebble-pebble friction to non-zero value

contact property fric 0.577 range contact type pebble-pebble

clump template create ...

      pebcalculate ...

      name BS1 ...

      pebbles 13 ...

              0.02,-0.02,-0.011547,0.03266 ...
```

```
                0.02,0.0, 0.02309401, 0.03266 ...
                0.02,0.0, 0.0, 0.0 ...
                0.02,-0.02,-0.034641016151378,0.0 ...
                0.02,-0.04,0.0,0.0 ...
                0.02,-0.02,0.034641016151378,0.0 ...
                0.02,-0.02,0.011547,-0.03266 ...
                0.02,0.0,-0.02309401, -0.03266 ...
                0.02,0.02,0.011547,-0.03266 ...
                0.02,0.02,0.034641016151378,0.0 ...
                0.02,0.04,0.0,0.0 ...
                0.02,0.02,-0.034641016151378,0.0 ...
                0.02,0.02, -0.011547, 0.03266
clump template create ...
      pebcalculate ...
      name BS2 ...
      pebbles 14 ...
                0.02,0.02,0.02,0.028284271247 ...
                0.02,0.0, 0.0, 0.0 ...
                0.02,-0.02,-0.02,-0.028284271247 ...
                0.02,0.02,-0.02,-0.028284271247 ...
                0.02,0.02,0.02,-0.028284271247 ...
                0.02,-0.02,0.02,-0.028284271247 ...
                0.02,-0.02,0.06,-0.028284271247 ...
                0.02,0.0, 0.04, 0.0 ...
                0.02,0.04,0.04,0.0 ...
                0.02,0.02,0.06,-0.028284271247 ...
                0.02,0.06,0.06,-0.028284271247 ...
                0.02,0.06,0.02,-0.028284271247 ...
                0.02,0.06,-0.02,-0.028284271247 ...
```

```
              0.02,0.04, 0.0, 0.0
clump template create ...
      pebcalculate ...
      name BS3 ...
      pebbles 28 ...
              0.02,0.02,0.02,0.028284271247 ...
              0.02,0.0, 0.0, 0.0 ...
              0.02,-0.02,-0.02,-0.028284271247 ...
              0.02,0.02,-0.02,-0.028284271247 ...
              0.02,0.02,0.02,-0.028284271247 ...
              0.02,-0.02,0.02,-0.028284271247 ...
              0.02,-0.02,0.06,-0.028284271247 ...
              0.02,0.0, 0.04, 0.0 ...
              0.02,0.04,0.04,0.0 ...
              0.02,0.02,0.06,-0.028284271247 ...
              0.02,0.06,0.06,-0.028284271247 ...
              0.02,0.06,0.02,-0.028284271247 ...
              0.02,0.06,-0.02,-0.028284271247 ...
              0.02,0.04, 0.0, 0.0 ...
              0.02,0.0, 0.0, -0.096568542494 ...
              0.02,-0.02,-0.02,-0.068284271247 ...
              0.02,-0.02,0.02,-0.068284271247 ...
              0.02,-0.02,0.06,-0.068284271247 ...
              0.02,0.02,0.06,-0.068284271247 ...
              0.02,0.0, 0.04, -0.096568542494 ...
              0.02,0.04,0.04,-0.096568542494 ...
              0.02,0.06,0.06,-0.068284271247 ...
              0.02,0.06,0.02,-0.068284271247 ...
              0.02,0.02,0.02,-0.068284271247 ...
```

```
              0.02,0.02,-0.02,-0.068284271247 ...

              0.02,0.06,-0.02,-0.068284271247 ...

              0.02,0.04, 0.0, -0.096568542494 ...

              0.02,0.02,0.02,-0.124852813741

def mpSetCommonParams

; Set common parameters.

  cm_matName = 'Ballast'

  ; ** Ballast aggregate of Ethio-Djibouti railway line (linear
parallel bonded material).

  cm_matType = 0

  cm_localDampFac = 0.7

  cm_densityCode = 0

  cm_densityVal = 2650.0

  ; Grain shape & size distribution group:

    cm_shape = 1

    cm_nSD = 5

    cm_typeSD = array.create(cm_nSD)

    cm_ctName = array.create(cm_nSD)

    cm_Dlo    = array.create(cm_nSD)

    cm_Dup    = array.create(cm_nSD)

    cm_Vfrac  = array.create(cm_nSD)

    cm_ctName(1) = 'BS1'

    cm_Dlo(   1) = 16.0e-3

    cm_Dup(   1) = 25.0e-3

    cm_Vfrac( 1) = 0.09

    cm_ctName(2) = 'BS2'

    cm_Dlo(   2) = 25.0e-3

    cm_Dup(   2) = 35.5e-3

    cm_Vfrac( 2) = 0.28
```

```
    cm_ctName(3) = 'BS3'
    cm_Dlo(   3) = 35.5e-3
    cm_Dup(   3) = 45.0e-3
    cm_Vfrac( 3) = 0.36
    cm_ctName(4) = 'BS3'
    cm_Dlo(   4) = 45.0e-3
    cm_Dup(   4) = 56.0e-3
    cm_Vfrac( 4) = 0.22
    cm_ctName(5) = 'BS1'
    cm_Dlo(   5) = 56.0e-3
    cm_Dup(   5) = 63.0e-3
    cm_Vfrac( 5) = 0.05
end
@mpSetCommonParams
def mpSetPackingParams
; Set packing parameters.
  pk_Pm = 150.0e3
  pk_procCode = 0
  pk_nc = 0.43
  ; Boundary-contraction group:
    pk_fricCA = 0.0
    pk_vLimit = 1.0
end
@mpSetPackingParams
;#####################################################
def mpSetLinParams
; Set linear material parameters.
  ; Common group (set in mpSetCommonParams)
  ; Packing group (set in mpSetPackingParams)
```

```
  ; Linear material group:

    lnm_emod = 500e6

    lnm_krat = 1.5

    lnm_fric = 0.4

end

@mpSetLinParams

@_mpCheckAllParams

@mpListMicroProps

return

;EOF: Ethio-Djibouti railway ballast.p3dat
```

### A.1.2 Triaxial compression test

```
;fname: compression-test.p3dat

; ** Triaxial test at 150 kPa confinement, with load-unload cycle
at 0.05% axial strain.

def ctSetParams

; Set Compression-Test Parameters.

  ct_testType = 0

  ct_Pc = 150.0e3

  ct_eRate = 0.01

  ct_loadCode =1

end

;------------------

def ctPerformStages ; redefinition of this function

  _ctPerformStage( 1, -0.0005 )

  _ctPerformStage( 2,  0.0005 )

end

@ctSetParams

@_ctCheckParams

@ctListProps
```

```
; Specify histories to be monitored during the compression test.
  history reset
  history nstep 10
  ; Servo pressures and strains:
  history add id=11 fish mv_wPx
  history add id=12 fish mv_wPy
  history add id=13 fish mv_wPz
  history add id=14 fish mv_wPr
  history add id=21 fish mv_wex
  history add id=22 fish mv_wey
  history add id=23 fish mv_wez
  ; Wall-based stresses and strains:
  history add id=101 fish mv_wsd
  history add id=102 fish mv_wsa
  history add id=201 fish mv_wea
  history add id=202 fish mv_wer
  history add id=203 fish mv_wev
  ; Measurement-based porosity:
  history add id=31 fish mv_mn
return
;EOF: compression-test.p3dat
```

## A.2 The remaining PFC$^{3D}$ triaxial compression test results

The results of triaxial compression test simulation under 30, 40, 80, 200, 500, 1000Kpa confining pressure are shown below.

***30kpa confining pressure***

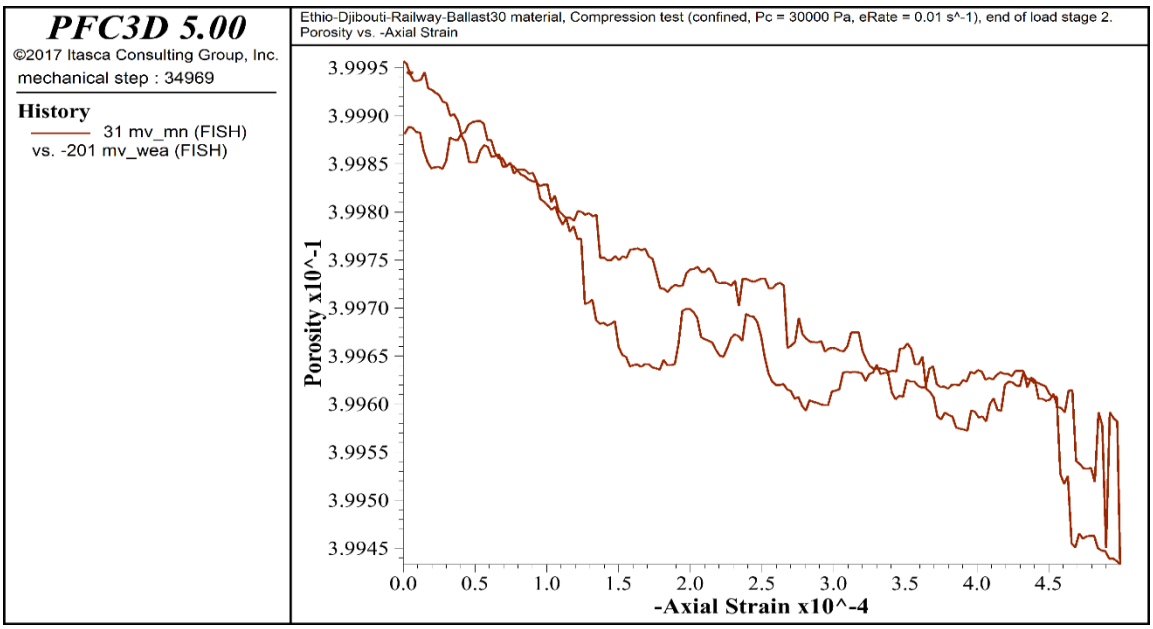


**Figure A.1: Porosity Vs. Axial Strain plot ($\sigma_c = 30Kpa$)**

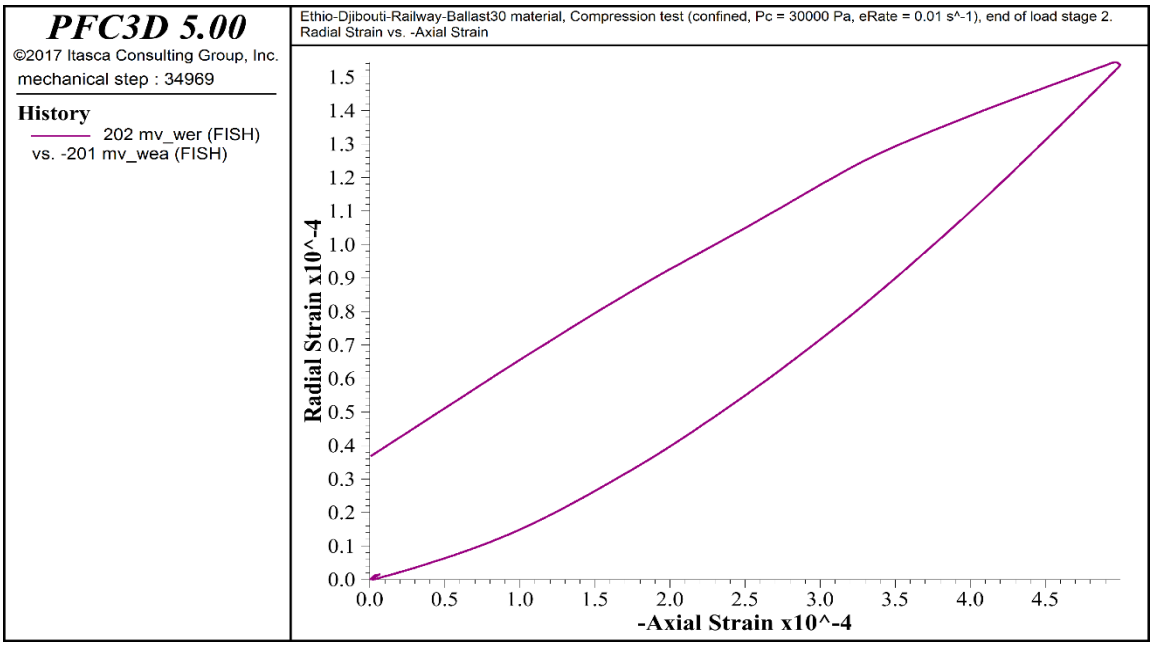


**Figure A.2: Radial Strain Vs. Axial Strain ($\sigma_c = 30Kpa$)**

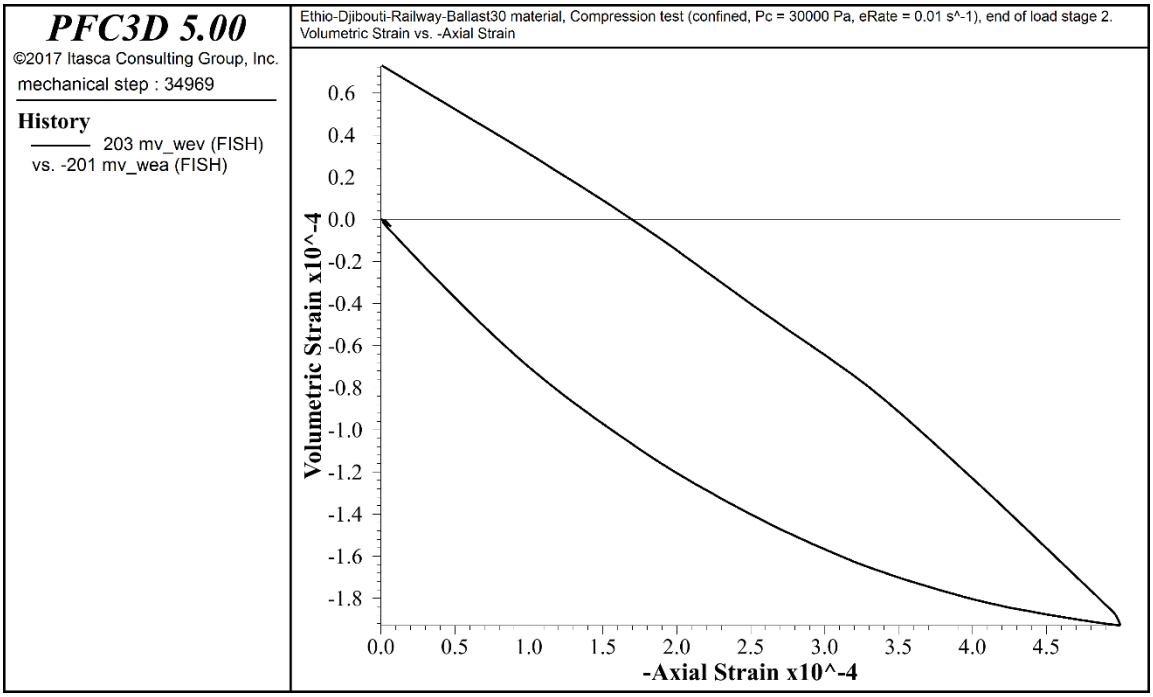


**Figure A.3: Volumetric Strain Vs. Axial Strain ($\sigma_c = 30Kpa$)**

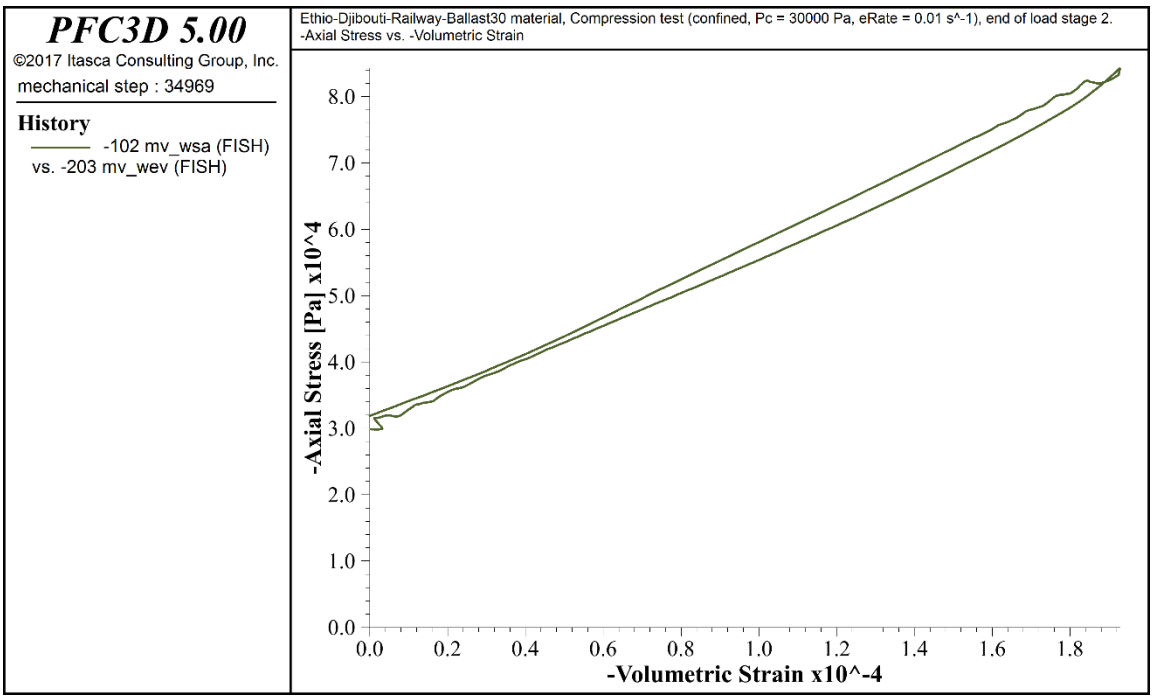


**Figure A.4: Axial Stress Vs. Volumetric Strain ($\sigma_c = 30Kpa$)**

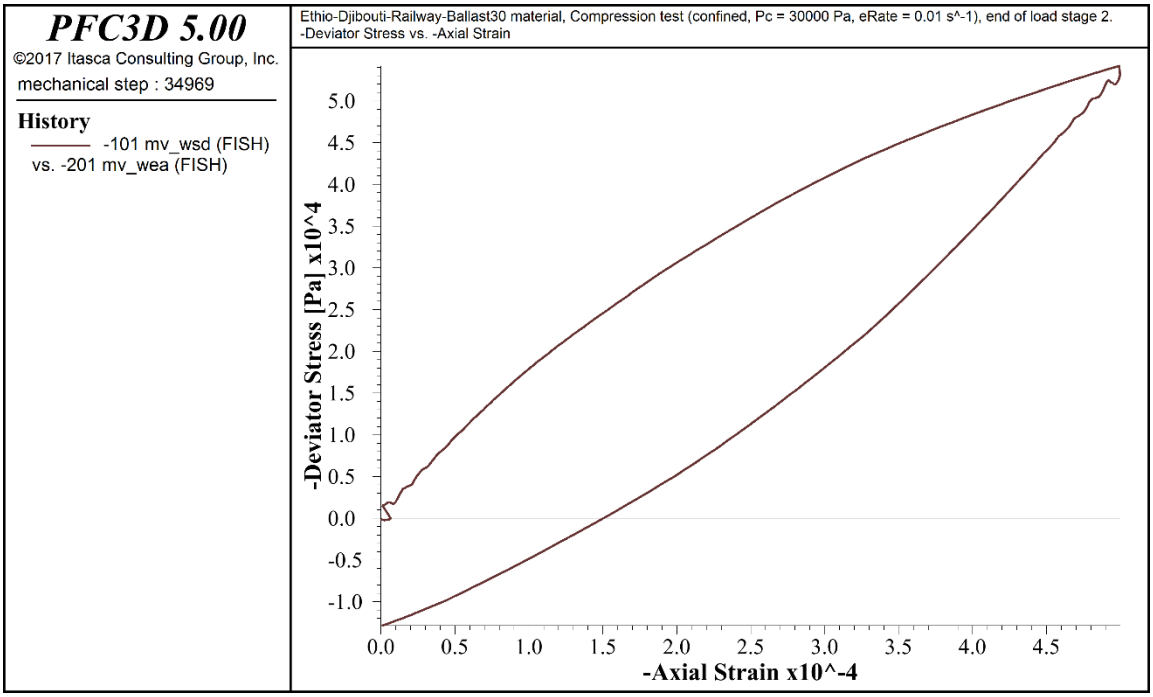


**Figure A.5: Deviator Stress Vs. Axial Strain ($\sigma_c = 30Kpa$)**

***80Kpa confining pressure***

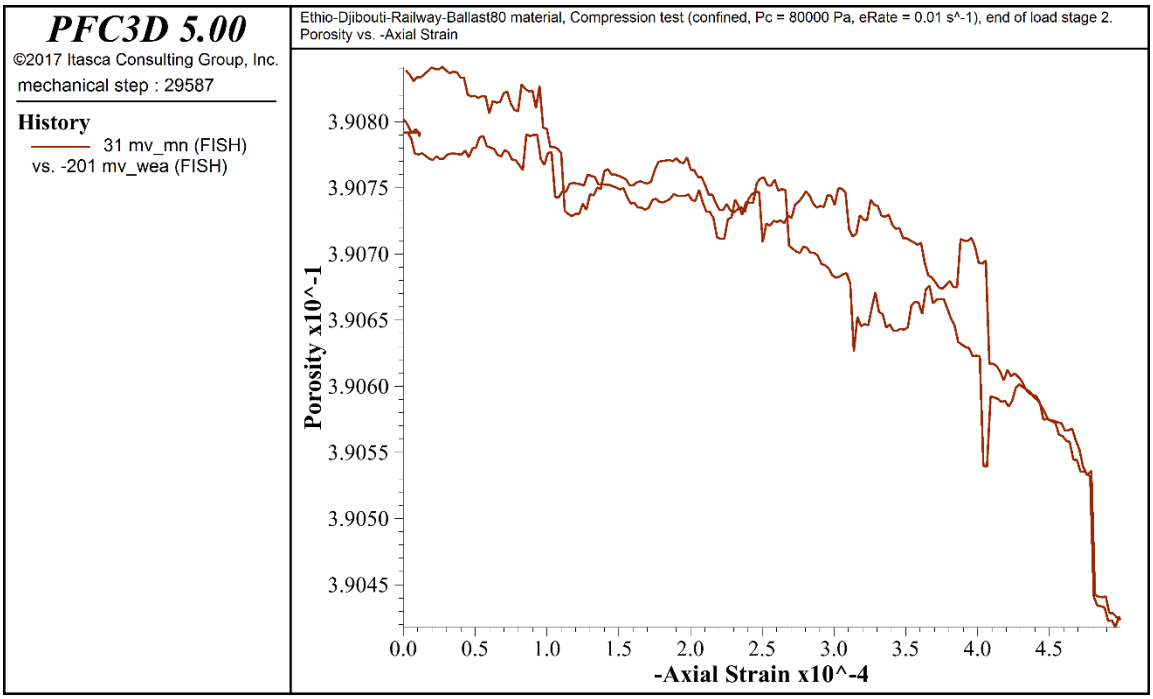


**Figure A.6: Porosity Vs. Axial Strain ($\sigma_c = 80Kpa$)**

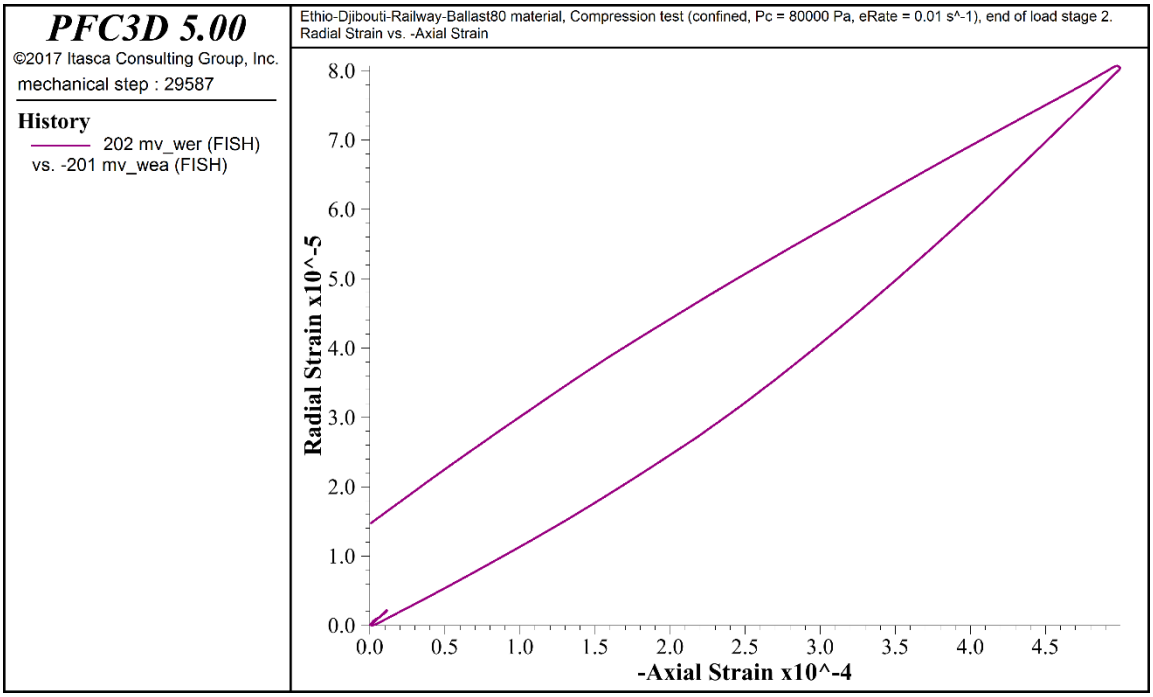


**Figure A.7: Radial Strain Vs. Axial Strain ($\sigma_c = 80Kpa$)**

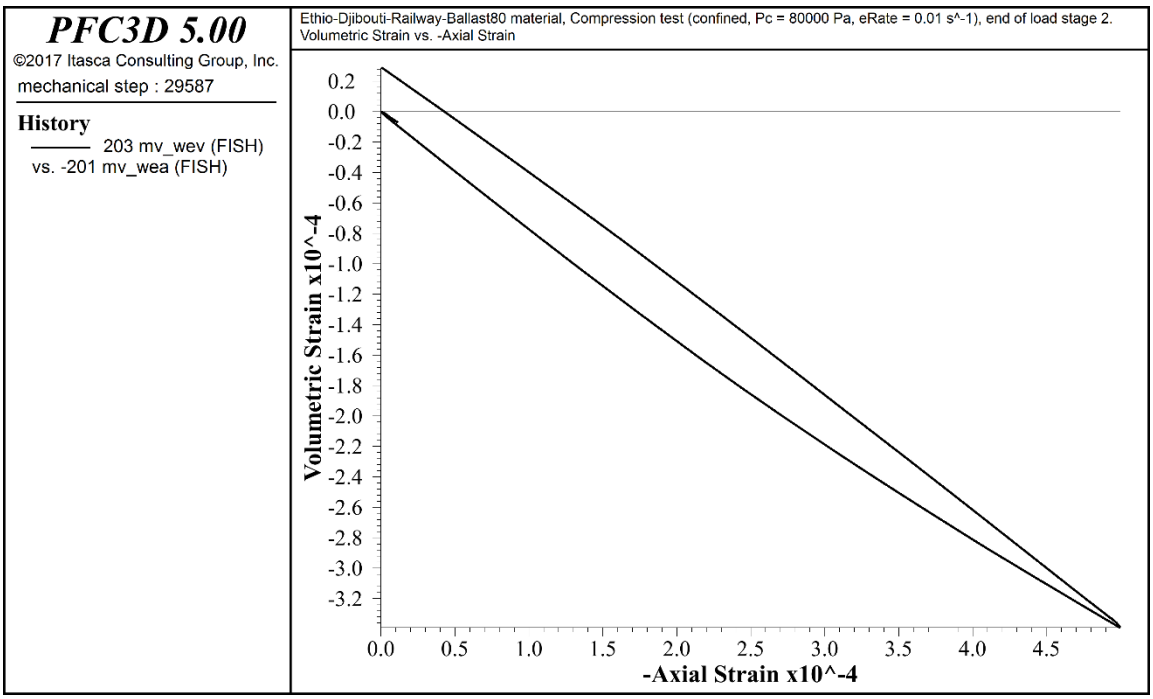


**Figure A.8: Volumetric Strain Vs. Axial Strain ($\sigma_c = 80Kpa$)**

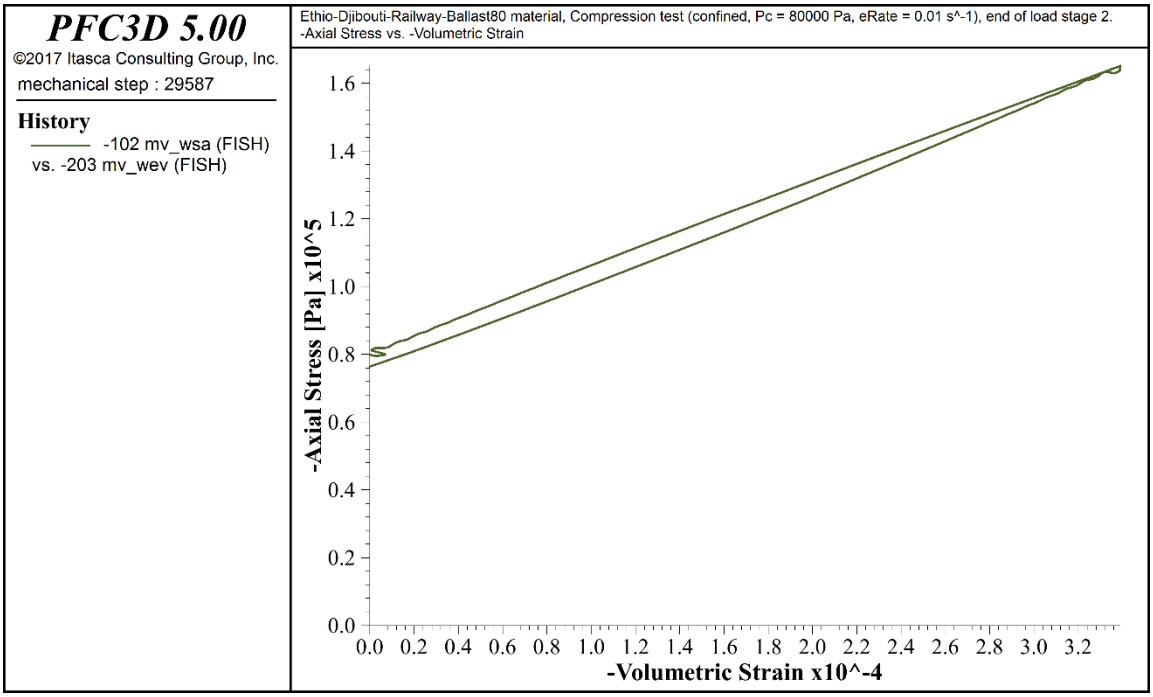


**Figure A.9: Axial Stress Vs. Volumetric Strain ($\sigma_c = 80Kpa$)**

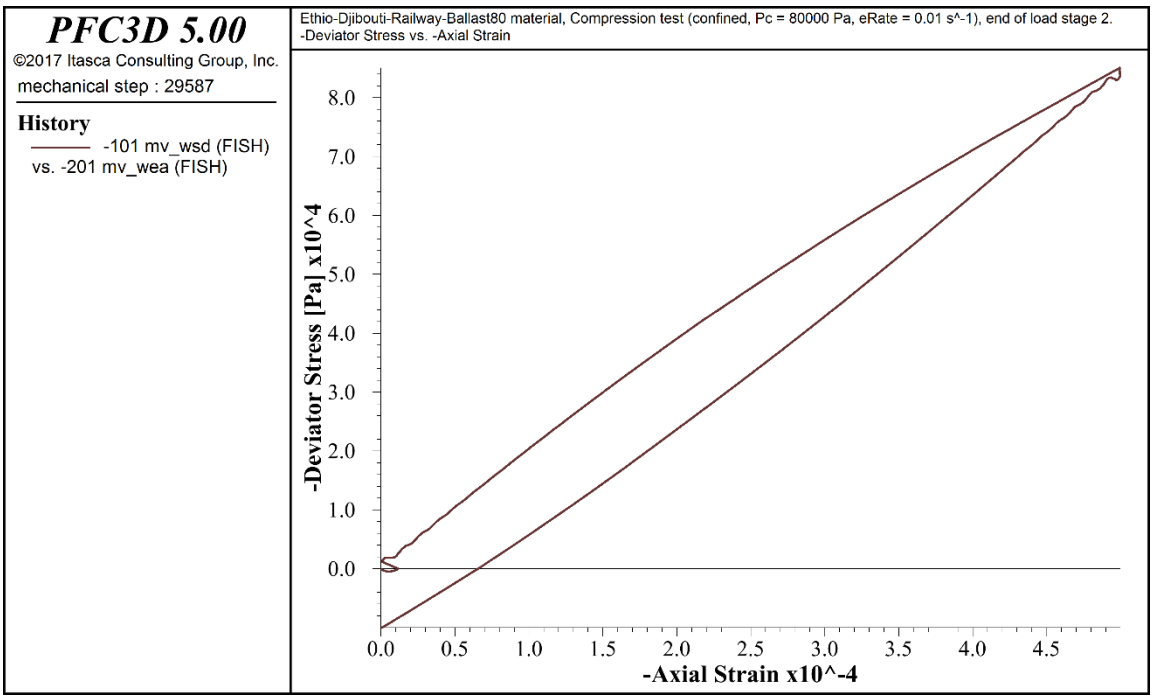


**Figure A.10: Deviator Stress Vs. Axial Strain ($\sigma_c = 80Kpa$)**

***150Kpa confining pressure***

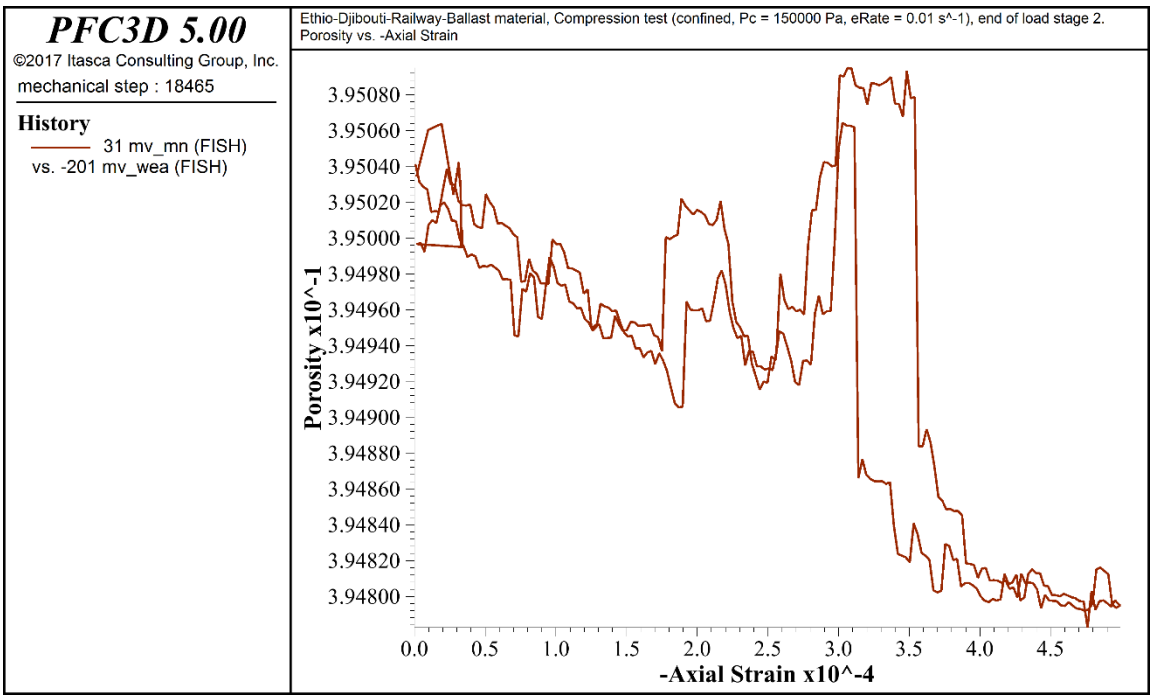


**Figure A.11: Porosity Vs. Axial Strain ($\sigma_c = 150Kpa$)**

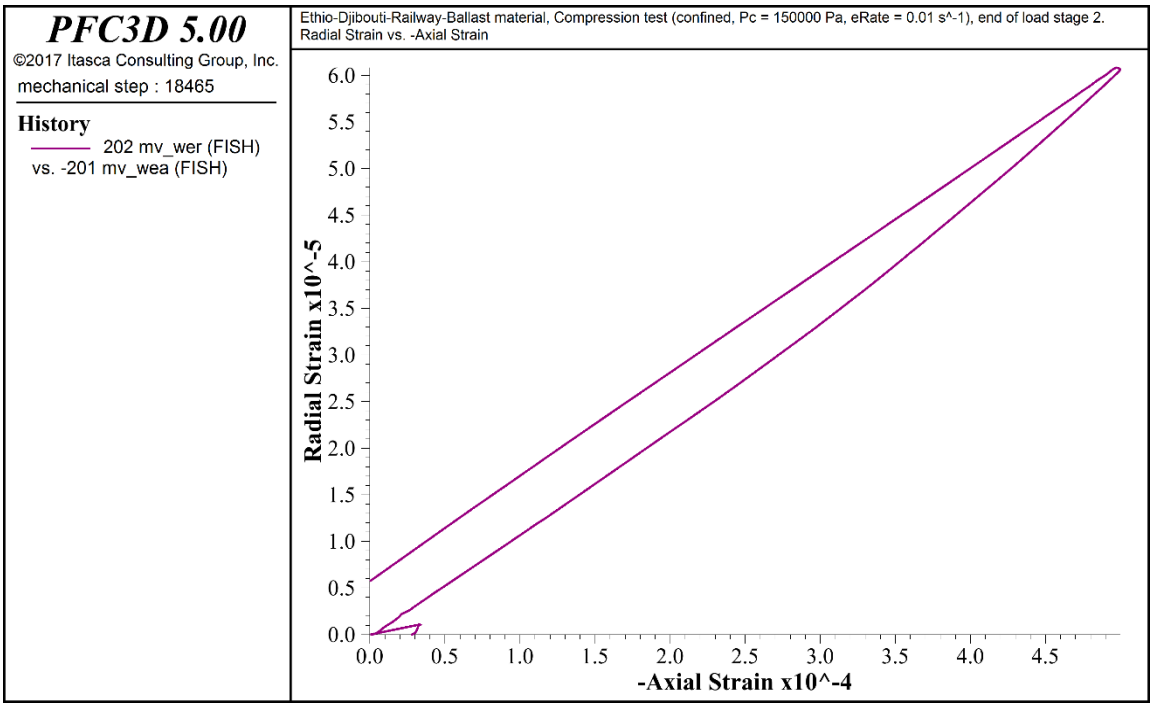


**Figure A.12: Radial Strain Vs. Axial Strain ($\sigma_c = 40Kpa$)**

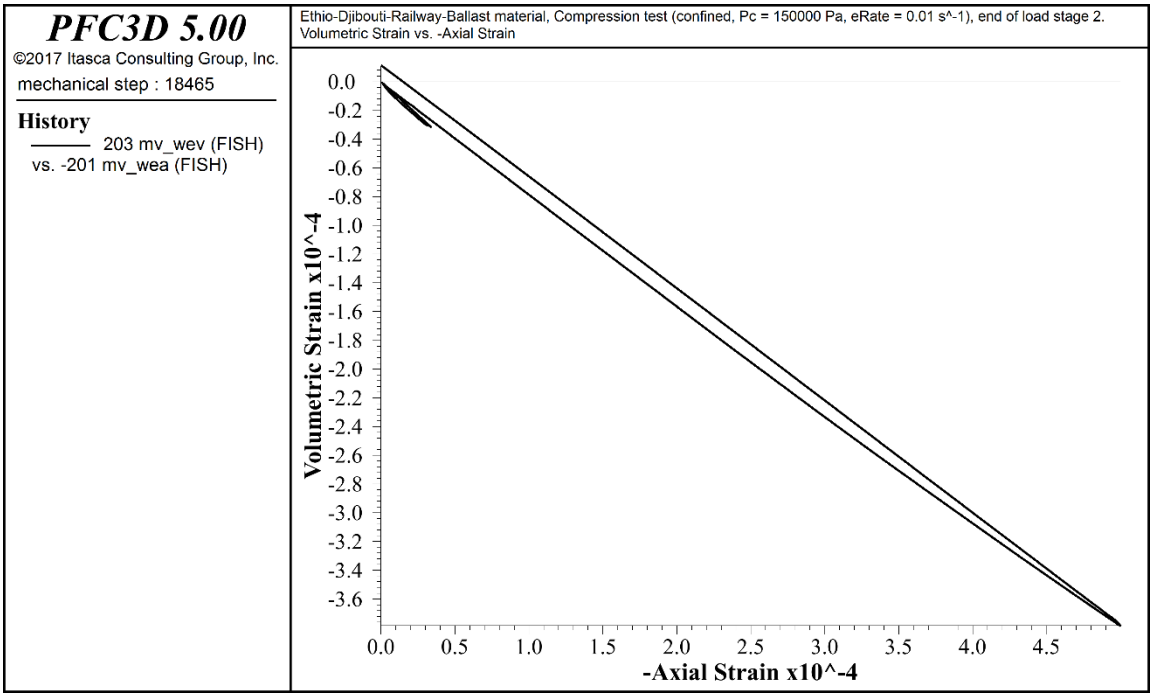


**Figure A.13: Volumetric Strain Vs. Axial Strain ($\sigma_c = 150Kpa$)**

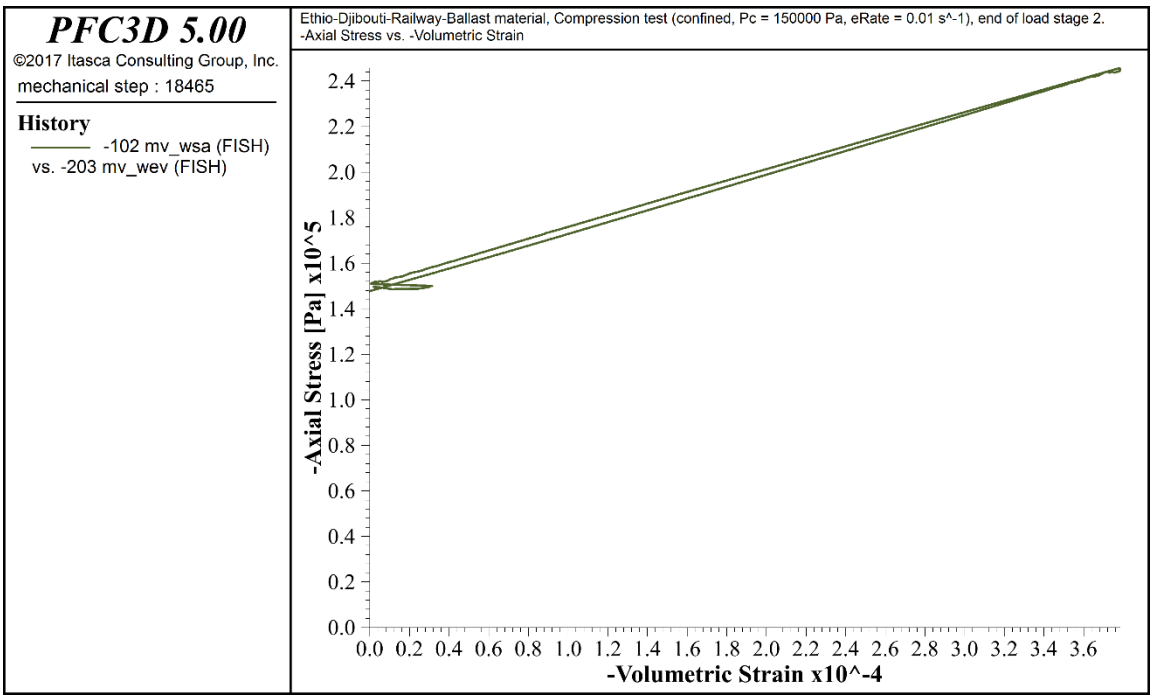


**Figure A.14: Axial Stress Vs. Volumetric Strain ($\sigma_c = 150Kpa$)**

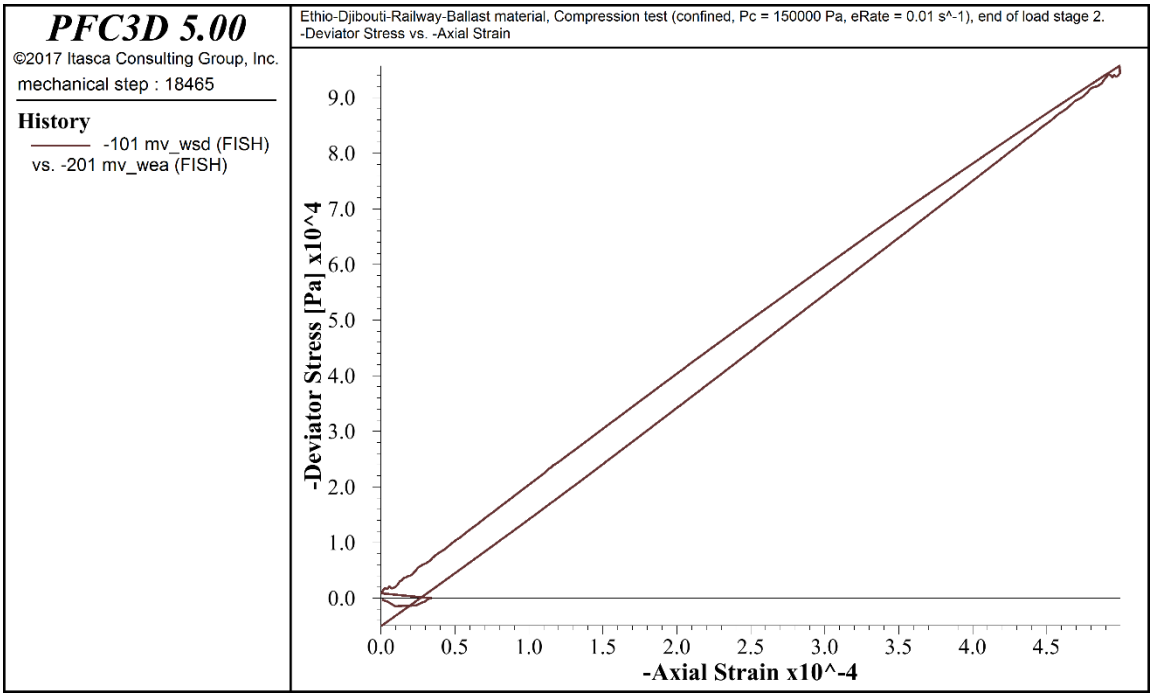


**Figure A.15: Deviator Stress Vs. Axial Strain ($\sigma_c = 150Kpa$)**

***200Kpa confining pressure***

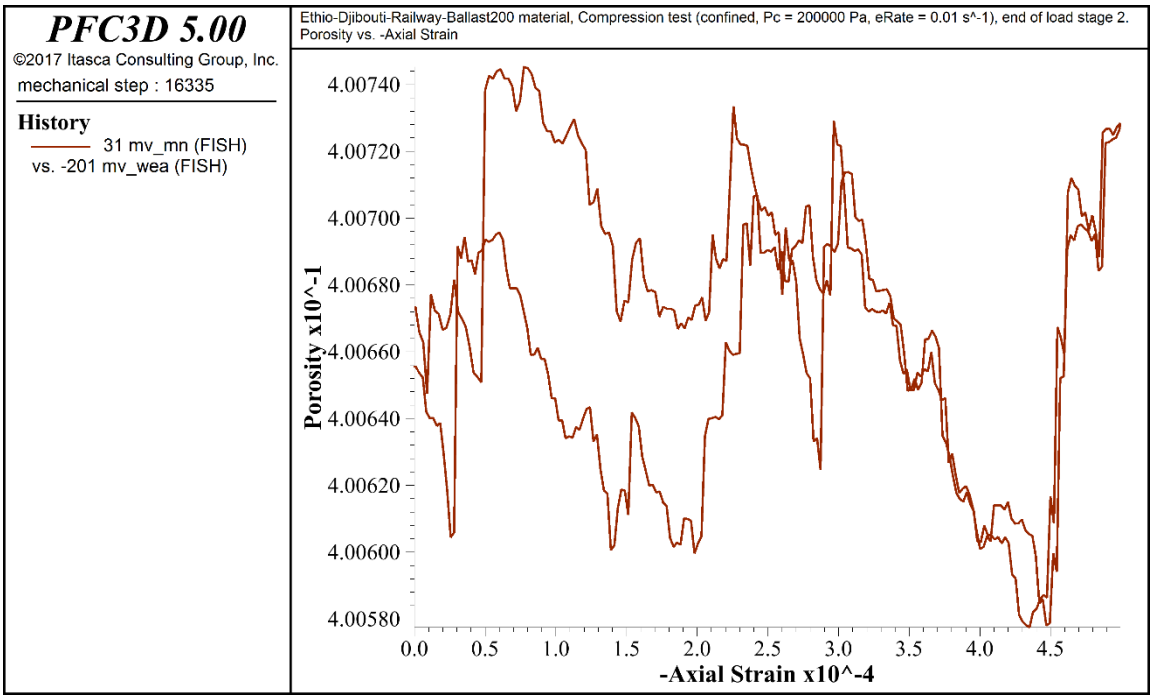


**Figure A.16: Porosity Vs. Axial Strain ($\sigma_c = 200Kpa$)**

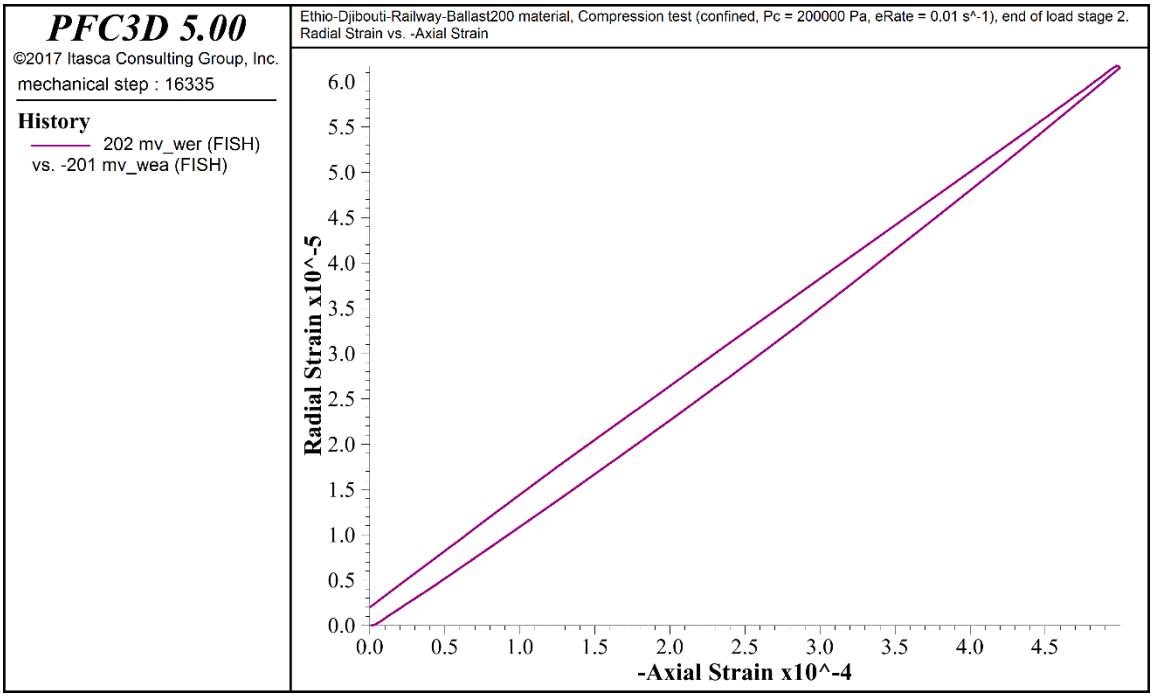


**Figure A.17: Radial Strain Vs. Axial Strain ($\sigma_c = 200Kpa$)**

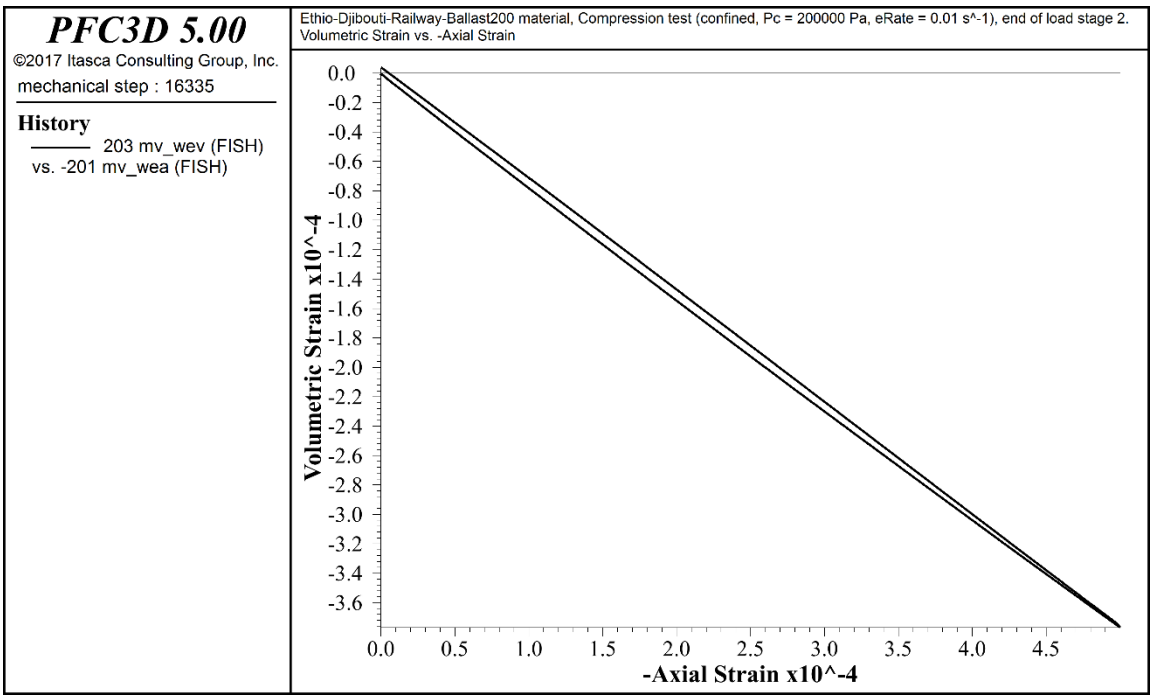


**Figure A.18: Volumetric Strain Vs. Axial Strain ($\sigma_c = 200Kpa$)**

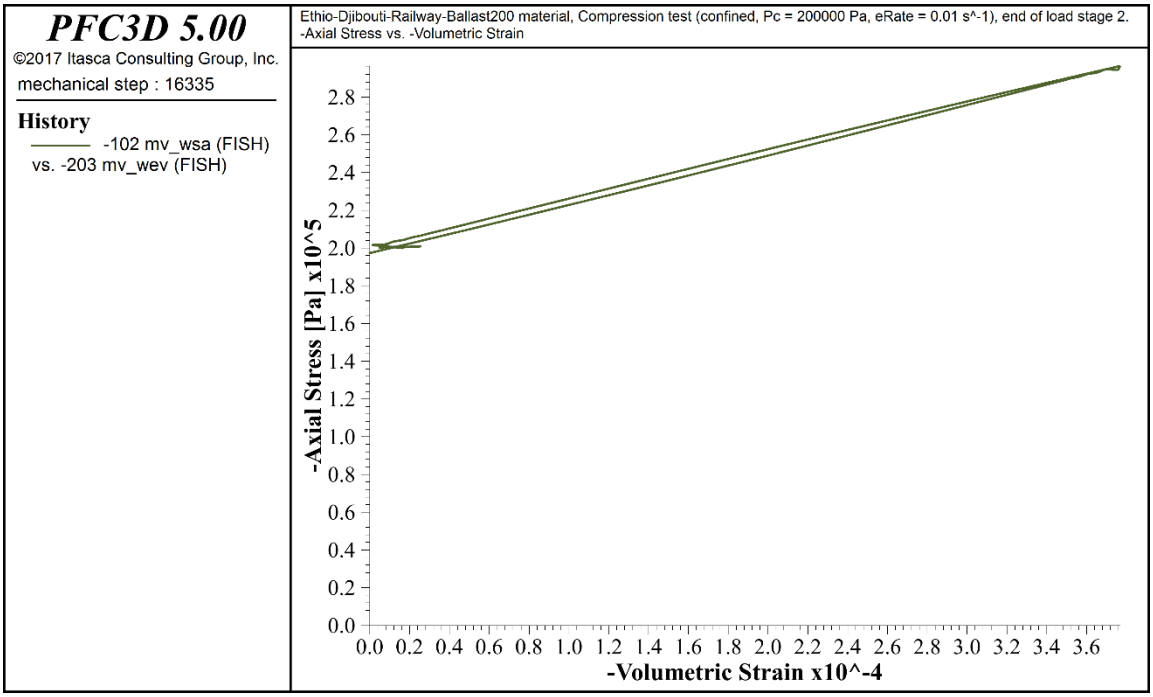


**Figure A.19: Axial Stress Vs. Volumetric Strain ($\sigma_c = 200Kpa$)**

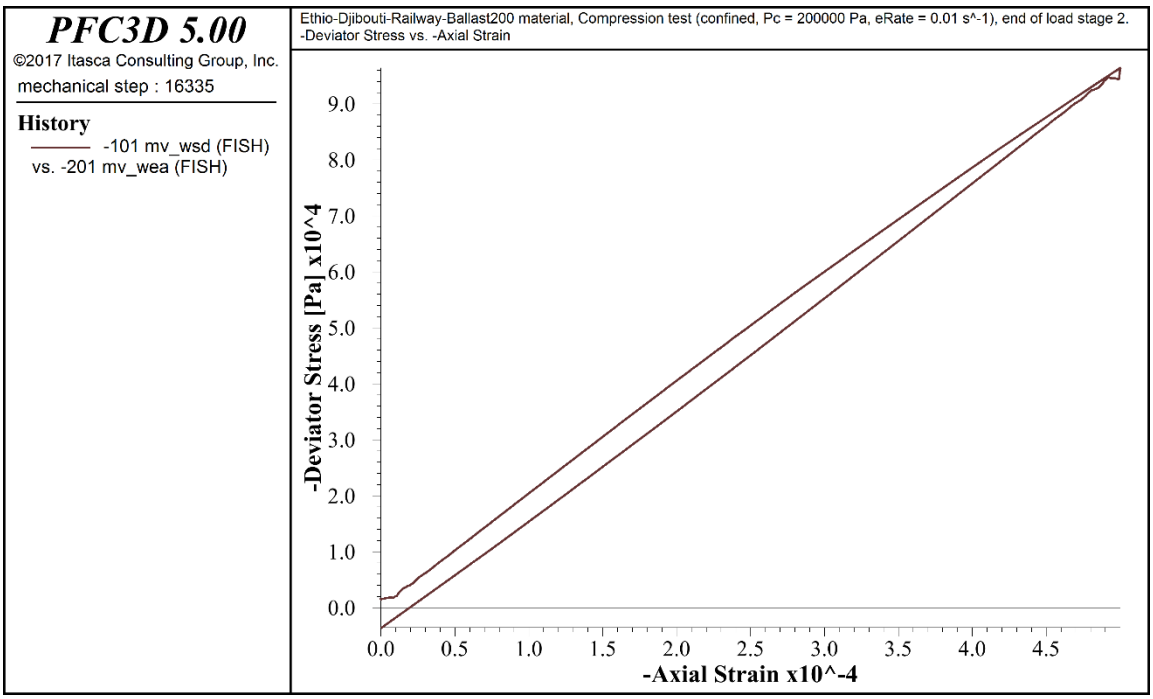


**Figure A.20: Deviator Stress Vs. Axial Strain ($\sigma_c = 200Kpa$)**

***500Kpa confining pressure***

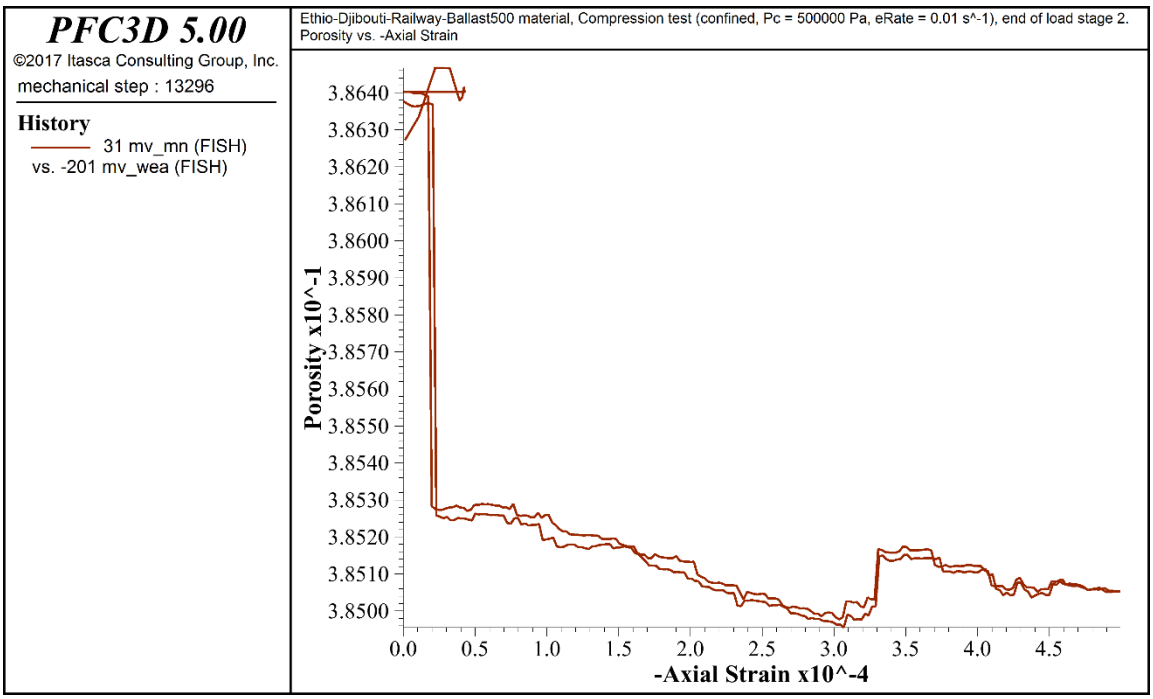


**Figure A.21: Porosity Vs. Axial Strain ($\sigma_c = 500Kpa$)**

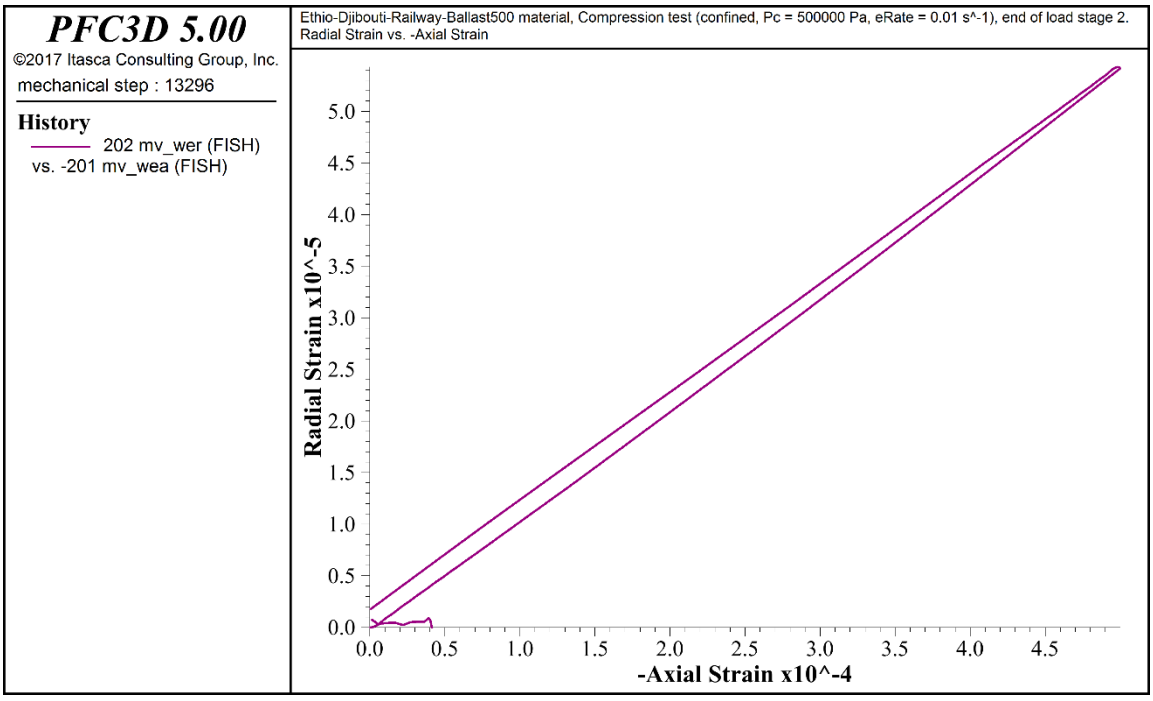


**Figure A.22: Radial Strain Vs. Axial Strain ($\sigma_c = 500Kpa$)**

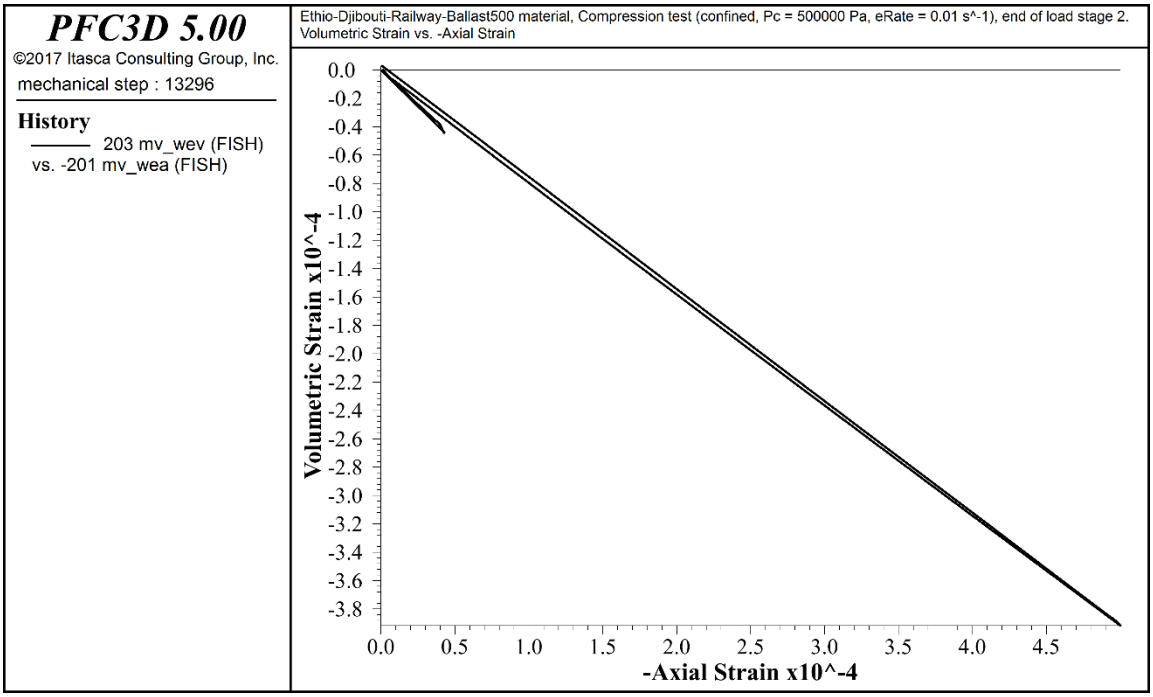


**Figure A.23: Volumetric Strain Vs. Axial Strain ($\sigma_c = 500Kpa$)**

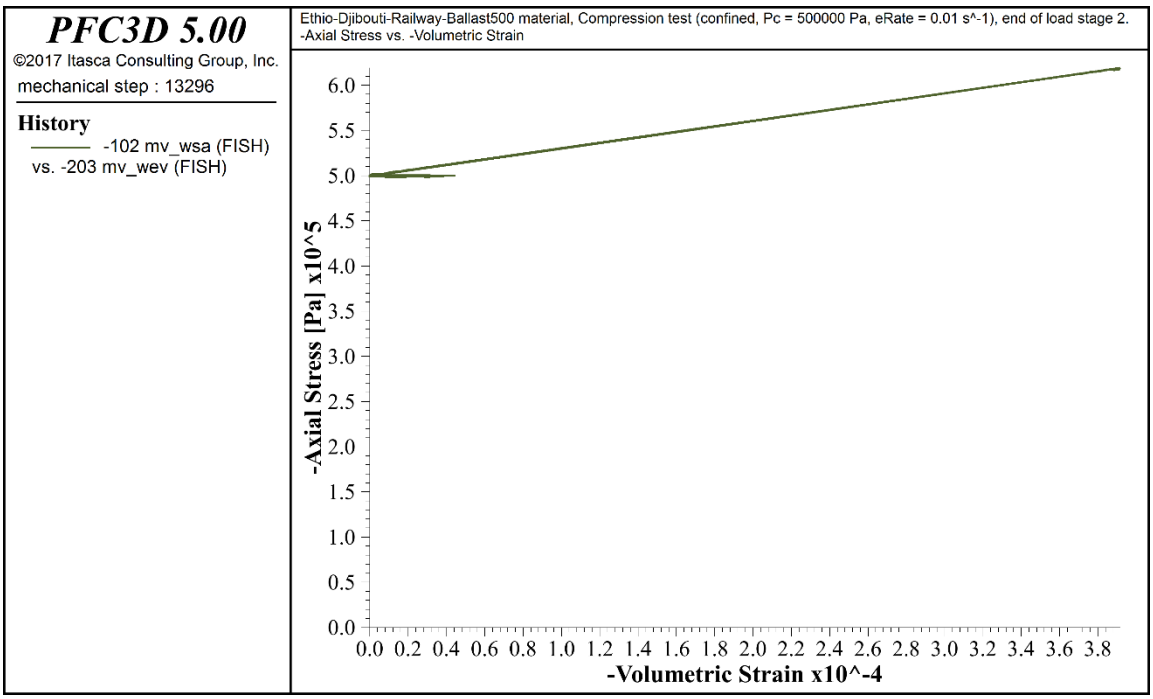


**Figure A.24: Axial Stress Vs. Volumetric Strain ($\sigma_c = 500Kpa$)**

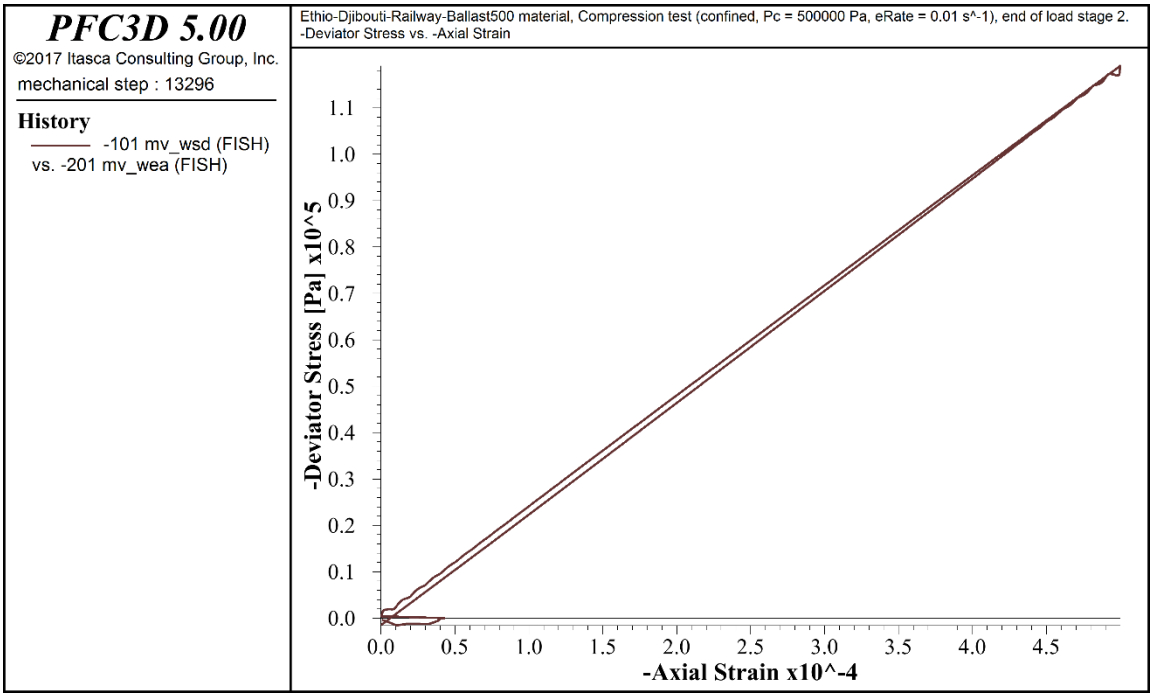


**Figure A.25: Deviator Stress Vs. Axial Strain ($\sigma_c = 500Kpa$)**

***1000Kpa confining pressure***

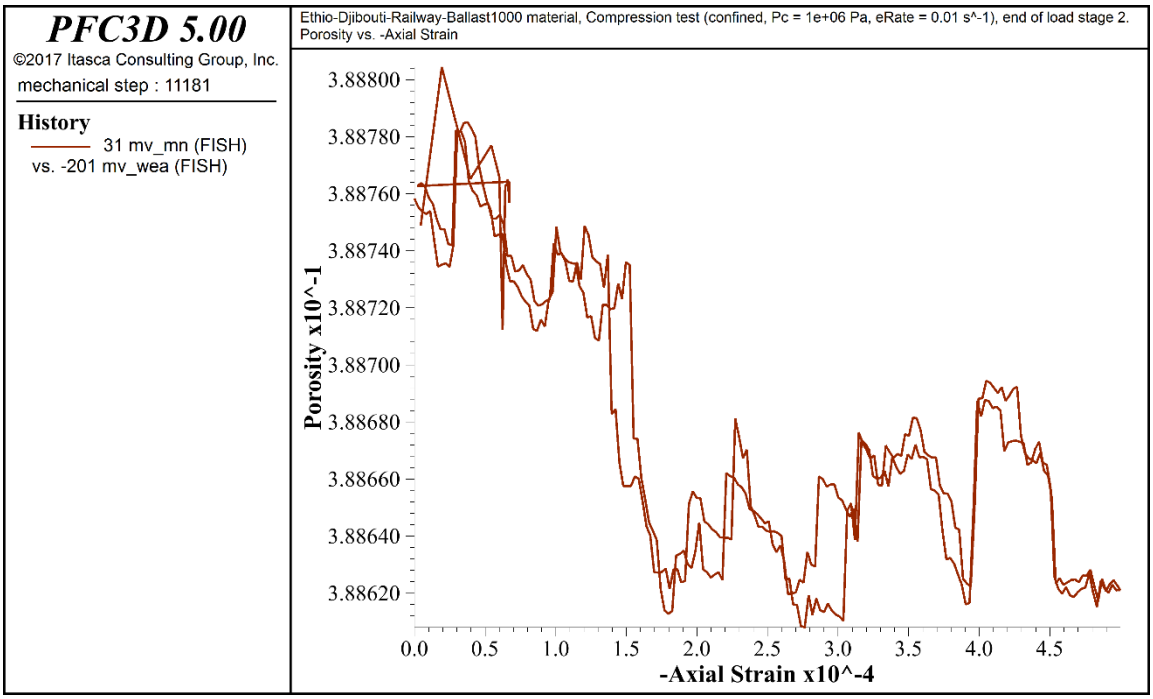


**Figure A.26: Porosity Vs. Axial Strain ($\sigma_c = 1000Kpa$)**

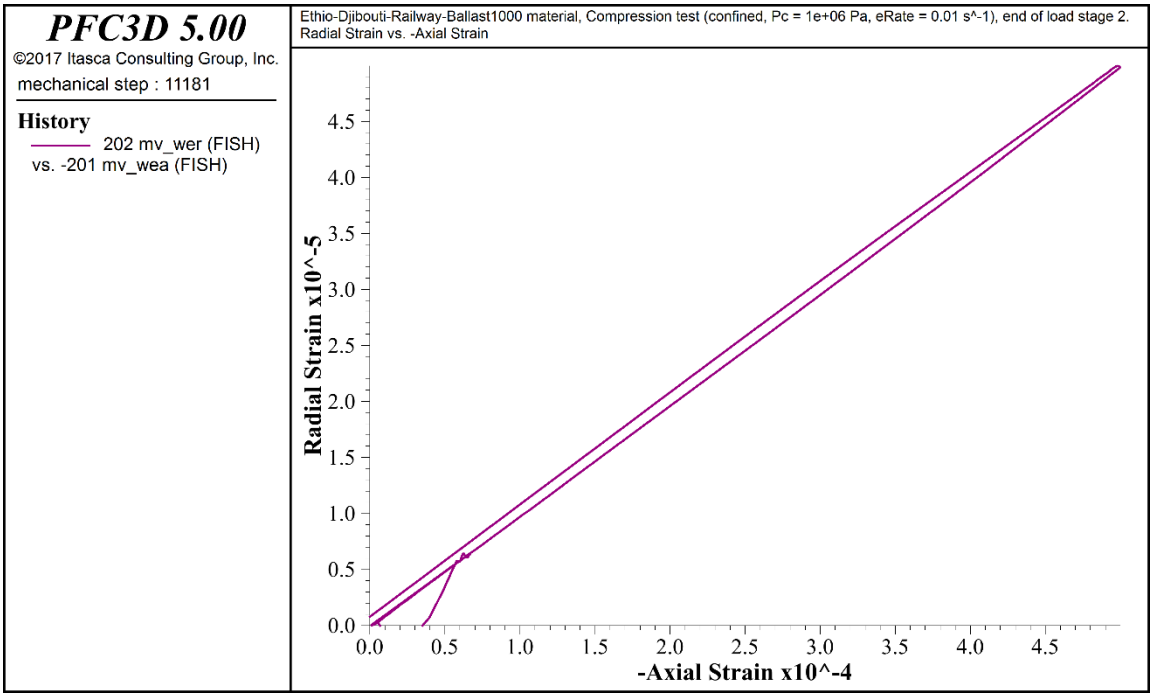


**Figure A.27: Radial Strain Vs. Axial Strain ($\sigma_c = 1000Kpa$)**

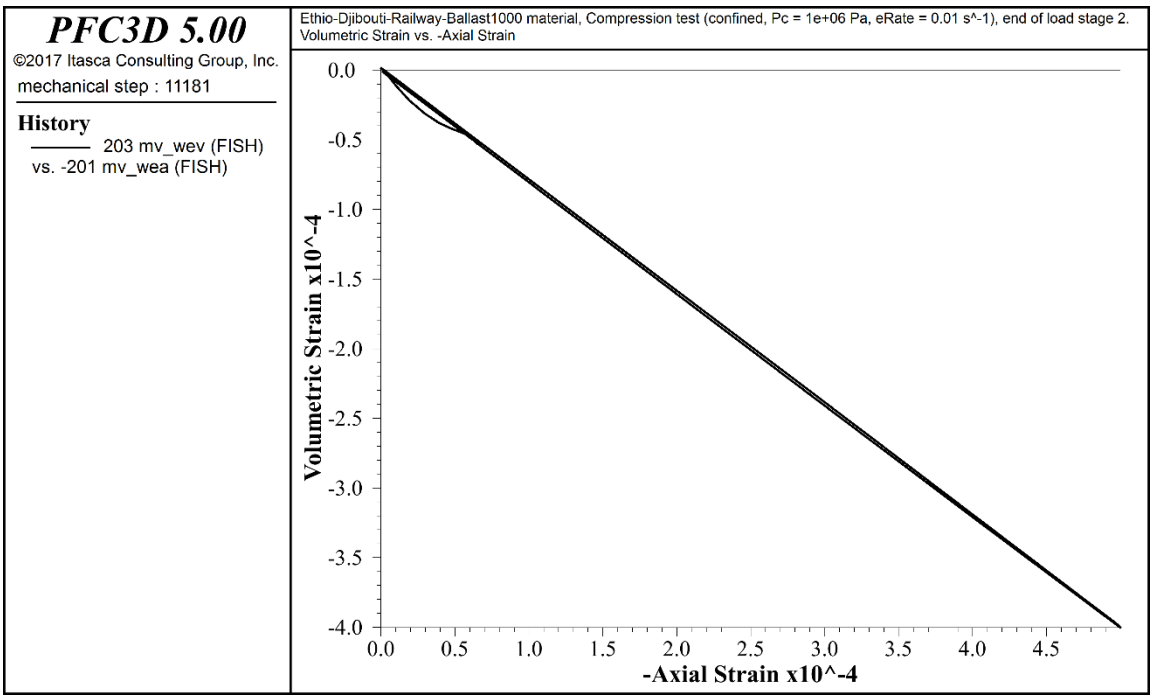


**Figure A.28: Volumetric Strain Vs. Axial Strain ($\sigma_c = 1000Kpa$)**

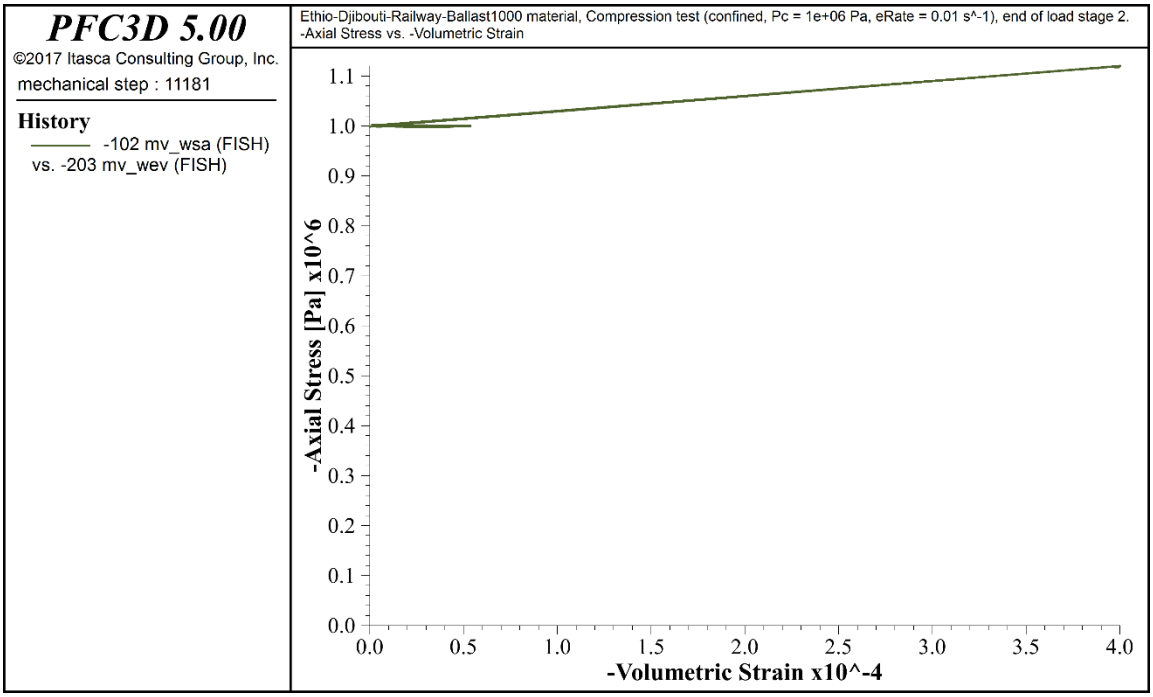


**Figure A.29: Axial Stress Vs. Volumetric Strain ($\sigma_c = 1000Kpa$)**

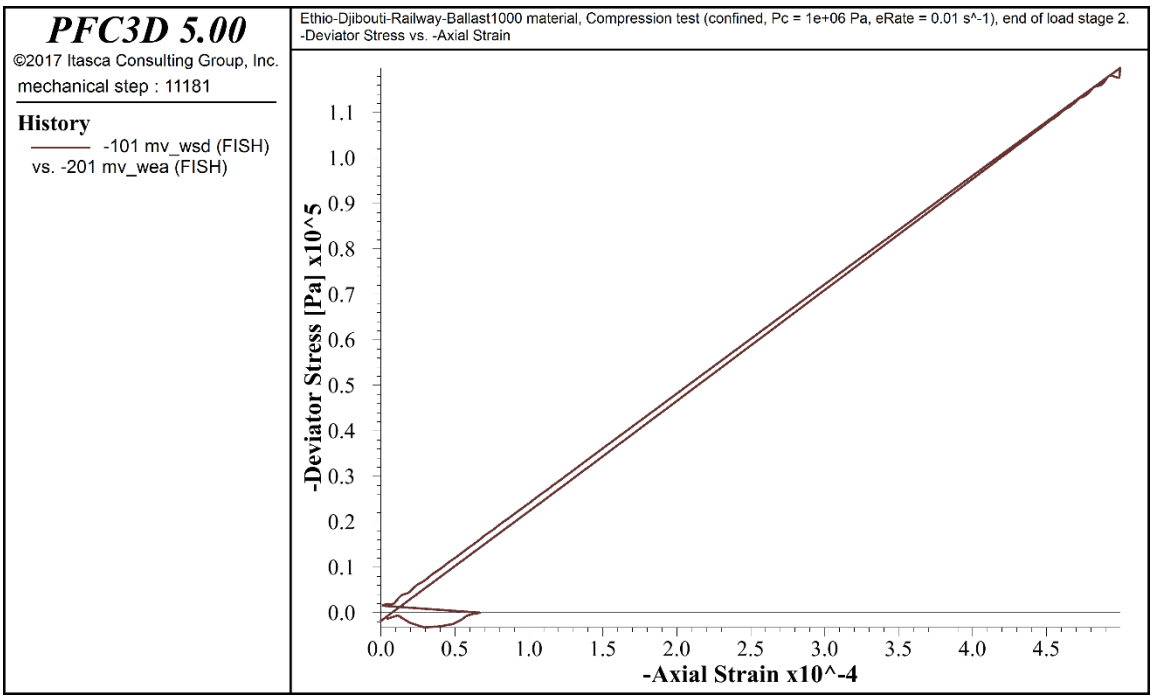


**Figure A.30: Deviator Stress Vs. Axial Strain ($\sigma_c = 1000Kpa$)**

# APPENDIX B

## B.1 Input data details

### B.1.1 Railway track classification

**Table B.1: The Classification of Main Track (Table 4.0.1 of [13])**

| Contents | | | | | Unit | Class 1 | Class 2 | | | Class 3 | Class 4 | Class 5 |
|---|---|---|---|---|---|---|---|---|---|---|---|---|
| Operating condition | Annual gross traffic tonnage | | | | Mt | >50 | 25~50 | | | 15~25 | 8~15 | <8 |
| | Design velocity for passenger train | | | | km/h | 160~120 | 160~120 | ≤120 | | ≤120 | ≤100 | ≤80 |
| Track structure | Rail | | | | kg/m | 75 | 60 | 60 | | 50 | 50 | 50 |
| | Sleeper | Concrete sleeper | | Type | — | Ⅲ | Ⅲ | Ⅲ | Ⅱ | Ⅱ | Ⅱ | Ⅱ |
| | | | | Number | piece /km | 1667 | 1667 | 1667 | 1760 | 1667 or 1760 | 1600 or 1680 | 1520 or 1640 |
| | Thickness of broken stone ballast | Soil subgrade | Double layer | Surface ballast | cm | 30 | 30 | 30 | | 25 | 20 | 20 |
| | | | | Subsurface ballast | cm | 20 | 20 | 20 | | 20 | 20 | 15 |
| | | Soil subgrade | Single layer | Ballast | cm | 35 | 35 | 35 | | 30 | 30 | 25 |
| | | Hard rock subgrade | Single layer | Ballast | cm | 30 | 30 | - | | - | - | - |
| | Ballastless track | Slab track | | Thickness of concrete base | cm | ≥15 | | | | | | |
| | | ballastless track with long-sleepers embedding concrete | | | | | | | | | | |
| | | ballastless track with elastic supporting blocks | | | | ≥17 | | | | | | |

Note: 1 Annual gross traffic tonnage includes net load, mass of locomotives and vehicles, and reciprocating gross traffic tonnage is calculated for single line, and gross traffic tonnage of each line is calculated for double lines.

2 The line with annual gross traffic tonnage more than 50 Mt may adopt 60 kg/m rail according to factually operating condition and technical-economical comparison.

3 The renovation of railwy track with the design velocity of train is 160 km/h may adopt type Ⅱ concrete sleepers.

4 When wooden sleepers are paved on open deck bridge, the number of sleepers per kilometer shall be designed according to *Fundamental Code for Railway Bridge and Culvert Design* (TB10002.1).

5 The thickness of concrete base of ballastless track with elastic supporting blocks is the concrete thickness under the block.

6 When wooden sleepers are used on special conditions, the number of sleepers may be defined according to design.

### B.1.2 Gradation test result

**Table B.2: Particle size distribution of ballast material used in Ethio-Djibouti rail track**

中国中铁

**CREC Addis Ababa-Mieso Railway Project**

**2nd Testing Report for Stone Ballast**

| | | | |
|---|---|---|---|
| Consignor | Xinyun Branch | Report No. | CRECxy-BT-2015001 (Gelan) |
| Rock Origin | Gelan | Date of Consignor | 2015-01-02 |
| Number of Samples Represented | Production Testing | Date of Report | 2015-01-12 |

| Test Items | | Standard Code | Test Results | |
|---|---|---|---|---|
| | | | Side Length of the Sieve Opening (mm) | Mass of Aggregate Passing the Sieve (%) |
| Particle Size Grading | 16mm | 0~5 | 16mm | 0 |
| | 25mm | 5~15 | 25mm | 9 |
| | 35.5mm | 25~40 | 35.5mm | 37 |
| | 45mm | 55~75 | 45mm | 73 |
| | 56mm | 92~97 | 56mm | 95 |
| | 63mm | 97~100 | 63mm | 99 |

| Test Items | 1st grade ballast | 2nd grade ballast | Test Result |
|---|---|---|---|
| Acicular Index (%) | ≤50 | | 14 |
| Flankiness Index (%) | ≤50 | | 8 |
| Content of Weathered Particles and Other Miscellaneous Stones (%) | ≤5 | / | 0.3 |
| Particle Surface Cleanliness (%) | ≤0.17 | / | 0.09 |
| Content of Powder with Particle Size of 0.1mm (%) | ≤1 | ≤1 | 0.4 |

Conclusion:
These ballast sample satisfies the techical standard of stair-class ballast of TB/T 2140-1990.

Report 罗七从 Approve 付勇 Stamp CREC ADDIS-MIESO RAILWAY PROJECT Xinyun Laboratory

### B.1.3 Rail profile

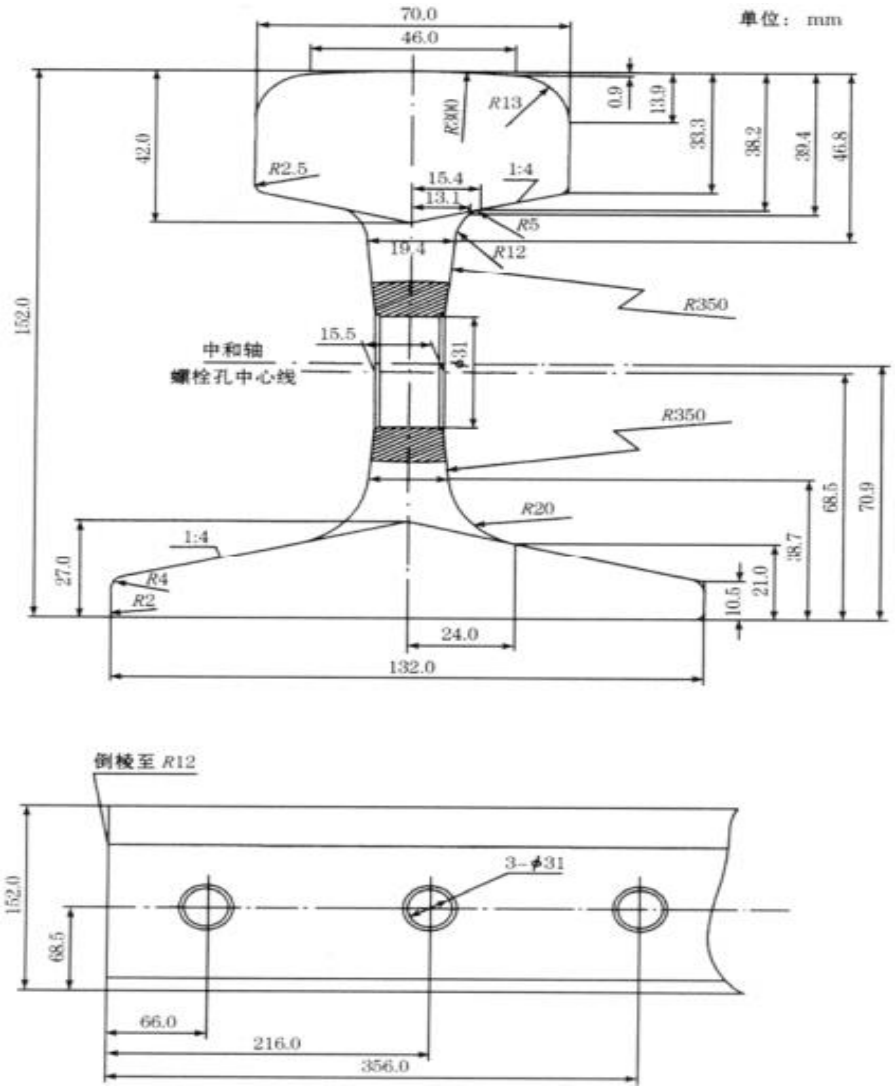


**Figure B.1: Rail profile 50kg/m (Figure A.4 of [12])**

### B.1.4 Sleeper detail

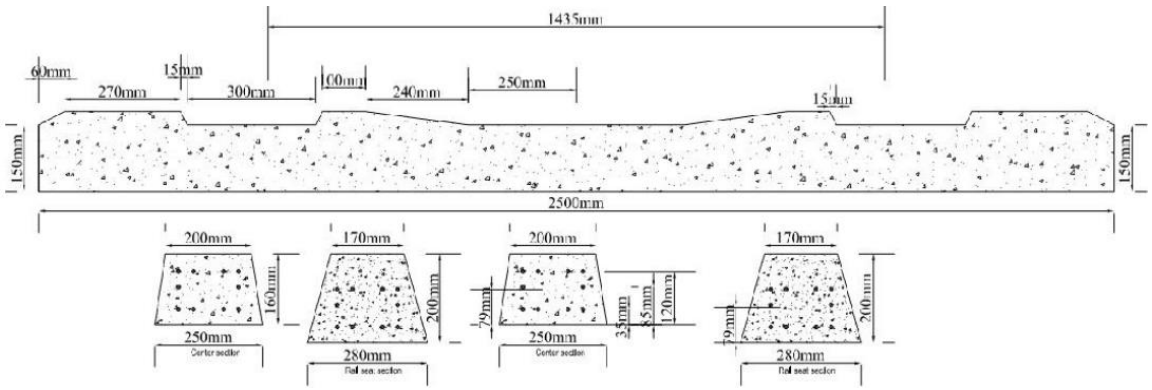


**Figure B.2: Sleeper section detail (Figure 3.2 of [21])**